1/21/94

Final Report

Artificial Plasma EXperiments.

Chemical release observations associated with the CRRES program.

Period Covered (April 12, 1985 - December 23, 1993)

Contract No. NAS-8-36630

Lockheed Palo Alto Research Laboratories,

Prepared for NASA, George C. Marshall Spaceflight Center
Marshall Spaceflight Center, Alabama 35812

by Stephen B. Mende

TABLE OF CONTENTS

1.0 Introduction

The CRRES program investigated earth plasma environment by active experiments in which metal vapors were injected into the upper atmosphere and magnetosphere. The vapor clouds perturb the ambient ionospheric/magneospheric environment and the effects could be monitored by passive observing instruments. Our part of the CRRES program, the Artificial Plasma EXperiment program, was a ground based and aircraft based investigation to observe artificial chemical releases by optical techniques.

The CRRES satellite was in a highly elliptical orbit with apogee above 30,000 km and this orbit permitted the injection of the chemical release clouds at low altitude near perigee and at high altitude near apogee. During the first CRRES campaign in which we participated, the releases took place at higher altitude at and near apogee. These experiments were intended to probe the magnetosphere in the equatorial region at an orbit altitude of about 5Re. This the so called "high altitude" campaign took place in the winter of 1991 with most releases occurring in January and a few in February. The major goals of these releases can be summarized as follows:

1. Stimulation of fast ambient electron/ion precipitation by the injection of cold plasma into the magnetosphere.

2. Studying the interaction of high velocity plasma clouds with the ambient environment electric and magnetic field and cold plasma.

In perigee region of the orbit the satellite is traveling at full orbital velocity. Releases made at full orbital velocity carry a great deal of momentum. Releases near perigee therefore were useful for studying the interactions between fast ion streams and the ionosphere. The major goals of these types of experiments were as follows:

1. Studying the momentum interchange of the ions released at orbital velocity into the ionosphere.

2. Studying the behavior of plasmas simultaneously in conjugate hemispheres. The fast moving ions were able to propagate along the field line to the other hemisphere because of the gradient B effects thus the method permitted the painting of a field line with Ba ions.

3. Using the ion clouds to modulate the radio wave propagation properties of the ionosphere.

2.0 Description of the Investigation

2.1 The 1991 High Altitude Campaign

The Lockheed group participated heavily in the CRRES high altitude campaign in January and February 1991. A field station was manned at Arecibo Puerto Rico with dual imaging capability. These cameras operated in the filtered mode and the filters could be changed. Most data was obtained with the ionized barium filter. In figure 1 we are including a collage of images of one of the Barium releases recorded by the camera at Arecibo. Note that this cloud was observed for several hours after release.

In addition to performance of ground based observations the Lockheed team supported the CRRES mission by simultaneously participating in the activities at the Satellite Control Center in Sunnyvale California. The release commands were given from here. Some of

Figure 1. CRRES release from Arecibo Puerto Rico.

R&DD

CRRES OBSERVATIONS FROM PUERTO RICO

Lockheed

10.8 kg OF BARIUM RELEASED AT 33,000 km ALTITUDE AT 05:30 UT

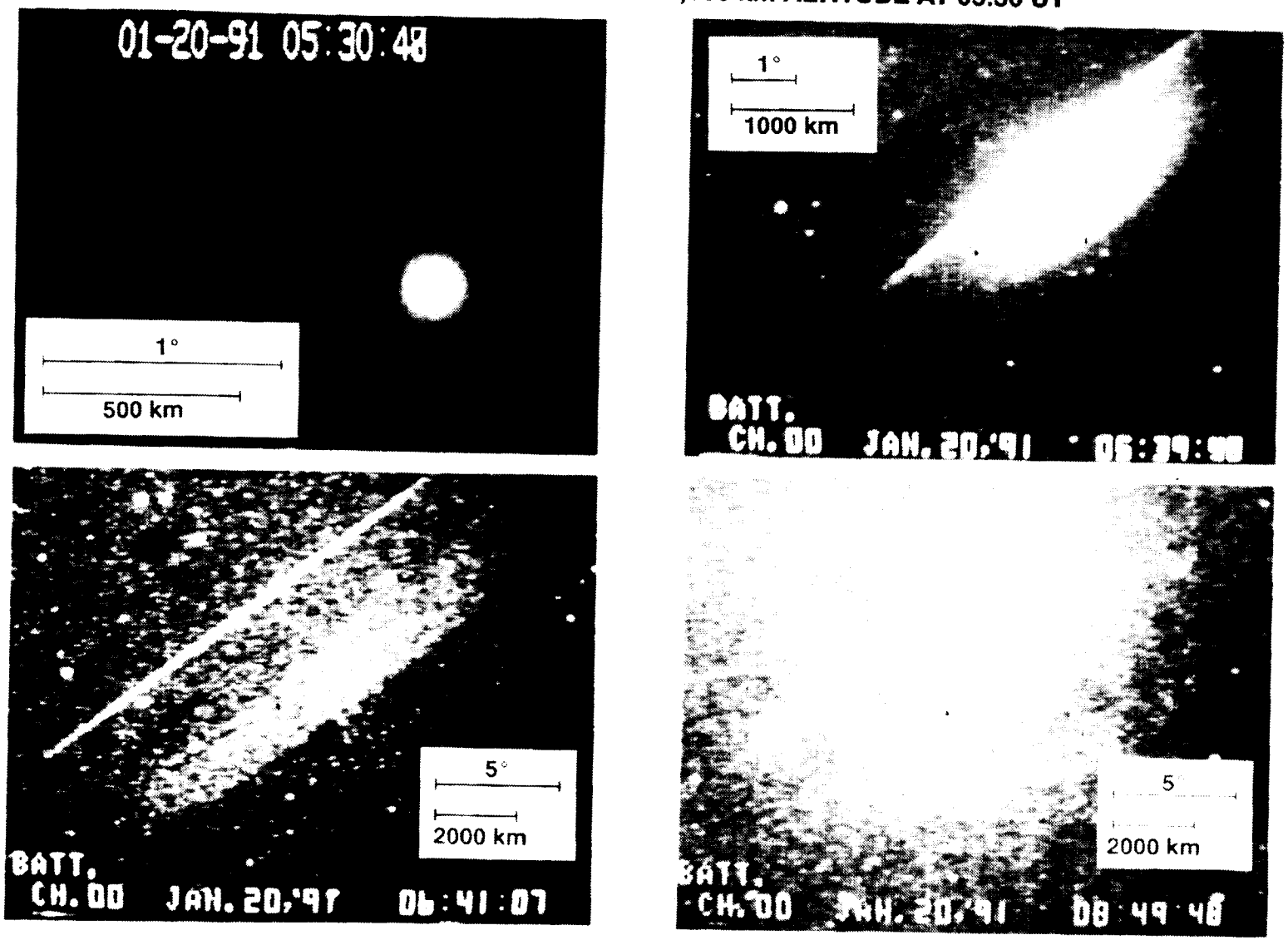

the high altitude releases had very complex release conditions. In addition to weather conditions at the optical sites the situation regarding the magnetic activity in the magnetosphere had to be taken into account.

For observation of the auroras at the end of the field line there were two instrumented aircrafts. On one of these aircrafts we have installed a low light level auroral camera. This camera was operated to support the entire high altitude campaign.

The CRRES Lithium releases were intended as cold plasma seeding experiments. It was proposed several years ago that when cold plasma was injected into a population of stably trapped energetic particles, waves would be produced which would perturb the trapped particles. The particles would precipitate, and the precipitation would be observable optically because of the aurora produced. The experiment was intended to test the cold plasma induced wave particle precipitation hypothesis. To conduct a successful experiment it was realized that very low ambient cold plasma density were needed at the satellite so that the plasma injection would represent a significant increase in the local ambient cold plasma. This generated a requirement of low quiescent ambient cold plasma density. The University of Iowa plasma wave instrument on CRRES satellite provided the monitoring capability of the cold plasma density at the satellite. Arrangements were made so that display capability was available for cold plasma monitoring at the Satellite Test Center. Dr. Roger Anderson, the PI on the Iowa experiment, was assisting in the monitoring activity.

Another important parameter was the intensity of the trapped energetic protons and electrons. There were two instruments which monitored energetic particles. One of them was the U. S. Air Force Phillips Laboratory experiment on the satellite with principal investigator Dr. Dave Hardy. The other hot particle experiment was operated by our colleagues at the Lockheed Palo Alto Research laboratories. Both of these experiments had adequate sensitivity to see particles in the intensity range of faint auroras. Both experiments were supported by the PI institutions during the entire high altitude release campaign.

The Lockheed team was at the Satellite Test Center during operation periods of the winter campaign and acted in a capacity of coordinating requirements and directing the releases.

Another set of high altitude releases G2, G3, and G4 were intended to compare the behavior of small barium clouds in the varying environment of different regions of the magnetosphere from low altitude, to regions just within the plasmapause, to regions just outside of the plasma pause. Thus the three small barium clouds were placed at three different geocentric distances. G2 and G3 releases were performed as planned. Observations were made from a number of observation sites. The weather permitted the observation at more than the minimum number of sites required for triangulation. The last release in this series was G4 which had to be released just outside the plasma pause. We followed the technique of measuring the position of the plasma pause on the inbound part of the orbit and used that data to predict the release time. The release command needed to be given about 30 minutes before actual release to permit the separation of the ejected canister from the main body of the satellite. Unfortunately, this delay ruled out the direct use of the instantaneous in situ measurements and invariably we needed to predict from the data taken during the prior orbit. In general it was found that prediction from orbit to orbit gave fairly reliable results. In the case of the G4 cloud, however, the technique of predicting let us down and the G4 cloud was released exactly on the plasmapause and not outside of it as it had been intended.

The G2, G3, and G4 clouds were tracked by several observing stations. The data was collected and the G2 and G4 cloud positions were triangulated by our team. The G3 cloud was triangulated by Mary Miller of Goddard Spaceflight Center. The cloud motions were determined and the cloud motion was related to parameters of the ambient environment. Fuselier et al., 1994 (pre-print enclosed).

During a prior program, the Active Magnetospheric Particle Tracing Experiment (AMPTE), while performing a release experiment in the geomagnetic tail we detected a sudden change in the external magnetic field at the cloud (Mende et al., 1989) and it was suggested that the plasma cloud might have induced a small substorm. It was thought that testing the validity of this suggestion would have significant impact on the understanding of magnetospheric substorms and would be of high scientific priority. In the latter phases of mission planning it was therefore decided to use two of the large canister barium releases to try to induce a substorm in a manner similar to the AMPTE tail release. G10 and G8 were reserved for such barium releases and they were performed in the magnetospheric tail. Both releases seemingly created some effect in the aurora which was monitored by aircraft borne instruments near the foot of the magnetic field line. Directly following the performance of the experiment, it was thought that the auroral disturbance was related to the release and the experiment was successful. However, during the months following the experiments we have scrutinized the data and found that the location and timing of the auroral disturbance was not consistent with the view that there was connection between the releases and the aurora.

The G-5, G-6, and G-7 investigations all involved release of two large canisters near (+/- 1.5 hours) local midnight at high altitude (r/Re > 5.5). The objective of the G-7 release was the direct observation of released lithium by in-situ ion mass spectrometers to provide new insight into ion transport and acceleration processes acting in the magnetosphere. The primary objective of the G-5 release was to see if the increase in local plasma density associated with the release would create an artificial aurora as predicted by Kennel and Petschek (1966). The primary objective of the G-6 release was to see if the increase in local plasma density associated with the release would create ion cyclotron waves that caused ion precipitation as predicted also by Kennel and Petschek (1966).

There were extensive optical observing (including aircraft) and geophysical condition restraints on the G-5 and G-6 releases. The physical constraints the G-5 and G-6 releases required CRRES apogee to be over eastern North America, and that there be indications from real time monitors of geophysical conditions that the particle energy density near synchronous orbit was increasing. The physical, as opposed to the geophysical, constraints on the G-5 and G-6 release allowed for approximately one release opportunity every two days for about 12 days in January and February of 1991. Obviously there were only a few selected time intervals where the relative positions of the DE-1, Akebono, and CRRES satellites were suitable for the G-7 release. Because the geophysical condition constraints on the G-5 and G-6 releases were so restrictive, it was decided to field the aircraft and ground observers and prepare for a release at each opportunity.

We used software developed especially for the CRRES program to determine the relative positions of the DE -1, CRRES, and Akebono satellites during each of the release opportunities for the G-5 and G-6 experiment. It was found that the position of the DE -1 spacecraft was most acceptable for the release opportunity on January 13, 1991. Acceptable release windows for the G-7 experiment were also identified in February and on January 15, 1991. The January 15 release required operations of the CRRES spacecraft for an extended period of time in the Earth's shadow. On January 11 and 12, in consultations with the Project Scientist, Dr. David Reasoner, Ball Aerospace personnel and a representative of Phillips Laboratory, it was decided the risks to the spacecraft associated

with the January 15 release were too high and it was eliminated from consideration. The February release opportunities were also ruled out because, at the time, the project wanted to complete all releases in January to avoid the expense of a February field campaign. The January 13 release for the G7 release was also favored because of concern over the continued operation of the DE -1 spacecraft. It was decided that the G-7 release would be made on January 13 independent of the geophysical or observing conditions.

The G-7 release was made at 07:05 universal time when CRRES was just past apogee and moving toward the dawn side of the magnetosphere. The natural motion of the magnetic field line transports cold ions dawnward toward the plane of the DE -1 orbit. DE -1 crossed the invariant latitude of the release (67.7 degrees) at 09:40 UT. The photo ionization time for lithium is on the order of 1 hour. During the hour required for the bulk of the lithium to photo ionize, the cloud of neutral lithium expands across and along magnetic field lines. Once photo ionized, lithium ions move along magnetic field lines. At the time of the release the CRESS satellite was at an altitude of ~33,000 km. Depending on the additional energy acquired from plasma wave heating or other acceleration processes lithium ions could have reached the location of DE -1 from ~08:40 when DE -1 was at 62.5 degrees invariant latitude and ~20,000 km altitude to ~ 10:40 (72 degrees invariant latitude and ~22,000 km altitude). Data was acquired on DE -1 during this interval in a special mode designed to maximize the sensitivity for detecting $^7Li^+$.

It was not possible to recover the data acquired on January 13 from the tape recorder on DE -1. The DE -1 satellite was near the end of its life. A special mode, designed to maximize the sensitivity of the SMS instrument to lithium ions was developed and up-linked to the Akebono satellite. However, no useful data were acquired by the Akebono satellite in support of the G-7 release. The on board RAM memory chip in the SMS instrument on Akebono experienced an upset event on January 10, shortly after the regularly scheduled RAM check procedure. The problem with SMS operations was not recognized until January 16 shortly after the next scheduled RAM check. The limited instrument health and safety monitoring is integral to the operation of the Akebono satellite. The Japanese do not rely on professional operators for scientific satellites. They use members of the various instrumental teams to command and control the satellite. They accept the inevitable loss of data associated with the reduced operating costs. Useful Akebono data were also not acquired on January 18 in support of the G-5 lithium release. Normal operations had not yet been re-established after the identification of the SMS instrument RAM problem noted above.

In summary, no lithium was detected from the DE -1 or Akebono space based ion mass spectrometers from the G-5, G-6, and G-7 releases. The lack of detection was the result of problems associated with satellite systems at the end of their useful life (Dynamics Explorer) and operational limitations associated with the low cost satellite operations and telemetry acquisition systems used by the Japanese (Akebono). To be fair to the Japanese, it must be pointed out that the probability of detection of lithium ions in the dusk side magnetosphere was minimal at best. For lithium ions to drift duskward after the release, they would have had to acquire energies of several keV. For this reason we did not request special, extra cost, operations and data acquisition in support of the CRRES chemical releases from the Akebono operators.

2.2 Other Coordinated High Altitude Campaign Observations:

In the course of obtaining the data from the various CRRES releases, particularly those that required specific geophysical conditions, a large body of coordinated observations were obtained from the then active suite of space and ground based instruments designed to

monitor aspects of the magnetosphere, ionosphere system. The software we developed to identify the best times for chemical releases was used after the releases to identify times during which extensive satellite data were acquired, and when the satellites were sampling nearly contiguous magnetic field lines. One such event, on February 18, 1991, was particularly interesting. The magnetosphere was quiet at this time and had been quiet (Kp * 1^+) for more than 24 hours. This provided an opportunity to characterize the quiet aurora zone and polar cap plasmas. We assembled the data and presented them as a poster paper at the 1991 Fall Meeting of the American Geophysical Union (Persoon et al., 1991).

During the January and February 1991 campaign, the magnetospheric conditions were monitored in real time prior to release in an attempt to predict conditions for each release. Data acquired in addition to those on the CRRES spacecraft were from the extensive array of ground and aircraft optical sites as well as the Millstone Hill Radar facility. Mende et al. (1991) have pointed out that during the campaigns excellent sets of data were gathered which characterized the aurora, the simultaneous particle and field measurement at the satellite and the accompanying convection in the ionosphere during various conditions. The times over which these data were acquired are given in Table 1, below.

Table 1. OBSERVATION PERIODS during which Extensive GEOPHYSICAL DATA were COLLECTED.

Day	Observation Interval		Release Times
Jan 13, 1991	0534 - 0827	G-2 G-7	02:17:00 07:05:00
Jan 15, 1991	0536 - 0954	G-3	04:11:00
Jan 16, 1991	0500 - 0730	G-4	06:25:00
Jan 18, 1991	0225 - 0700	G-5	05:20:00
Jan 20, 1991	0304 - 0811	G-10	05:30:00
Jan 22, 1991	0524 - 0843		none
Feb 10, 1991	2350 (2/9/91) - 0600		none
Feb 12, 1991	305 - 0505	G-6	04:15:00
Feb 14, 1991	243 - 0730		none
Feb 17, 1991	0009 - 0500	G-8	03:30:00

2.3 Perigee Caribbean Campaign (Summer 1991)

As stated earlier barium releases which were performed at perigee had the property that the ions inherited the velocity of the satellite at the time of injection. This velocity which is about 8 km/sec allows the ions to escape along the magnetic field and in favorable situations travel to the opposite hemisphere. A series of experiments wee carried out which had this as a technological goal. In addition these experiments permitted the investigation of the interaction of the fast ions with the ambient atmosphere. Our objective was to study the processes associated with the momentum dissipation of fast ions in the ionosphere.

The Lockheed group fielded a special air borne Fabry Perot Imager. The Fabry Perot allows the detection of the Doppler velocity distribution of the barium ions. The airborne instrument was installed on an air force operated KC-135 airplane. The instrument was used to observe the barium clouds and obtained high wavelength resolution interferograms. The results are discussed in a paper attached as Appendix B to this report (Rairden et al., 1994)

3.0 Conclusions

The CRRES high latitude releases did accomplish the mission goal of experimentally testing various active techniques to induce auroral precipitation. The effectiveness of these techniques to produce the precipitation has not been proven. When the lithium releases took place the geophysical conditions were relatively disturbed and even if some precipitation enhancement had taken place it would have been impossible to detect. At the time when the canister was ejected prior to the release the conditions during G5 and G6 were excellent. However during the half hour between canister ejection and cloud release the situation deteriorated. In order to perform this experiment and increase the probability of success it would be essential to reduce the delay between canister ejection and release.

The small barium releases G2, G3, and G4 , worked extremely well. The data was triangulated, analyzed and the paper is attached as appendix A of this report.

During the Caribbean campaign our group flew an imaging Doppler Fabry-Perot interferometer on an aircraft. Data was taken to study the interaction of the fast ions with the atmosphere. These experiments were successful and showed that there are other complex interactions are involved in addition to just plain classical ion neutral collisions. These experiments are described by Rairden et al., 1994 (Pre-print enclosed).

Another unexpected benefit of the CRRES optical and space based observations are the extensive coordinated data sets obtained. In particular the data from February 18, 1991 are perhaps the most extensive data set yet acquired during an extended period of geophysically quiet conditions. Prolonged intervals of quiet geomagnetic conditions are relatively rare. These intervals are generally ignored in the particle and field literature, because of the lack of distinctive plasma signatures. Nevertheless the plasma conditions that obtain during periods of prolonged magnetic quiet conditions are important because they represent as close to a base level magnetosphere as will ever be observed.

4.0 Acknowledgments

Dr. David Reasoner was the very effective NASA project scientist of the CRRES Chemical Release Team. His insight and efforts in organizing the diverse group of investigators involved in the chemical releases is largely responsible for the success of the CRRES Chemical release investigations.

5.0 References

Kennel, C.F., and H.E. Petschek, Limit on stably trapped particle fluxes, J. Geophys. Res. 71, 1, 1966.

Mende, S.B. G.R. Swenson, S.P. Geller, J.H. Doolittle, G. Haerendel, A. Valenzuela, and O.H. Bauer, Dynamics of a barium release in the magnetospheric tail, J. Geophys. Res 94, 17063, 1989.

Mende, S.B., H.L. Collin, W.K. Peterson, T.A. Fritz, G. Haerendel, R.R. Anderson, D.A. Hardy, H.J. Singer, J.C. Foster, and D.L. Reasoner, Real time monitoring of the geophysical parameters in support of the CRRES chemical releases, (Abstract) EOS, Trans. Am. Geophys. U. 72, No. 17, p. 230, 1991.

Persoon, A.M., R.R. Anderson, W.K. Peterson, H.L. Collin, R.M. Robinson, H.J. Singer, K. Kerns, D.A. Hardy, W.F. Denig, N.C. Maynard, J.R. Wygant, J.A. Slavin, C.J. Pollock, and T.E. Moore, Observations of a quiet magnetosphere and polar cap by CRRES, DE -1, and DMSP, (Abstract) EOS, Trans. Am. Geophys. U. 72, No. 44, p. 413, 1991.

APPENDIX A

Dynamics of the CRRES Barium Release in the Magnetosphere

by Fuselier S. A.,
S.B. Mende, S.G. Geller, M. Miller, R.A. Hoffman. J.R. Wygant, M. Pongratz,
N.P. Meredith,
and
R.R. Anderson

Paper to be submitted to J. Geophys Res., 1994

DYNAMICS OF THE CRRES BARIUM RELEASES IN THE MAGNETOSPHERE

S. A. Fuselier, S. B. Mende, S. G. Geller
Lockheed Palo Alto Research Laboratory
Palo Alto, CA 94304

M. Miller, R. A. Hoffman
Goddard Space Flight Center
Greenbelt, MD 20771

J. R. Wygant
Space Sciences Laboratory
University of California
Berkeley, CA 94720

M. Pongratz
SST-7, Los Alamos National Laboratory
Los Alamos, NM 87545

N. P. Meredith
Atmospheric Physics Lab
University College London
W1P 7PP London, England

and

R. R. Anderson
Department of Physics and Astronomy, University of Iowa
Iowa City, IA 52242

23 December 1993

Abstract

The Combined Release and Radiation Effects Satellite (CRRES) G-2, G-3, and G-4 ionized and neutral barium cloud positions are triangulated from ground based optical data. From the time history of the ionized cloud motion perpendicular to the magnetic

field, the late time coupling of the ionized cloud with the collisionless ambient plasma in the magnetosphere is investigated for each of the releases. The coupling of the ionized clouds with the ambient medium is qualitatively consistent with predictions from theory in that the coupling time increases with increasing distance from the Earth. Quantitative comparison with simple theory for the coupling time also yields reasonable agreement. Other effects not predicted by the theory are discussed in the context of the observations.

1. Introduction

Chemical releases in the ionosphere and magnetosphere are a type of active experiment that is designed to probe the ambient plasma and elucidate the interactions between newly created plasma and the ambient medium. In early January 1991, a series of barium releases by the Combined Release and Radiation Effects Satellite (CRRES) were performed at different altitudes. Each release in the series (identified as G-2, G-3, and G-4) contained identical amounts of barium (1.7 kg) and were done under similar quiet magnetospheric conditions (e.g., Kp$\sim$3- for G-3). The objectives of the releases were to study diamagnetic cavity formation, unstable velocity distributions, and coupling of the ionized cloud to the ambient plasma. Table 1 shows the dates, times, geographic coordinates, and altitudes of the three releases.

Several ground stations participated in the release campaign. Stations in both North and South America tracked the barium clouds sometimes for periods of over an hour using image intensified cameras. Individual ground stations were used in a preliminary study comparing the early time (<1-2 min) behavior of the barium clouds [*Huba et al.*, 1992] and in a study concentrating on the early time behavior of the G-2 release closest to the Earth [*Bernhardt et al.*, 1993].

The early time behavior of a release at the distances of the G-2, -3, and -4 releases is dominated by the formation and collapse of a diamagnetic cavity. This cavity forms because a current loop at the edge of the cloud created by the newly ionized barium ions and cold electrons on the surface of the cloud cancels the magnetic field inside the cloud. The maximum size of the cavity is attained when the kinetic energy of the release roughly equals the magnetic energy swept up by the expansion of the cloud [*Huba et al.*, 1992]. Diamagnetic cavities were observed for all three releases in Table 1 [*Singer et al.*, 1991; *Bernhardt*, 1992]. However, the cavity that is formed is unstable to several possible plasma instabilities and the cloud will structure and collapse on a time scale of seconds when it is still quite dense [*Huba et al.*, 1992]. After this time, the ambient magnetic field penetrates the cloud and the barium ions striate along this field.

Later time behavior of the ionized barium cloud depends on the size of the perturbation in the ambient medium. For large releases far from the Earth, the cloud acts like a large inertial object. It striates along the magnetic field but continues to move in the direction of the spacecraft motion at the time of the release, dragging the imbedded ambient field with it [e.g., *Mende*, 1973]. For smaller releases closer to the Earth, the

cloud represents a small perturbation in the ambient medium and is expected to rapidly couple to the ambient plasma motion. Theoretical study of this later time coupling of the cloud to the ambient medium suggests a relatively simple interpretation [e.g., *Scholer,* 1970]. The motional electric field of the cloud created by the differential motion between it and the ambient medium is transferred along the magnetic field as an Alfven wave at the local Alfven velocity. The cloud couples to the ambient plasma when this disturbance has swept up a volume of plasma along the flux tube that has a mass equal to the mass of the ionized cloud. After this time, the cloud should have approximately the same velocity as the ambient plasma perpendicular to the ambient magnetic field but will continue to striate along the magnetic field.

The determination of the late time coupling for the CRRES releases requires combining ground station data using triangulation procedures to determine the cloud position in space as a function of time. In this paper, triangulation results from the three releases in Table 1 are presented. From these results, the motions of the clouds are determined and compared to the simple theory of the later time coupling of the clouds to the ambient plasma outlined above. Section 2 of this paper contains a description and examples of the triangulation procedure. Section 3 contains a discussion of the verification of the triangulation results and the uncertainties in the procedure. Section 4 contains the determination of the cloud motion from the triangulated positions and a comparison of the three releases. Section 5 contains a discussion of the observational results and a comparison of these results with theory. Section 6 contains the conclusions.

Triangulation Data and Procedure

Although a large number of ground stations participated in the release campaign, ground station pairs that had large east-west baselines were better suited for the purposes of this paper (see below). An example of the G-2 release data from such a pair of stations is shown in Figure 1. This example will serve to illustrate the triangulation procedure used in this study. The procedure is semi-automated in that several computer programs do most of the computations but key decisions are left to the operator. It is similar to the procedure employed to triangulate one of the AMPTE magnetospheric tail releases [*Mende et al.*, 1989].

The top left-hand panel of Figure 1 shows data from Rosemary Hills, FL (Lat. 29.4 N, Long. 82.5 W) approximately one minute after the G-2 release. These data were acquired from an image intensified CCD camera with a field of view of 10° although the

full field of view is not shown in Figure 1. Bright stars in the image are approximately 5th magnitude. The orientation of the magnetic field line, the location and direction of motion of the spacecraft at the time of the release as seen from the Rosemary Hills location are shown in the upper right-hand panel of Figure 1. The full field of view of the camera is shown by the dashed box in that panel. The large, asymmetric, and bright circle in the upper left hand panel of Figure 1 is the expanding neutral barium cloud. At the time of observation, the CRRES spacecraft (large square) was still located in the expanding cloud and both were moving ~6 km/s primarily in the direction of increasing elevation as shown in the upper right-hand panel. The thin line marked at one point by the cross is the ionized barium cloud striating along the ambient magnetic field near the release point. In subsequent images, the neutral cloud expanded, continued to separate from the ionized cloud, became fainter, and was lost from view approximately 2 min after release. In contrast, the ionized cloud continued to striate along the field and was tracked for over 10 min after the release.

The bottom left-hand panel of Figure 1 shows data from Los Alamos (Breezy Point), NM (Lat. 35.8 N, Long. 106.2 W) at the same time as the Rosemary Hills image in the top panel. These data were also from an image intensified CCD camera with a field of view of 4.5° although again, the full field of view is not shown. Stars in the image (for example near the line in the image) are 8th-9th magnitude. Similar to the image from Rosemary Hills, the Los Alamos image in the lower panel also shows the neutral cloud well separated from the ionized cloud that is striating along the magnetic field. Due to the aspect angle of the observations from Los Alamos (see the lower right-hand panel), the neutral cloud appears to be offset from the ionized cloud mainly in the azimuthal direction.

Image pairs from both ground stations were digitized from the original data for as many nearly simultaneous observations as possible after the initial release time. In the first part of the triangulation procedure, the star fields in each image pair are identified using standard star charts. The right ascension and declination of the stars in the field of view are placed in a computer file and the pixel locations in the image are identified for two stars which act as reference stars. The star field is then plotted on the image to verify the location of other stars and the aspect ratio of the plotted star field is adjusted to fine tune the fit. The reference stars are then used to linearly interpolate pixel location on the image to right ascension and declination in the sky for the second part of the triangulation procedure.

To triangulate the ionized part of the cloud that is striating along the magnetic field, a point at the center of the striation such as the one shown by the cross in the top left-hand image in Figure 1 is selected. Then, using an estimate for the distance of the ionized cloud from the Earth (based on the release distance), the computer draws a line segment 0.2 R_E long on the image acquired at the second site that corresponds to the line of sight in the direction of the point chosen on the first image. The center of the line segment is the estimated distance of the ionized cloud. Continuing with the example, this line is shown in the bottom left-hand panel of Figure 1. If the estimate of the distance from the Earth to the cloud is good, then the line should cross the striated cloud in the second image as illustrated in Figure 1. By selecting the position where the line crosses the center of the striation in the second image, the triangulated position for a point in the striated cloud is obtained. This procedure is repeated to determine other positions along the striated cloud. The entire procedure, including redefining the reference stars, is repeated for other image pairs from the releases. The end product of the triangulation procedure is a set of points (in Geographic coordinates) along the center of the ionized cloud for each image pair. This set should be the locus of points along a magnetic field line in geographic coordinates. For the G-2 release, it was also possible to triangulate the neutral cloud position and size for approximately the first two minutes after the release (see Figure 1).

Since the cloud striates along the magnetic field which is approximately north-south, large east-west baselines are preferred for the triangulation. For these baselines, the line of sight direction for the first image is nearly perpendicular to the ionized cloud in the second image as illustrated in Figure 1. For north-south baselines, the line of sight direction would be nearly parallel to the cloud and the triangulation would be difficult [e.g., *Mende et al.*, 1989].

Uncertainties in the triangulation procedure increase with increasing altitude of the release. Choosing station pairs with larger baselines partially compensates for this effect but the almost 3 R_E difference between the G-2 and G-4 release distances (see Table 1) is too big to be fully compensated by the available baselines. To illustrate this, Figure 2 shows an image pair from the G-4 release. The format is the same as in Figure 1, with the left hand panels showing the observations and the right hand panels showing the location of the magnetic field line and spacecraft as viewed from the observing site. The upper panel shows an image taken approximately 6.5 min after the release by an image intensified CCD camera at Arecibo, PR (Lat. 18.34 N, Long. 66.75 W). The corresponding image from

Los Alamos (Breezy Point) is shown in the lower panel. The same triangulation procedure discussed above was used on this image pair to produce the selected point shown by the cross in the upper panel and the corresponding 0.2 R_E line shown in the lower panel. Despite the larger baseline used in the G-4 triangulation, it is clear from comparison of the line segments in the images in the lower panels of Figure 1 and 2 that the uncertainty in the triangulated cloud location for G-4 will be considerably larger than that for G-2.

Also, uncertainties in the triangulated points from a release will be largest in the radial direction from the Earth independent of the baseline used. This is because positions in the planes of the images (perpendicular to the radial direction) are much more accurately determined than positions perpendicular to that plane. This will have additional effects on the results (discussed below).

Verification of the Triangulation Procedure

There are several ways to verify the accuracy of the triangulation results. In this section only two of these ways are considered. Further checks that concern the details of the interaction of the ambient plasma with the cloud will be discussed in the next section.

The first obvious verification of the triangulation results is to compare the triangulated position of the cloud at (or soon after) the release with the known location of the CRRES spacecraft. This single point comparison provides a measure of the absolute uncertainty (or offset) in the triangulated position of the cloud. For the G-2 release (closest to the Earth), the triangulated position of the cloud at the release time and the spacecraft position were indistinguishable, indicating an absolute error of less than 30 km (the limit of the resolution of the G-2 images). The differences in the triangulated and spacecraft positions for G-3 and G-4 were approximately 70 km. These larger absolute errors reflect the greater distance of the releases from the Earth when compared to that for the G-2 release.

The second verification is to use the well known fact that the ionized cloud will striate along the magnetic field after the rapid collapse of the diamagnetic cavity [e.g., *Mende*, 1973]. Unlike releases in the magnetotail where the model magnetic field is somewhat uncertain and the release is used at least partially to identify the magnetic field [e.g., *Mende et al.*, 1989], the G-2, G-3, and G-4 releases were sufficiently near the Earth and were done under sufficiently quiet conditions to have confidence in the model magnetic field. Therefore, an additional test of the data that provides some information on the relative uncertainty in the measured points of the cloud is to compare the model magnetic

field with a least squares fit through the triangulated points from an image pair. Table 2 shows the results of this comparison for all triangulated data in this study.

For each release in this table, the left hand columns show the time in UT and the right hand column shows the angle between the model magnetic field (from the CRRES spacecraft ephemeris) and the least squares fit line through the triangulated points for that time. The angle can be relatively large (see for example the angle at 062557 UT for G-4) soon after the release because the line segment is short and the direction inferred from this segment has a large uncertainty. Angles for the last times listed (for example 022703 UT for G-2) can be also relatively large because the ion cloud becomes faint and difficult to triangulate. However, for most times, Table 2 shows that the direction of the magnetic field inferred from the triangulation results agrees quite well with the model magnetic field direction. On average, the discrepancy is largest for the G-4 release. This is likely a combination of the decreasing accuracy of the model field and, more importantly, the greater distance for the G-4 release from the Earth, resulting in larger statistical errors in the triangulation. Even for this release, the average difference between the model field and the triangulated field is less than 10°. This provides confidence that the triangulation procedure is reasonably accurate.

Cloud Motion

The later time barium cloud motion can be separated into striation along the ambient magnetic field and motion of the flux tube perpendicular to the ambient magnetic field direction. Determining the changes in the cloud size along the magnetic field has several observational problems. First, the the cameras used to image the releases had relatively small fields of view. In the bottom left-hand panel of Figure 1, it is clear that the entire ionized cloud along the magnetic field is not within the field of view of the camera. This problem becomes particularly acute at later times when the cloud subtends an angle of many degrees in the sky. Ground observers were instructed to track one end of the cloud after the cloud moved out of the field of view. Triangulation of only the part of the cloud that was tracked produces an apparent motion along the field with time. A second problem with the observations is that the image intensity is not calibrated for the cameras used in this study. Therefore, the apparent length of the cloud even at early times is a function of the (uncalibrated) images from different sites.

Because of these observational problems, we deconvolve the motion along and perpendicular to the ambient magnetic field direction and concentrate only on the latter motion.

In terms of the late time coupling of the cloud to the ambient plasma, the latter motion is more important since the barium ions are essentially free to move along the magnetic field.

The deconvolution is accomplished by rotating the coordinate system from the original geographic coordinates to a system where the magnetic field direction (defined by the least squares fit through the triangulated data) is along the z-axis. An additional rotation is also made so that the y-axis is along the direction of the component of the spacecraft velocity (at release) that is perpendicular to the magnetic field (after the co-rotational velocity is accounted for). The x-axis completes the right-handed coordinate system. Finally, this coordinate system is translated so that the origin is at the spacecraft location at the release time. It is important to note that this coordinate system is non-inertial because the original geographic coordinate system is co-rotating with the Earth. Thus, the coordinate rotation must be done for the triangulated data from each image pair separately.

For each image pair in a release, the triangulated points along the magnetic field are projected into the x-y plane of this new coordinate system. Motion of the flux tube perpendicular to the magnetic field is then determined by the change in position of the clusters of points in the x-y plane as a function of time.

These projected points for the G-2, G-3, and G-4 releases are shown in Figures 3, 4, and 5, respectively. The component of the spacecraft velocity perpendicular to the magnetic field at the time of release (in units of 0.01 R_E = 1 km/s) is shown in the figures by the arrow along the y-axis. Short arrows in the figures show the radial direction from the Earth. The G-2 and G-3 releases occurred on the outbound part of the CRRES orbit so that the radial direction and spacecraft velocity are in similar directions. The G-4 release occurred on the inbound part of the CRRES orbit so that the radial direction and the spacecraft velocity are in nearly opposite directions. The corotation direction is perpendicular to the radial direction. In the G-2 and G-4 releases, the corotation direction was nearly in the X direction in Figures 3 and 5. However, for the G-3 release, the corotation direction has a substantial component in the y direction in Figure 4.

For the G-2 release, it was possible to triangulate the center and outer radius of the neutral cloud for approximately the first 2 minutes. In the last image pair at 021903, the center of the neutral cloud was not in the field of view of the camera at one of the observing sites and had to be estimated from the curvature of the part of the outer radius of the neutral cloud in the field of view. The velocity of the neutral cloud is expected

to be that of the spacecraft velocity at the release time. Figure 3 shows that the G-2 neutral cloud moved approximately in the +y direction in agreement with expectations. (The magnitude of the cloud velocity is discussed below.) The cloud also expanded with an expansion velocity of about 1.6 km/s. This velocity is somewhat higher but similar to previous estimates of the neutral cloud expansion [e.g., *Bernhardt et al.*, 1993]. The ionized cloud motion is in stark contrast to this neutral cloud motion and expansion. The ionized cloud initially moved approximately in the direction of the spacecraft velocity vector for a distance of ~0.01 R_E from the release point and then stopped for the rest of the approximately 11 minutes of observations. Evidence of the separation of the neutral cloud and the ionized cloud one minute after the release can be seen in Figure 1. Because the coordinate system is co-rotating with the Earth, Figure 3 actually shows that after the first minute, the ionized cloud acquired the co-rotational velocity of the ambient plasma but the neutral cloud moved with the spacecraft velocity and direction as if there were no co-rotational forces on it.

For the G-3 release, only the ionized cloud could be tracked. Its motion perpendicular to the magnetic field in the co-rotating frame is shown in Figure 4. One of the obvious features of the "clusters" of triangulated points that are projected into the x-y plane in Figure 4 is that they line up along the radial direction from the Earth. If the statistical uncertainty in the triangulated position was the same in all directions, then the projected points would form a true cluster around the least squares position of the magnetic field in the Figure. However, the uncertainty is not the same in all directions. As discussed above, the uncertainty in the radial direction is larger. Therefore, the points that form short line segments for each time period show the uncertainty in the radial direction is on the order of 0.01 R_E but it is much smaller perpendicular to that direction. The G-3 ion cloud motion is significantly different from that for G-2. Because the motion is complicated, the dashed line connecting the centers of each group of points shows the motion of the average position of the cloud with time. Considering the motion in the y direction first, Figure 4 shows that the G-3 cloud moved approximately along the spacecraft velocity vector for the first 1.5 min and then reversed its motion. It then moved in the -y direction for approximately another 2.5 min before stopping its y motion for the rest of the observing time.

The motion in the x direction for the G-3 release is unique to the three releases. The motion is nearly uniform after the first minute because the distance covered is approximately constant as is the time between observations (with the exception of a data gap

between 0416 and 0419 UT). The velocity computed from the change in x position with time is approximately equal and opposite the co-rotation velocity of the plasma at the G-3 distance, indicating that the cloud was stationary with respect to the rotating Earth.

Like the G-3 release, only the ionized cloud could be tracked for G-4. However its motion was much less complicated when compared to that of the G-3 release. The G-4 motion perpendicular to the magnetic field is shown in Figure 5. The motion is relatively simple in that the cloud initially moved away from the release point along the spacecraft velocity vector direction (also the radial direction) for over 5 minutes after release and then slowed its y motion for the duration of the observation period. The offset of the motion in the x direction reflects the 0.01 R_E offset in the triangulated and actual release positions. No motion in the x direction for the entire period indicates that the ionized cloud was co-rotating with the Earth throughout. Triangulation beyond 8 min after the release was not possible because the cloud became too faint at one of the observation sites to be reliably tracked.

Using consecutive triangulated y positions and the time between them, the y velocity of the cloud as a function of time for the three releases was computed. These velocity profiles are shown in Figure 6. The dashed line in each panel shows the component of the spacecraft velocity perpendicular to the magnetic field at the time of the release. Error bars on the velocity measurements of the ionized clouds are computed from the uncertainty in the triangulated y position and are based on the scatter of the points for an individual triangulated position in Figures 3, 4, and 5. These error bars are smaller than the symbol size for the G-2 release but increase significantly with increasing release distance from the Earth. Since the errors are computed using the statistical uncertainty in the location, if only one point is triangulated, (for example near the beginning of the release), then the uncertainties in Figure 6 do not fully represent the actual uncertainty in the measurements. This is apparently the problem with the initial measurements of the G-3 and G-4 releases, which indicate very low initial velocities.

For the G-2 release, the neutral cloud center could be triangulated reasonably accurately except for the last point at 120 s after the release. For this point, the uncertainty in the position may be larger than shown because the cloud was dissipating rapidly and the center had to be estimated from the curvature of the cloud in the field of view. Thus, the apparent acceleration of the neutral cloud at 120 s is probably not real. In general, the neutral cloud moved away from the release point with the spacecraft velocity, in agreement

with expectations. This provides additional confidence in the triangulation procedure. Also for the G-2 release, it is apparent that even with the first velocity measurement one minute after the release, the ionized cloud had slowed considerably. The velocity rapidly decays to zero and remains close to that value for the duration of the observations.

The G-3 ionized cloud velocity profile is considerably different from that of the G-2 release. The first velocity point is somewhat below the spacecraft velocity; however, the basic trend is a positive velocity until 100 s after the release, then the velocity passes through zero and stays negative until 300 s after the release at which time the velocity returns to zero for the duration of the observations. The velocities for the last three points are somewhat suspect because the cloud was beginning to dissipate and move out of the field of view of the camera at one of the observing locations.

For the G-4 release, the velocity appears to be higher than the spacecraft velocity at the release time. We do not have a physical interpretation for the higher velocity. However, the y velocity is almost entirely along the radial direction (Figure 5), where the uncertainties in the position are the largest. It is possible that the error bars which are based only on the standard deviation of the y positions for adjacent times may not fully represent uncertainties in the positions in this case. This apparent higher velocity notwithstanding, the trend in the G-4 release is similar to the early time trends in the other releases. The release initially moves away with nearly constant velocity and then stops after approximately 300 s.

Discussion

The time required for a release to acquire the ambient plasma motion is proportional to the size of the perturbation on ambient medium. Since identical amounts of chemical were used in the G-2, G-3, and G-4 releases, the size of the perturbation depends only on the ambient plasma conditions, primarily the ambient density. Qualitatively, the density decreases with decreasing distance from the Earth so the time needed to acquire the ambient plasma motion (in these cases zero velocity in the y direction perpendicular to the magnetic field and perpendicular to the co-rotating direction) should increase for G-2 through G-4. The observations in Figure 6 are consistent with this expectation. The vertical dashed lines show where the ionized cloud velocity is 1/e of its initial velocity. These velocity decay times increase with increasing distance from the Earth. For the G-2 release, the decay time was estimated by assuming that the velocity decreased linearly with time from the spacecraft velocity to the first observed velocity. For the G-3 and G-4 releases,

the initial velocity was assumed to be the spacecraft velocity and the average measured velocity, respectively.

Quantitative theory suggests that the decay time should be the time required for an alfven wave to propagate along the ambient field and sweep over a mass equal to the mass of the ionized cloud [*Scholer*, 1970]. Assuming that the Alfven velocity does not change along the field line from the observation point to the ionosphere, then

$$\frac{M}{A} = 2\rho V_A \tau. \tag{1}$$

Where M is the mass of the cloud, A is the cross sectional area of the cloud, ρ is the ambient mass density (here we assume protons only), V_A is the local Alfven velocity, and τ is the decay time or the time required for the cloud velocity to decrease to 1/e of its initial value. The factor of 2 comes from the fact that there are Alfven waves launched in both directions along the magnetic field. A more accurate estimate of τ would be obtained by modeling the change in the alfven velocity along the magnetic field. However, measurement uncertainties in Figure 6 suggest that this level of sophistication is not necessary. Each release contained 1.7 kg of Barium. Assuming that 40% of the released chemical ionized [*Huba et al.*, 1992], the mass of the cloud was 700 g. Other quantities in (1) for the 3 releases are in Table 3.

The Alfven velocity and the ambient density in Table 3 were determined from the in situ magnetic field and plasma wave data and are probably quite accurate when compared to other quantities in Table 3. We chose to estimate the cloud radius from the images. The estimates are about a factor of 20 times larger than a barium ion gyro-radius at the release distances and are also larger by about a factor of 4 than the confinement radius [e.g., *Huba et al.*, 1992]. Since the decay time is inversely proportional to the square of the cloud radius, using the gyro-radius or the confinement radius in (1) would result in decay times of 400 and 20 times larger than those listed in Table 2, respectively. Table 3 shows that the estimated decay time is a factor of 2 larger than the observed decay time. However, the ratio of the estimated and observed decay times for the three releases are in reasonable agreement. Therefore, we conclude that, although there is not detailed agreement between the observations and the predictions from (1), there is good enough quantitative agreement to conclude that the concept of the coupling of a release with the ambient medium suggested by *Scholer* [1970] is reasonable.

Also listed in Table 3 is the Alfven transit time from the equator (at the distance of the release) to the ionosphere. This transit time was estimated from *Mende et al.* [1980,

equation 3], using a dipole magnetic field. It is clear from Table 3 that the time required for the release to couple to the ambient medium is considerably longer than an Alfven transit time. In fact, the coupling would require on the order of 10 transit times or many reflections of the Alfven wave disturbance off the ionosphere. Using the Alfven transit time and the initial speed of the ionized cloud perpendicular to the magnetic field, the possibility that an Alfven wave will return to the cloud before the cloud moves a substantial distance away can be estimated. By multiplying the Alfven transit time by the spacecraft velocity perpendicular to the magnetic field (5.9, 2.88, and 2.1 km/s for the G-2, G-3, and G-4 releases, respectively) it is apparent that in all three cases, the Alfven wave will return to the release point at about the same time that the release has moved approximately one ionized cloud radius away. Thus, the Alfven wave has the possibility of re-encountering the release in all three cases.

Reflection of the Alfven wave off the ionosphere was considered in the original model of *Scholer* [1970]. One of the predictions from this reflection was that the cloud could over-brake and acquire a velocity in the opposite direction of the original release velocity. The observations of negative velocities in Figure 6 for the G-3 release may be evidence for this over-braking.

In addition, the G-3 release was the only release that had a substantial initial velocity in the corotation direction. Perhaps not by coincidence, the G-3 release was the only release that exhibited motion counter to the corotation direction. Using the in situ measurement of the electric field inside and outside of the G-2, G-3, and G-4 releases [*e.g., Wygant et al.,* 1994], we determined that in all three cases, the ambient plasma was corotating. Therefore, the G-3 release was clearly not moving with the ambient plasma in the X direction in Figure 5. It is possible that the same over-braking observed in the Y direction and predicted by *Scholer* [1970] is responsible for the X motion of this release. However, further work on the modeling of this and the other releases and the comparison of these models with the observations in this paper is needed to confirm this possibility.

Acknowledgments

Research at Lockheed was funded through NASA contract NAXX-XXXXX. The authors would like to thank the CRRES team for their effort in assembling these data. E. Aamodt was in charge of the cameras at Arecibo.

References

Bernhardt, P. A., Probing the magnetosphere using chemical releases from the Combined Release and Radiation Effects Satellite, *Phys. Fluids B*, **4**, 2249, 1992.

Bernhardt, P. A., J. D. Huba, M. B. Pongratz, D. J. Simons, and J. H. Wolcott, Plasma irregularities caused by cycloid bunching of the CRRES G-2 barium release, *J. Geophys. Res.*, **98**, 1613, 1993.

Huba, J. D., P. A. Bernhardt, and J. G. Lyon, Preliminary study of the CRRES magnetospheric barium releases *J. Geophys. Res.*, **97**, 11, 1992.

Mende, S. B., Morphology of the magnetospheric barium release, *J. Geophys. Res.*, **78**, 5751, 1973.

Mende, S. B., R. L. Arnoldy, L. J. Cahill, Jr., J. H. Doolittle, W. C. Armstrong, and A. C. Fraser-Smith, Correlation between λ4278-A optical emissions and a Pc 1 pearl event observed at Siple Station, Antarctica, *J. Geophys. Res.*, **85**, 1194, 1980.

Mende, S. B., G. R. Swenson, S. P. Geller, J. H. Doolittle, G. Haerendel, A. Valenzuela, and O. H. Bauer, Dynamics of a barium release in the magnetospheric tail *J. Geophys. Res.*, **94**, 17,063, 1989.

Scholer, M., On the motion of artificial ion clouds in the magnetosphere, *Plant. Space Sci.*, **18**, 977, 1970.

Singer, H. J., W. J. Hughes, R. Anderson, J. Wygant, W. McNeil, and D. L. Reasoner, Diamagnetic cavities formed by the CRRES high altitude chemical release experiments, *EOS Trans. Amer. Geophys. U., (Supplement)* **72**, 230, 1991.

Wygant, J. R., P. Harvey, F. S. Mozer, M. Pongrantz, D. J. Simons, and H. Singer, CRRES electric and magnetic field measurements during the Alfven wave mediated braking of a barium release in the ionosphere, *J. Geophys. Res.*, submitted, 1994.

Figure Captions

Figure 1. Observations of the CRRES G-2 barium release (one minute after the release) from Rosemary Hills, FL (top panel) and Breezy point (Los Alamos), NM (bottom panel). The large, asymmetric circle is the expanding barium neutral cloud while the thin line is the ionized cloud. The spacecraft position is shown by the large square. The cross in the upper panel and the 0.2 R_E line in the lower panel through the ionized cloud were used in the triangulation technique and are explained in the text.

Figure 2. Observations of the CRRES G-4 barium release (6.5 min after the release) from Arecibo, PR (top panel) and Los Alamos, NM (bottom panel). The format is the

same as in Figure 1. This release was much further from the Earth and, at this late time in the release, no neutral cloud is visible. The 0.2 R_E line in the bottom panel is significantly shorter than in the same panel in Figure 1, indicative of the much further release distance for the G-4 release.

Figure 3. The position of the ionized and neutral clouds for the G-2 release for several observation times. The plane of the plot is perpendicular to the ambient magnetic field and the y-axis is parallel to the component of the spacecraft velocity vector perpendicular to the magnetic field. The entire coordinate system rotates with the co-rotational velocity of the plasma. The neutral cloud expands and convects approximately in the direction of the spacecraft motion while the ionized cloud moved only a short distance from the release point before stopping for the duration of the observations.

Figure 4. The position of the ionized cloud for the G-3 release for several observation times. The format is the same as in Figure 3. Triangulated positions along the magnetic field that are projected into this coordinate system form short line segments aligned with the radial direction from the Earth because of the larger uncertainty in the measurements in this direction. The G-3 ionized cloud initially moved in the direction of the spacecraft motion. Later, it reversed it motion before stopping for the duration of the observations.

Figure 5. The position of the ionized cloud for the G-4 release for several observation times. The format is the same as in Figures 3 and 4. The G-4 cloud moved along the spacecraft velocity vector for several minutes before stopping.

Figure 6. The y velocities of the ionized clouds for G-2, G-3, and G-4. The G-2 neutral cloud moved with at least the spacecraft velocity for as long as it was reliably observed (the last point may be suspect). The ionized clouds all had the characteristic of moving at a velocity other than zero but eventually decaying to zero. Decay times for the three releases are shown by the vertical dashed lines.

Table 1

Name	Date	Time	Latitude	Longitude	Altitude
G-2	13 Jan 1991	0217:03 UT	16.9°	-103.1°	6,180 km
G-3	15 Jan 1991	0411:00 UT	17.9°	-97.5°	15,063 km
G-4	16 Jan 1991	0625:00 UT	-0.7°	-53.8°	23,977 km

Table 2.

G-2 Release hmmss	13-Jan-1991 $B_{tri} \cdot B_{mod}$	G-3 Release hmmss	15-Jan-1991 $B_{tri} \cdot B_{mod}$	G-4 Release hmmss	16-Jan-1991 $B_{tri} \cdot B_{mod}$
21700	(release)	41100	(release)	62500	(release)
21759	4.7	41200	1.9	62557	30.4
21935	1.6	41231	0.6	62629	14.5
22011	1.3	41300	1.1	62656	5.6
22048	1.0	41331	5.3	62727	5.7
22125	2.2	41400	3.7	62806	6.4
22233	3.3	41500	0.9	62858	10.7
22339	1.8	41600	3.0	62940	8.7
22407	2.3	41900	4.8	63028	6.8
22453	2.6	42000	4.4	63133	10.1
22703	8.8	42100	7.0	63252	7.0
		42202	9.4		
		42303	10.4		
		42400	9.0		
		42505	12.1		
		42600	9.9		

Table 3.

Release:	G-2	G-3	G-4	
Cloud Radius (km)	12.8	30.	64.	(estimated from images)
Alfven velocity (km/s)	2400	1300	780	(CRRES s/c data)
ambient density (cm-3)	2075	278	49	(CRRES s/c data)
tau = vel decay time (s)	82	205	426	(equation 1)
Ratio	1	: 2.5	: 5.2	
tau observed (s)	40	100	310	
observed Ratio	1	: 2.5	7.8	
Alfven transit time (s)	3.1	10.3	25.1	

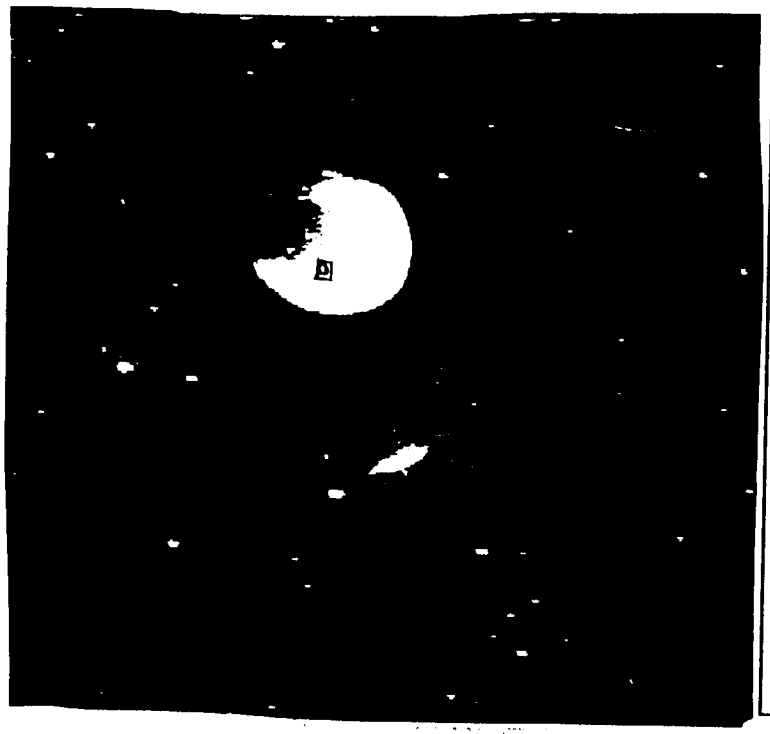

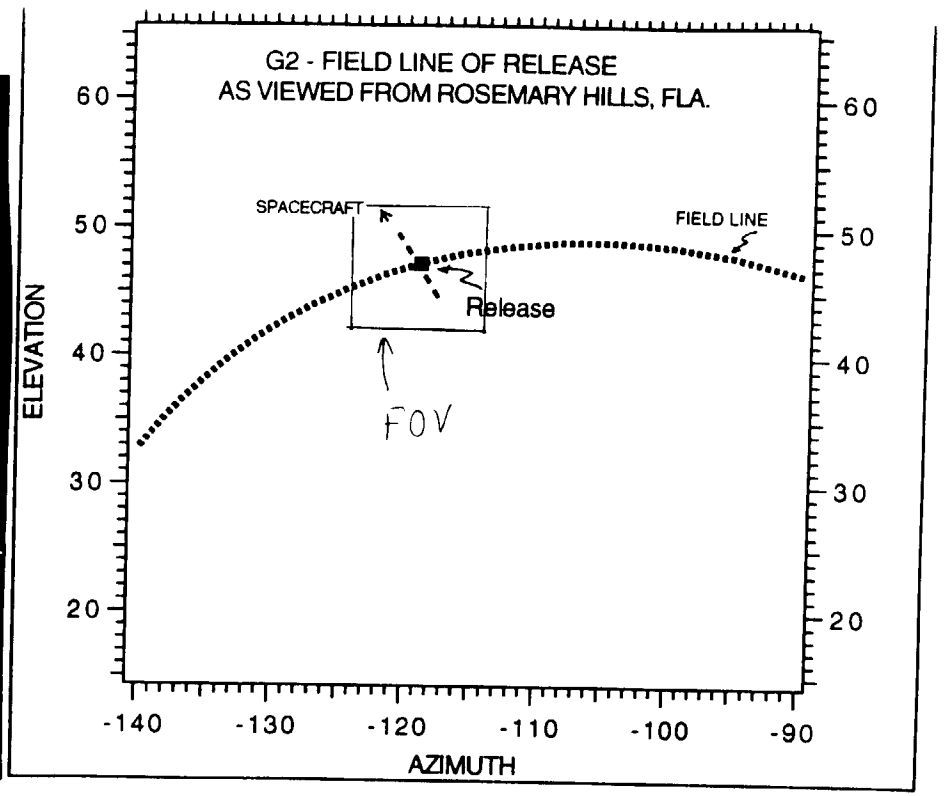
G2 - FIELD LINE OF RELEASE
AS VIEWED FROM ROSEMARY HILLS, FLA.
SPACECRAFT
FIELD LINE
Release
FOV
ELEVATION
AZIMUTH
60
50
40
30
20
-140
-130
-120
-110
-100
-90

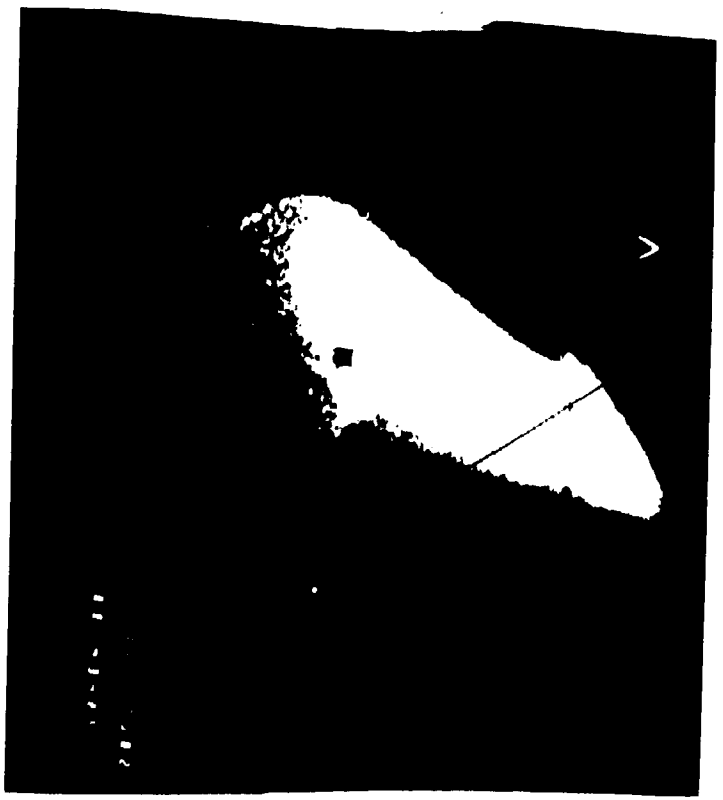

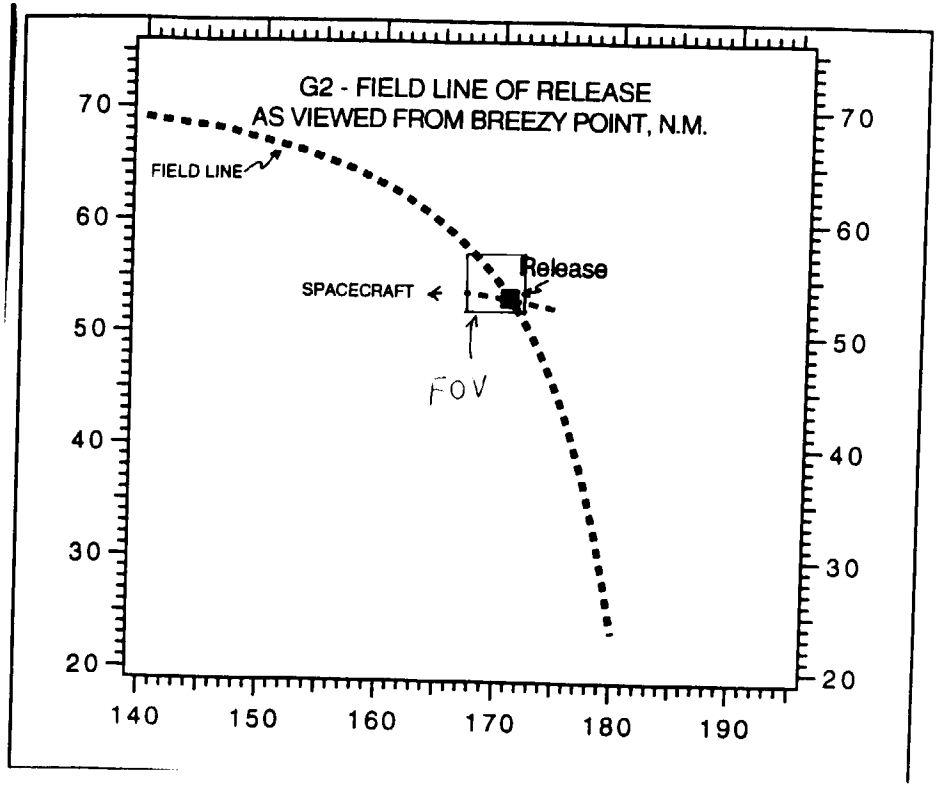
G2 - FIELD LINE OF RELEASE
AS VIEWED FROM BREEZY POINT, N.M.
FIELD LINE
Release
SPACECRAFT
FOV
70
60
50
40
30
20
140
150
160
170
180
190

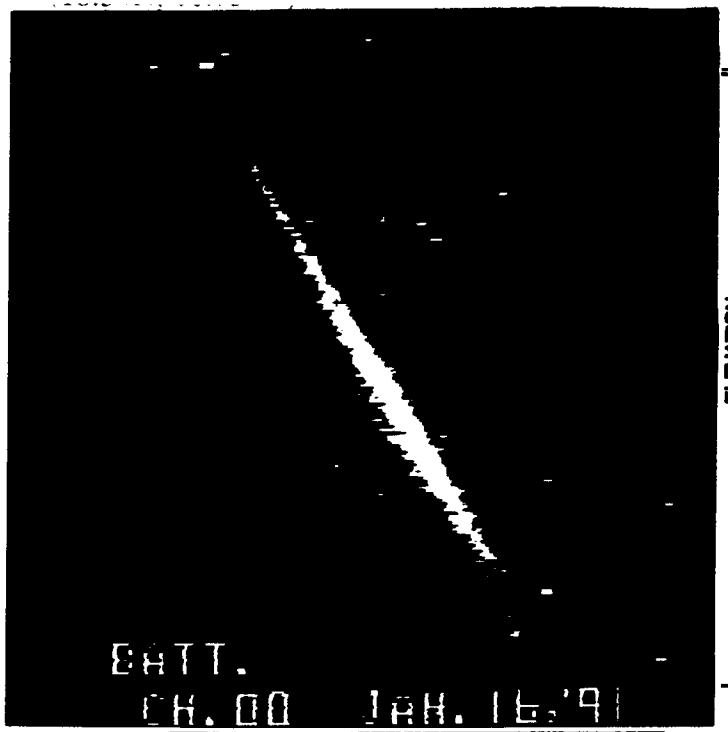
EXIT.
CH.00 JAN.16.'91

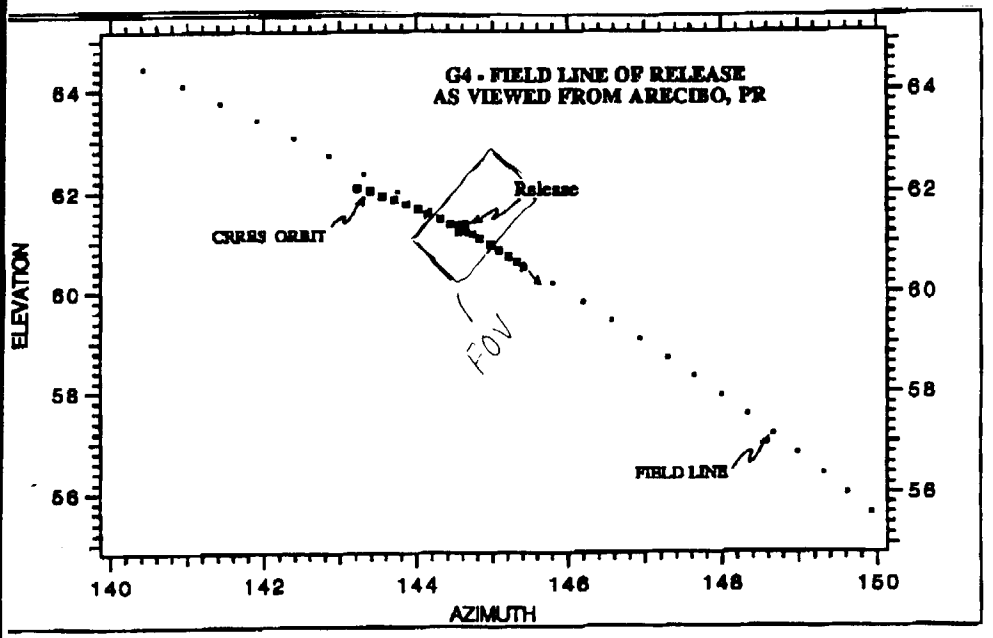
G4 - FIELD LINE OF RELEASE
AS VIEWED FROM ARECIBO, PR
Release
CRRES ORBIT
FOV
FIELD LINE
ELEVATION
AZIMUTH
64
62
60
58
56
140
142
144
146
148
150

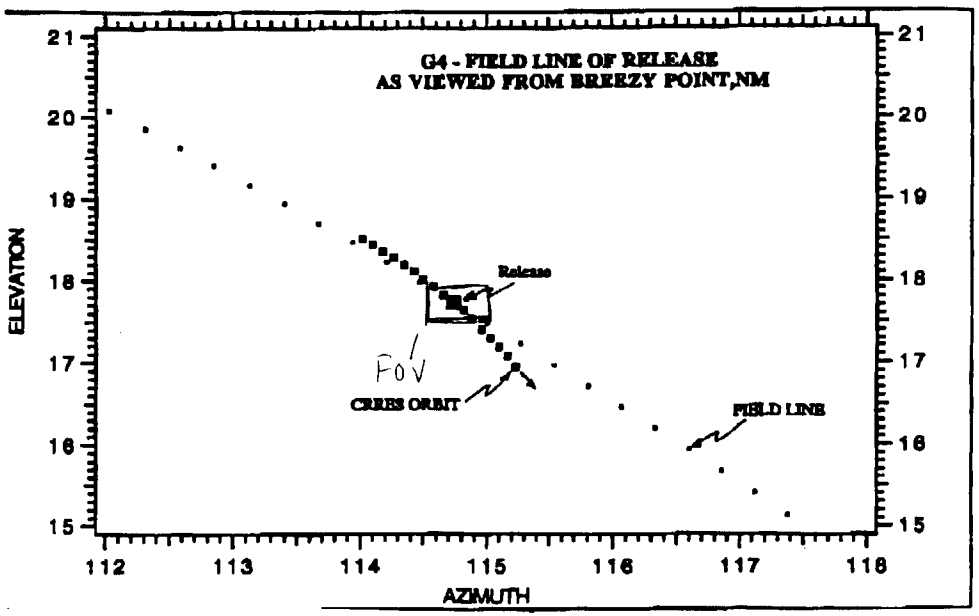
G4 - FIELD LINE OF RELEASE
AS VIEWED FROM BREEZY POINT,NM
Release
FOV
CRRES ORBIT
FIELD LINE
ELEVATION
AZIMUTH
21
20
19
18
17
16
15
112
113
114
115
116
117
118

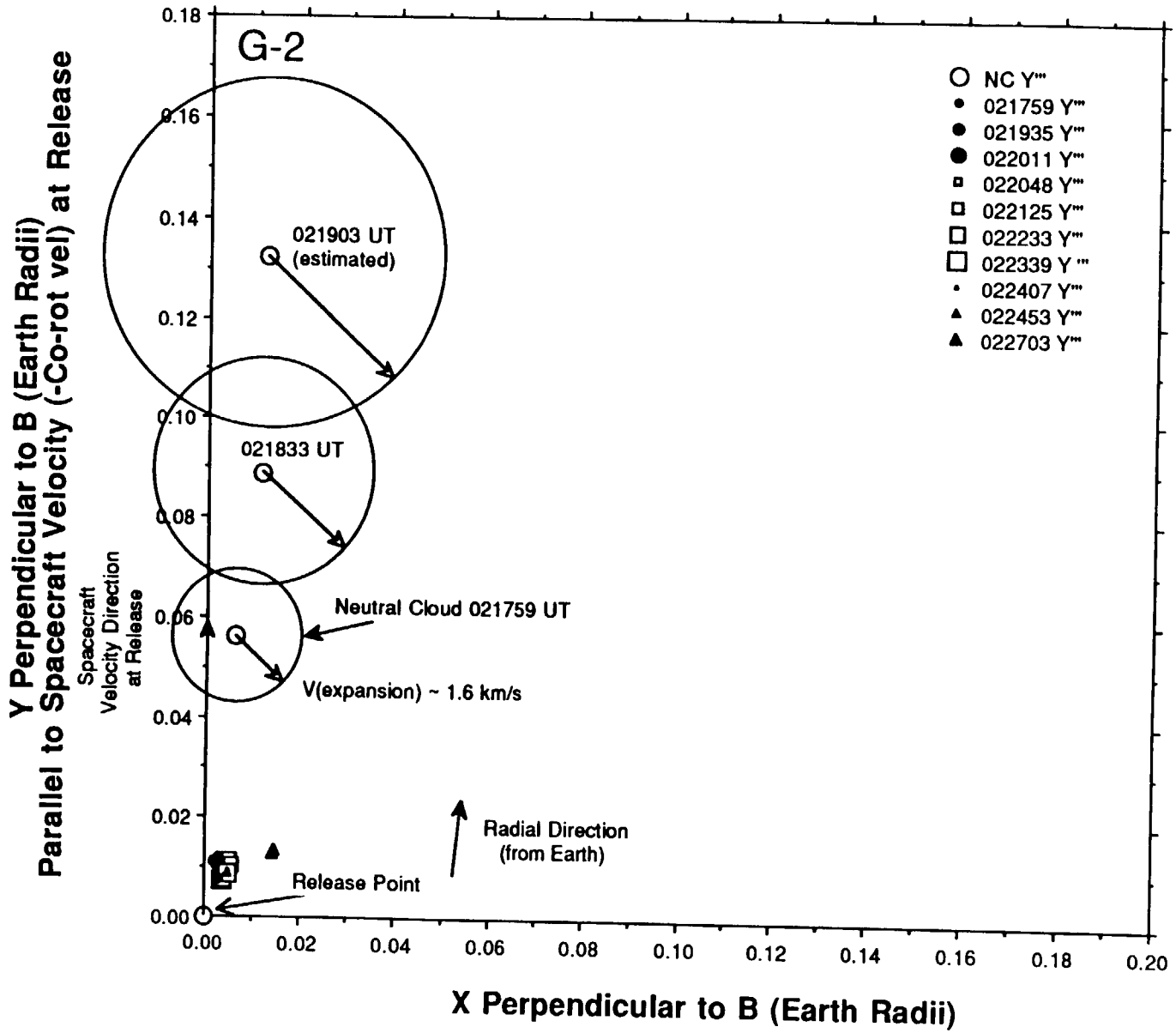
G-2
NC Y'''
021759 Y'''
021935 Y'''
022011 Y'''
022048 Y'''
022125 Y'''
022233 Y'''
022339 Y '''
022407 Y'''
022453 Y'''
022703 Y'''
021903 UT
(estimated)
021833 UT
Neutral Cloud 021759 UT
V(expansion) ~ 1.6 km/s
Spacecraft
Velocity Direction
at Release
Radial Direction
(from Earth)
Release Point
Y Perpendicular to B (Earth Radii)
Parallel to Spacecraft Velocity (-Co-rot vel) at Release
X Perpendicular to B (Earth Radii)
0.00
0.02
0.04
0.06
0.08
0.10
0.12
0.14
0.16
0.18
0.20

Figure 3

Data from "G-3 triang B perp/Vsc-co rot"

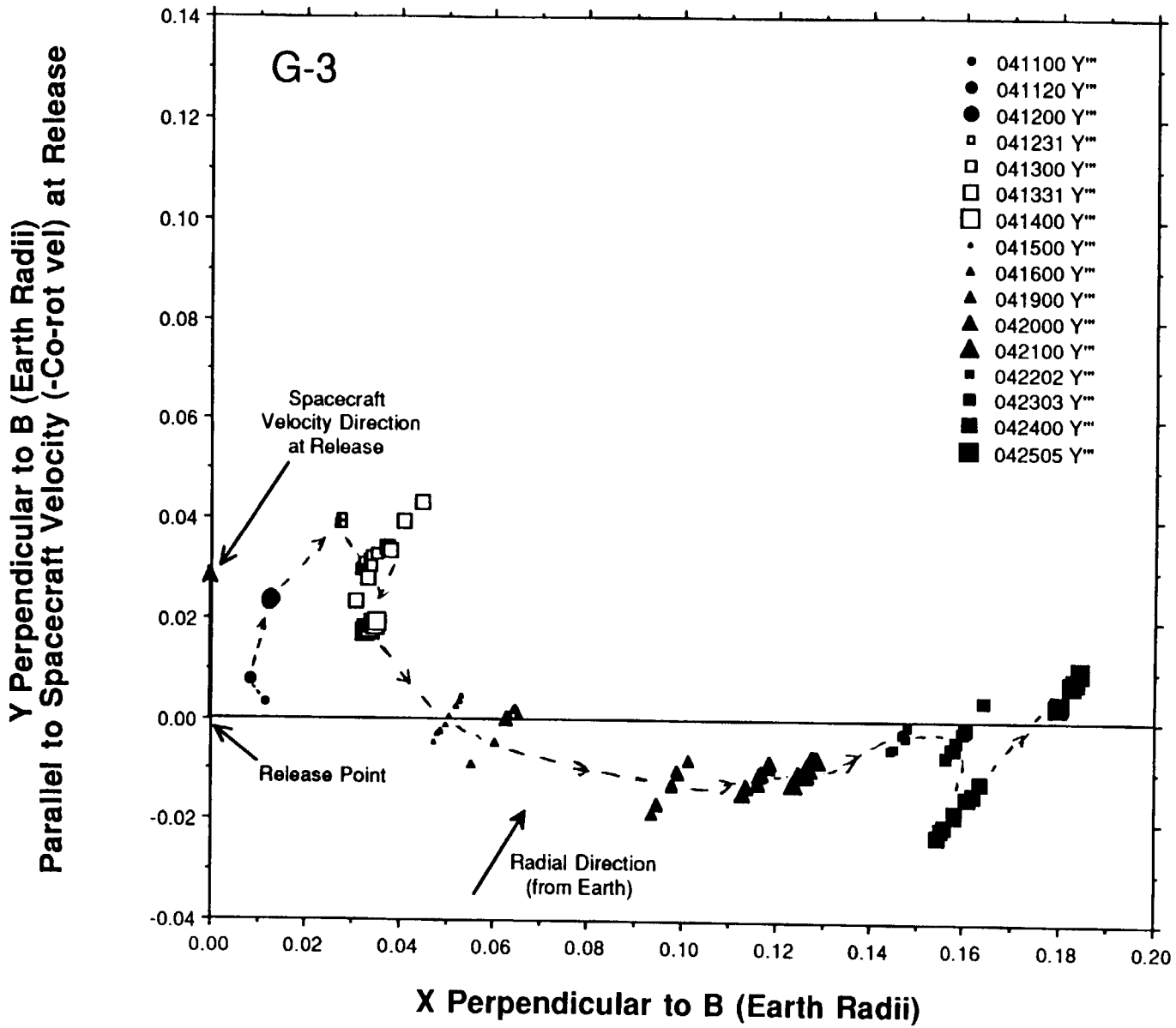

Figure 4

Data from "G-4 triang B perp/ Vsc-co rot"

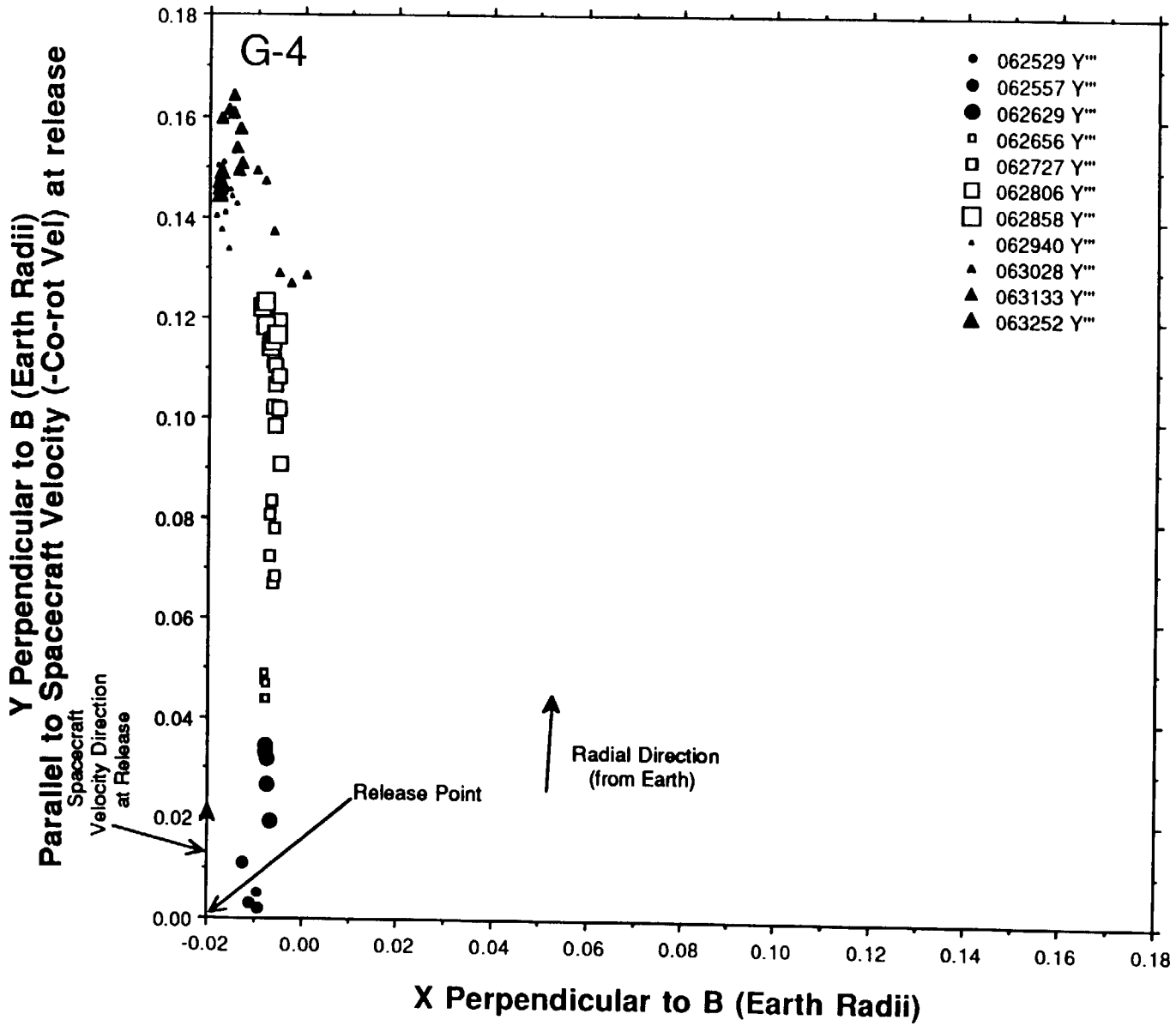

Figure 5

Data from "cloud vel compared"

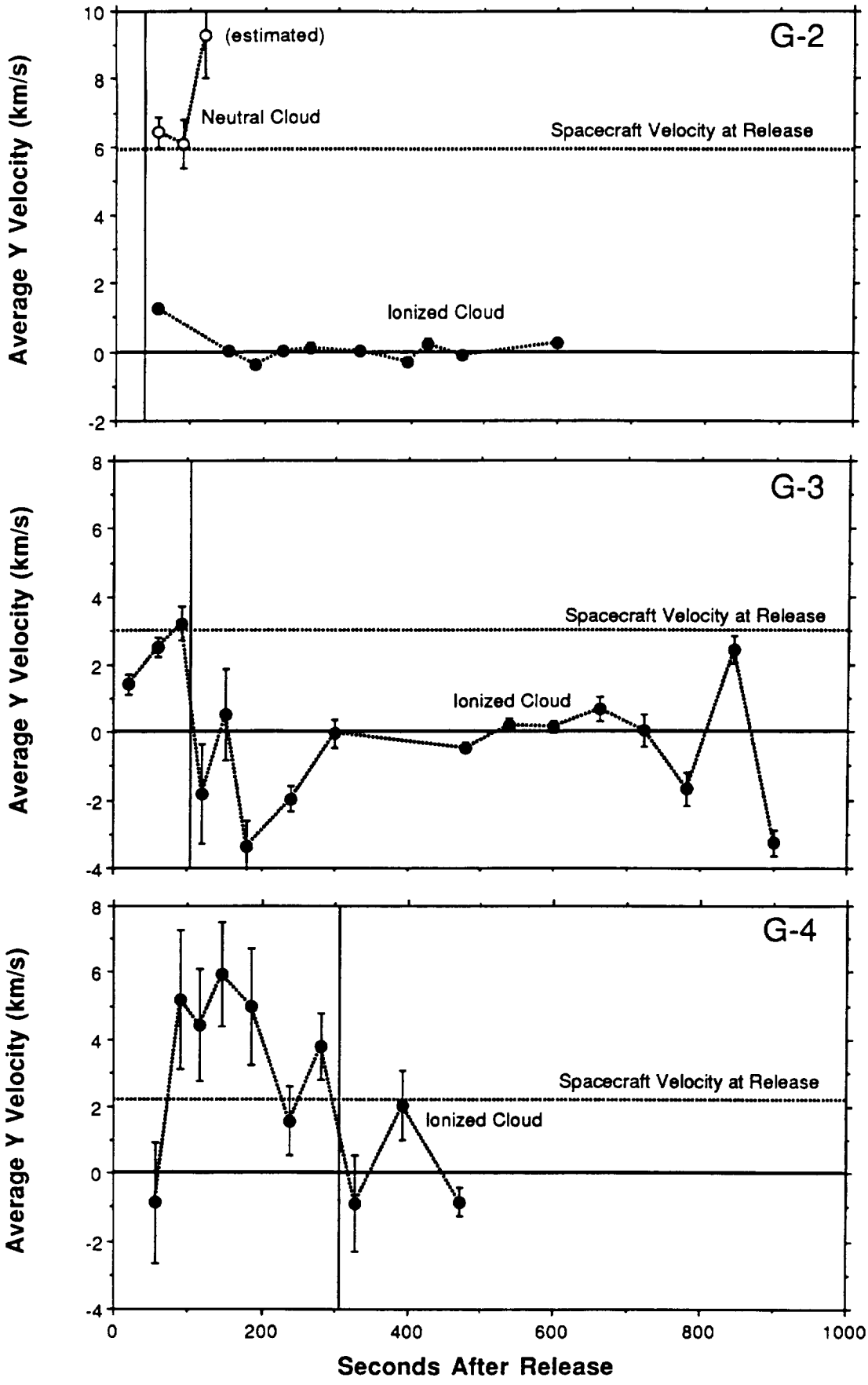

APPENDIX B

Ion Doppler Velocity Distributuions Observed in Fabry-Perot Images of CRRES Low-Altitude Barium Release

by

Rairden R.L., S.B. Mende, M.B. Pongratz

Paper to be Submitted to J. Geophys. Res. 1994

Ion Doppler Velocity Distributions Observed in Fabry-Perot Images of CRRES Low-Altitude Barium Releases

R. L. Rairden and S. B. Mende
Lockheed Palo Alto Research Laboratories, Palo Alto, California

M. B. Pongratz
Los Alamos National Laboratory, Los Alamos, New Mexico

Abstract. During the CRRES equatorial low-altitude release campaign of July-August 1991, ion Doppler velocity measurements were recorded by aircraft-based Lockheed Fabry-Perot imaging instrumentation. The barium releases were typically performed in sunlight over the morning terminator, at the satellite perigee velocity of > 9 km/sec nearly perpendicular to the geomagnetic field direction. Velocity profiles early in a release (t < 5 minutes) show a marked double-peak resulting from ion gyromotion toward and away from the instrument at close to the release velocity. Modeled ion Doppler velocity profiles for the particular viewing geometry of each release agree qualitatively with these measurements. Narrowing of the velocity profiles indicates that the ion momentum is lost on a time-scale of minutes. Releases at three different altitudes show a progressive increase in momentum loss rate with decreasing altitude, consistent with ion-neutral collisional slowing. Monte Carlo calculations of the momentum loss due to ion-neutral collisions are fitted to the observations, and residual differences indicate the presence of additional loss mechanisms where energy is dissipated in collective plasma effects. A sudden dramatic momentum loss is exhibited in the 100 to 120 second interval following event G-9, the largest chemical release.

(Index terms: 2403 Ionosphere, active experiments
2451 Ionosphere, particle acceleration
2471 Ionosphere, plasma waves and instabilities)

Introduction

The chemical release portion of the Combined Release and Radiation Effects Satellite (CRRES) program was designed to further the understanding of a wide variety of magnetospheric and ionospheric plasma processes. Though originally conceived as a shuttle-deployed vehicle with a low orbit phase and subsequent boost to geosynchronous transfer orbit (GTO), circumstances eventually dictated an Atlas-Centaur launch of a reduced payload configuration in July 1990 directly into the final GTO. The twenty-four chemical canisters

were distributed among several release objectives. Bernhardt [1992] presents an overview of the CRRES releases and some initial findings.

A first pair of nighttime release experiments was performed in September 1990 at near-perigee altitudes to investigate Critical Ionization Velocity (CIV) effects [Wescott et al., 1991]. The second campaign, in the winter of 1991, comprised the high-altitude series of magnetospheric releases which occurred in regions of differing magnetic field strengths and low ambient plasma densities. The resulting diamagnetic cavities, ion coupling to the magnetic field, and associated plasma instabilities have been under study [Huba et al., 1992a].

During the summer of 1991 the remaining canisters were expended in a series of near-perigee releases over the Caribbean observed by several participants at various sites. These ionospheric releases are characterized by high velocities (> 9 km/s) directed nearly perpendicular to the geomagnetic field. Kinetic instabilities compete with polarization fields in slowing the introduced material as it ionizes, with the final plasma state being dependent on the coupling process. Optical measurements during the first minute are essential in the investigation of these effects. Later measurements from the network of observing sites are able to track the barium ions as they paint the field lines (L~1.3) into the opposite hemisphere, the objectives being, for example, to determine the weak parallel and transverse electric fields and to establish how closely the magnetic field lines can be regarded as equipotentials.

In this paper we present and interpret portions of the Lockheed video imaging data from the summer 1991 low-altitude release experiments. Emphasis is placed on the early evolution (first five minutes) of the barium ion Doppler velocity distributions, which are unique measurements obtained through our Fabry-Perot imagery. The ions are found to lose energy more quickly than predicted from Monte Carlo calculations of ion-neutral collisional slowing alone. Non-collisional plasma coupling mechanisms are suspected to be responsible for the differences. The equipment set-up and data gathering operations are described in some detail for the benefit of those who might be considering Fabry-Perot imaging or airborne geoscience missions in general.

Subjects not addressed in this paper are the abundance of release products, their motions transverse to the line of sight, and the longer time scale behavior of the chemical clouds. These aspects are among the objectives for the optical data from other sites in the observing network.

Instrumentation and Operations

In addition to the numerous ground sites, a total of four aircraft were deployed as observation platforms for several investigator teams during the CRRES campaigns. These provided great flexibility in avoiding poor weather conditions and in optimizing the viewing

geometry for each release. The Lockheed cameras occupied one of three large optical grade windows on the left side of one of these aircraft, a U. S. Air Force KC-135.

The optical layout is shown in Figure 1, drawn roughly to scale. Two thermo-electrically cooled image-intensified CCD video cameras shared a large elliptical gyroscopically stabilized pointing mirror. The incoming light was intercepted by a dichroic multilayer beamsplitting mirror which reflected the 455.4-nm singly ionized barium (BaII) image into the narrow field path, and transmitted the 493.4-nm BaII image through to the widefield camera. Both cameras were generally operated with narrowband (3.5 nm FWHM) interference filters centered on those respective wavelengths. A temperature stabilized four-position filter wheel in the optical path of the narrow field camera carried three solid Fabry-Perot etalons and one vacant aperture. The equivalent air gap for each etalon and the corresponding free spectral range (FSR) for the BaII 455.4-nm line are listed in Table 1.

TABLE 1. Fabry-Perot etalons in narrow-field camera filter wheel, equivalent air gap and free spectral range.

Position	Etalon	FSR
1	8-mm	8.5 km/sec
2	2-mm	34 km/sec
3	0.5-mm	136 km/sec
4	open	-----

A hollow cathode barium calibration lamp completes the setup, verifying temperature stability and giving the precise locations for effectively zero velocity F-P fringes in each etalon. The calibration beam entered the system by reflection from a white diffusing surface opposite the source, returning to an uncoated pellicle beamsplitter placed at a 45-degree angle in the optical path. Ghost images or aberrations introduced by the thin (five micron) pellicle membrane are negligible.

The co-alignment and relative fields of view for the two cameras are illustrated by starfield images in Figure 2. The constellation is Orion, viewed in white light (BaII filters removed). The widefield camera achieves dimensions of 15 by 18.5 degrees using a 50-mm f/1.2 lens, and a fiber-optic taper to couple the intensified image to a 15-mm CCD. The narrow field camera uses a 135-mm f/2.0 lens and an untapered fiber-optic coupling for its 3.5 by 4.3 degree view. Both fields are mirror reversed. Realtime pointing operations were accomplished through commanding biases to the gyro-stabilized pointing mirror using a joystick. The

stabilization effectively countered small maneuvers by the aircraft, although large heading changes would drive the mirror into its limit switches. The unvignetted pointing envelope was approximately 0 to 40 degrees elevation (relative to level flight) and 20 degrees forward to 20 degrees aft, somewhat elevation dependent. Additional system features shown in the images of Figure 2 are the date and time annotation, and a bar code at the left edge indicating the image integration time.

Software in a small computer controlled the image integration times for a series of bracketing exposures or other preprogrammed sequences realtime commandable at the keyboard. Computer inputs were time-tagged and logged to disk. It is noted that joystick inputs were part of an independent system and not tracked or logged. Few stars are sufficiently bright to be seen through the narrow band filters, so little absolute pointing information is available. However, this is of no consequence for the primary objectives of determining barium release initial expansion rates and radial velocity distributions. For observations several minutes into the release, the general look direction could be derived from the aircraft heading.

A pair of monitors, a date/time generator, a frame memory unit, a 3/4-inch video recorder and an 8-mm backup video recorder were installed for each of the two cameras. A microphone was connected to an audio channel of one video recorder for verbal notations. Other equipment included image intensifier high-voltage supplies, the calibration lamp power supply, and the filter wheel controller. All components and cables on the optical bench and in the electronics racks were strictly required to be securely fastened to withstand the most severe accelerations which could be imparted by inflight turbulance or ground mishaps.

Radio contact with the ground operations teleconference was maintained on each flight to indicate readiness to the Project Scientist. The 25-minute interval between canister ejection and thermite initiation gave adequate time for a release confirmation message to reach the aircraft well before each event. Due to the extreme cold at altitude, care was required to avoid fogging or frosting the single-pane fuselage windows. Small warm air blowers were located at each station, and before each release the windows were wiped with alcohol. Heavy black cloth shrouded the optical bench area from the cabin operations, and interior lighting was kept minimal. A popularized account of the flight activities, relating the flavor of the campaign and additional background information, is reported by Shiner [1992].

OBSERVATIONS

The release events and their geographic coordinates are identified in Table 2. The aircraft track is available as a digital recording of Global Positioning Satellite (GPS) receiver fixes at two-second intervals. Large canisters were always released in pairs due to CRRES satellite

dynamical constraints. The small canisters could be released singly, or paired for greater effect. Large and small canisters contained ~5 and ~1.5 kg barium, respectively; Stenbaek-Nielsen et al. [1993] list precise chemical quantities for each release. Figure 3 provides an overview of the release and observation locations on a map of the Caribbean. The lines of sight are directed looking toward sunrise from the nightside of the terminator. Each release occurred in sunlight, with the exception of G-11B, a critical ionization velocity (CIV) experiment which occurred in darkness just to the nightside of the terminator.

TABLE 2. CRRES Caribbean Campaign Release Events

Date	Time UT	Label	Canisters	Release location lat°N	lon°E	alt(km)	Aircraft location lat°N	lon°E	Range to release, km
July 13, 1991	08:35:23	G-1	One small	17.8	297.1	495	12.90	292.51	903
July 19, 1991	08:37:07	G-9	Two large	17.4	297.2	441	13.04	292.64	837
July 22, 1991	08:38:21	G-11A	One small	16.8	299.7	411	13.01	291.99	1039
July 25, 1991	08:37:10	G-11B	One small	17.3	290.5	478	16.37	285.16	757
Aug 12, 1991	09:31:18	G-12	Two small	9.1	296.5	507	14.99	289.52	1154

G-11B, a Critical Ionization Velocity experiment, occurred in darkness just to the nightside of the terminator. All others were in sunlight. Aircraft altitude was 10 to 12 km. Aircraft velocity was approx 200 m/s (400 knots), roughly perpendicular to the line of sight.

In each case the azimuth and elevation coordinates of the imaging field of view were aligned to the predicted release point, providing characteristic initial measurements such as the example of G-12 video images presented in Figure 4. Wide-field and narrow-field images at 8, 19, and 28 seconds after this release show the early ion cloud evolution. The barium neutral population, not visible through these filters, expands spherically as its bulk velocity follows the satellite orbit. In sunlight the neutrals photoionize with a time constant on the order of 28 seconds, leaving behind an expanding cone of BaII stopped in the geomagnetic field. The fringes from the 2-mm Fabry-Perot etalon in the narrow-field view reveal a double peak in the ion radial velocity distribution during this time regime. Figure 5 shows Fabry-Perot images from G-9 selected at times sufficiently after release for the ion spread to fill the field of view. The decrease of fringe width during the first minutes is clearly evident. The quantitative interpretation of these fringes as Doppler velocity distributions is discussed in the following paragraphs.

Fabry-Perot interferometry. The principles of Fabry-Perot interferometry are presented in many optics textbooks (e.g. Born and Wolf, 1980). Briefly, the constructive interference of multiple internal reflections within a solid etalon causes monochromatic light to be preferentially transmitted at given angles away from normal incidence, resulting in a pattern of concentric circular fringes with maxima obeying the expression

$$2T\cos\varphi = m\lambda \qquad (1).$$

Here T is the equivalent air gap thickness of the etalon, which is the physical thickness multiplied by μ, the index of refraction of the etalon material. Lambda is the wavelength, m is the order of interference (an integer), and φ is the angle of refraction within the material. Successively larger values of φ satisfy this equation for orders m–1, m–2, etc., giving rise to fringes of successively larger angular radii. If λ_0 satisfies (1) at an internal angle of incidence φ_0, then the fringe radius for $\lambda_0 + \Delta\lambda$ in the same order can be found by differentiation of (1). The external angle of incidence follows from Snell's law. The corresponding Doppler velocity

$$v = c\,\Delta\lambda/\lambda \qquad (2)$$

of a given emission line can thus be measured by the change in fringe radius. In (2), v is the radial velocity and c is the speed of light ($v << c$). A receding (redshifted) source is found to result in a fringe of smaller radius than that of a stationary source (e.g. a local calibration lamp).

The free spectral range (FSR) of an etalon at a given wavelength is the value of $\Delta\lambda$, or equivalent radial velocity, which would shift a fringe to the position of the next order fringe. A radial velocity spread in excess of the FSR will cause fringes to overlap. For our T = 2mm etalon, the order m for λ = 455.4nm (BaII) is roughly 2 × 2mm/455.4nm, or ~8800. A change in wavelength of 455.4nm/8800, which is 0.052 nm, would produce an identical fringe pattern, with the order m stepped by one unit. The simple expression for the FSR is $\lambda^2/(2T)$. The equivalent Doppler velocity in this example is c/8800, or 34 km/s. Absolute velocities of the observed barium ions are determined relative to the fringes of the zero-velocity 455.4-nm emission line from the BaII calibration lamp. Figure 6 illustrates these results for the three etalons used. The video images are digitized, the fringe pattern center is determined, and radial profiles are measured and plotted. In this example we compare the profile calculated for an infinitely narrow line with measured profiles from the calibration lamp and profiles from representative barium images obtained many minutes after release. A spurious neon emission in the calibration lamp appears within the 3.5-nm width of our 455.4-nm filter, producing an additional fringe which does not materially interfere with establishing the barium line zero-

velocity radius on the images. (A laboratory spectrometer measurement found this line to be 1.0 nm shorter than the BaII line.) The width of the fringe for an infinitely narrow line is a function of etalon surface reflectivity, which is enhanced at the operational wavelength by appropriate multilayer coatings. Finer velocity resolution is thus obtained at the expense of a decreased intensity throughput. The ratio of free spectral range divided by this fringe width is generally termed the transmissive finesse, N_T.

Temperature stabilization is required to maintain a constant value for an etalon's effective thickness T. The fused silica index of refraction, $\mu = 1.465$, increases with temperature by $\sim 10^{-5}$ per degree C (near room temperature). A change of one degree C moves a fringe by the same amount as would a wavelength change of $\sim 10^{-5}\lambda$, equivalent to a Doppler shift of $10^{-5}c$, or 3 km/s. The calibration lamp is activated every few minutes to monitor temperature stability. The effect of thermal expansion in this substrate is an order of magnitude less significant. The radial dispersion for Doppler shift (km/s per pixel) is effectively independent of effective thickness T. The fringes may appear to exhibit inherent small departures from circularity or concentricity over the full field of view due to geometric distortions in image acquisition, reproduction or digitization, therefore the respective calibration image fringes must always be used as fiducials for zero velocity. The above considerations are important for realizing the full precision of this measurement technique.

Double-peak velocity distribution. In Figure 7 we display the early time evolution of the ion Doppler velocity for releases G-9, G-11A, and G-12. Profiles of the innermost (highest resolution) fringe from 2-mm etalon images acquired during the first minute or two after each release are stacked to make the trends most evident. The bottom profile in each series is of the calibration lamp, used to locate the zero-velocity position (right hand peak of the lamp profile is BaII, left hand peak is a neon line). The abscissa is linear in image-space, labeled in Doppler velocity.

Profiles from the first minute of G-11A and G-12 clearly show the double-peaked velocity distribution which is expected to arise from the ion gyromotion component toward and away from the observing point. Profiles of the much larger G-9 release have a more uniform intensity across the Doppler spread. The initial G-9 and G-11A distributions are spread ±7 to 8 km/s centered around the zero-velocity wavelength, while the G-12 profiles show a smaller spread and are red shifted 4 to 5 km/s. A quantitative demonstration that this behavior is expected requires some detailed modeling of the chemical release velocity and geometry. This modeling is described in the next section.

MODELING THE DOPPLER PROFILE AND ENERGY LOSS RATES

The release observation geometry is described by four vectors, referring to the satellite velocity, the solar direction, the local geomagnetic field direction, and the line-of-sight or "look" direction. These vectors are given in Table 3 for each event, in terms of azimuth and elevation at the release point. (The satellite orbital velocity vector is given in the earth-rotating frame.) Angles between the various pairs of directions are also listed. The geometrical situation is sketched pictorially for G-9, G-11A, and G-12 in Figure 8. For G-9 and G-11A both the satellite velocity vector and the look direction are nearly perpendicular to the magnetic field, while for G-12 a larger component of the release velocity is up the field line (southward) and the look direction is within 33 degrees of being up the field line.

TABLE 3. Local geometry at each release point.

	G-1	G-9	G-11A	G-11B	G-12
Satellite velocity, V					
azimuth, deg	91.6	94.2	96.7	95.0	106.2
elevation, deg	–6.8	–5.5	–3.1	–6.0	7.2
velocity, km/s	9.6	9.6	9.6	9.6	9.5
Magnetic field, B					
azimuth, deg	348	348	347	352	350
elevation, deg	–46.5	–45.9	–44.3	–47.2	–35.8
flux density, nT	31,500	32,000	32,000	32,000	27,500
Direction to Sun					
azimuth, deg	60.4	61.5	63.3	59.7	73.0
elevation, deg	–15.4	–15.7	–13.9	–21.7	–9.0
Direction to aircraft					
azimuth, deg	222.8	226.1	244.0	260.4	311.4
elevation, deg	–35.7	–34.1	–26.8	–40.7	–29.8
Angles between directional vectors					
Look-Sun, deg	53.7	51.9	40.7	65.3	68.3
Look-V, deg	62.5	60.3	43.5	48.6	32.8
Look-B, deg	95.8	95.4	99.9	117.8	147.3
V-Sun, deg	31.8	33.7	34.7	37.6	36.3
V-B, deg	94.1	97.0	101.7	94.2	115.5
B-Sun, deg	66.6	67.2	70.6	59.2	79.2

Look direction is opposite of direction to aircraft.
Some numbers are from Stenbaek-Nielsen et al. [1993].

Taking the initial G-9 barium cloud velocity to be the satellite velocity vector at the time of release, the ions are created at a pitch angle of 97 degrees, with $v_{\|}$ at 1.18 km/s southward and $v_{\perp}$ at 9.46 km/s. The angle between the magnetic field and the camera look direction is 95.6 degrees, giving an apparent radial component of gyromotion equal to $9.46 \times \sin(95.6) = 9.41$ km/s, both toward and away from the observer. For G-12 the parameters are $v_{\|} = 4.17$ km/s southward and $v_{\perp} = 8.46$ km/s. The viewing direction is 32.8 degrees relative to the magnetic field, giving plus and minus 4.58 km/s for the radial component of the gyromotion. The radial component of $v_{\|}$ is 3.50 km/s away from the aircraft, causing the observed shift of the G-12 velocity profile (Figure 7).

For modeling purposes Bernhardt [1992] assumes a neutral barium release cloud to be a shell centered on the satellite orbit track, expanding at a radial speed $V_r = 1.38$ km/s, with the shell thickening at a rate $V_t = 0.26$ km/s. In our modeling we adjust the V_r parameter to fit ground-based imaging measurements; for example the radial expansion rateV_r of release G-9 is found to be 1.7 km/s based on video imaging observations from the island of St. Croix. The ionization rate for barium in full sunlight is 0.0357/s, or $\tau_i = 28$ s, and the cloud may be regarded as optically thin after the first few seconds following the release event [Huba et al., 1992b]. A factor complicating the profile appearance presents itself in the shape of the illumination source, the solar spectrum, near 455.4 nm. The deep BaII Fraunhofer absorption is shown in Figure 9, as used by Stenbaek-Nielsen [1989] in a detailed modeling of barium cloud emission rates.

Monte Carlo simulations. A simulation software routine named PTRACE, developed at Los Alamos, models the single-particle dynamics within the chemical release cloud. Photo-ionization, collisions, ion drift, and mirror force are included. Collective plasma effects are not included in the PTRACE simulation code. A hard sphere model is used for neutral barium collision with neutral oxygen, and a Langevin potential is used for Ba^+ collision with O. An estimate of the density of ambient neutral atoms at the release altitudes is obtained from the appropriate MSIS model. The density is adjusted for consistency with ground-based measurements of the drag on the neutral barium cloud (slowing of translational velocity), which is derived from image differencing. Results of the simulations for G-9 and G-11A are shown in Figure 10, plotted in the form of predicted Fabry-Perot profiles at various times following release, as viewed from the aircraft location. Evolution of the velocity profile shape is readily apparent during the first few minutes while ions are quickly losing momentum. The widths of the simulated profiles in Figure 10 compare well with the observed profile widths at corresponding post-release times displayed in Figure 7. The qualitative shape of the profiles is also reproduced, showing a more pronounced double-peak structure for G-11A while the G-9 profile is more flat across the top.

The modeled rates of ion momentum loss due to ion-neutral collisions are illustrated in Figure 11. Average ion speed is plotted versus time after release for three events. The differing energy loss rates result primarily from the different ambient neutral atom densities at the altitude of each release.

The measured rates of ion momentum loss are represented in Figure 12 by plots of the Fabry-Perot fringe half-width at half-maximum versus time after release. Curves covering the first six minutes are shown for G-9, G-11A, and G-12. Release altitudes are indicated, and it is seen that steeper loss rates appear for lower altitude releases. The width of the G-12 profile begins at a lower value than that of the other releases because a smaller component of the satellite orbital velocity is perpendicular to the geomagnetic field. The curves for G-9 and G-11A, where the release velocities are nearly perpendicular to the magnetic field, are comparable with the modeled curves in Figure 11. (Results for the PTRACE simulation of G-12 have not been plotted yet.) The G-9 profile exhibits a sudden dramatic narrowing in the 100 to 120 second interval following release. Interpreting this discontinuity as a sudden loss of ion momentum, candidate causes are plasma instabilities or wave-particle interactions of a sort that would abruptly manifest itself when the plasma density decays to a certain level. Possibly Alfven waves were generated early in the release, and have reflected back from the southern hemisphere on this time-interval.

Ground based imagery of G-9 shows nothing remarkable occurring in the release cloud at this point in time. The wide-field camera images from the aircraft, co-aligned with the Fabry-Perot instrument, show the barium ion 455.4-nm emissions continuing to dim at a regular rate. The images also show that no appreciable change occurred in the camera look direction over the interval in question. Sets of these images are displayed in Figure 13. The third wide-field image appears brighter because the CCD frame integration time was doubled at this point to keep the fading cloud intensity within the instrument dynamic range.

Discussion

Acknowledgments. We wish to thank Test Directors Lt. Tim Heywood and Capt. Bryon Pedersen, and the many other U. S. Air Force personnel of the 4950th Tactical Wing at Wright-Patterson A.F.B. who made these campaigns possible. The efforts of the flight crews, ground crews, and the aircraft modification center staff are greatly appreciated. CRRES Project Scientist David Reasoner is remembered for his enthusiasm and energy in coordinating the efforts of all the participating investigator groups to maximize the science return of this program. In the Lockheed group we thank Steve Geller for software, Earl Aamodt and Francis Pang for hardware, and Hank Hancock, Jack Doolittle, and Gary Swenson for valuable assistance. This work was funded in part by NASA grant number NAS8-36630.

REFERENCES

Bernhardt, P. A., Probing the magnetosphere using chemical releases from the CRRES satellite, Phys. Fluids B, 4, 2249-2256, 1992.

Bernhardt, P. A., J. D. Huba, M. B. Pongratz, D. J. Simons, and J. H. Wolcott, Plasma irregularities caused by cycloid bunching of the CRRES G-2 barium release, J. Geophys. Res., 98, 1613-1627, 1993.

Born, M. and E. Wolf, Principles of Optics, 6th edition, p. 329, Pergamon Press, Oxford, 1980.

Drapatz, S. W., The radiative transfer problem in freely expanding gaseous clouds and its application to barium cloud experiments, Planet. Space Sci., 20, 663-682, 1972.

Foppl, H., G. Haerendel, L. Haser, J. Loidl, P. Lutjens, R. Lust, F. Melzner, B. Meyer, H. Neuss, and E. Rieger, Artificial strontium and barium clouds in the upper atmosphere, Planet. Space Sci., 15, 357-372, 1967.

Gatsonis, N. A., and D. E. Hastings, A three-dimensional model and initial time numerical simulation for an artificial plasma cloud in the ionosphere, J. Geophys. Res., 96, 7623-7639, 1991.

Haerendel, G., R. Lust, and E. Rieger, Motion of artificial ion clouds in the upper atmosphere, Planet. Space Sci., 15, 1-18, 1967.

Horak, A., and C. Whitaker, Resonance-fluorescence in barium ion clouds, Planet. Space Sci., 30, 897-907, 1982.

Huba, J. D., P. A. Bernhardt, and J. G. Lyon, Preliminary study of the CRRES magnetospheric barium releases, J. Geophys. Res., 97, 11-24, 1992a.

Huba, J. D., H. G. Mitchell, J. A. Fedder, and P. A. Bernhardt, 'Skidding' of the CRRES G-9 barium release, Geophys. Res. Lett., 19, 1085-1088, 1992b.

Mende, S. B., Morphology of the magnetospheric barium release, J. Geophys. Res., 78, 5751-5767, 1973.

Mende, S. B., G. R. Swenson, S. P. Geller, J. H. Doolittle, G. Haerendel, A. Valenzuela, and O. H. Baker, Dynamics of a barium release in the magnetospheric tail, J. Geophys. Res., 94, 17063-17083, 1989.

Mitchell, H. G., J. A. Fedder, J. D. Huba, and S. T. Zalesak, Transverse motion of high-speed barium clouds in the ionosphere, J. Geophys. Res., 90, 11091-11095, 1985.

Reasoner, D. L., Chemical release mission of CRRES, J. Spacecraft and Rockets, 29, 580-584, 1992.

Scholer, M., On the motion of artificial ion clouds in the magnetosphere, Planet. Space Sci., 18, 977-1004, 1970.

Shiner, L., Come to Aruba when the barium blooms, Smithsonian Air & Space, vol. 17, number 2, 56-65, February/March 1992.

Simons, D. J., M. G. Pongratz, and S. P. Gary, Prompt striations in ionospheric barium clouds due to a velocity space instability, J. Geophys. Res., 85, 671-677, 1980.

Stenbaek-Nielsen, H. C., Calculated emission rates for barium releases in space, Planet. Space Sci., 37, 1441-1452, 1989.

Stenbaek-Nielsen, H. C., E. M. Wescott, and T. J. Hallinan, Observed barium emission rates, J. Geophys. Res., 98, 17491-17500, 1993.

Wescott, E. M., H. C. Stenbaek-Nielsen, and D. Hampton, Results from the CRRES Ba, Sr, and Ca critical velocity experiments (abstract), Eos trans. AGU, supplement, 72, 230, 1991.

Wescott, E. M., H. C. Stenbaek-Nielsen, D. L. Hampton, and P. A. Delamere, Results of critical velocity experiments with barium, strontium and calcium releases from CRRES satellite, submitted to J. Geophys. Res., 1993.

R. L. Rairden and S. B. Mende, Lockheed Palo Alto Research Laboratories, Dept. 91-20, Bldg. 255; 3251 Hanover Street, Palo Alto, CA 94304.

M. B. Pongratz, Group SST-7, Mailstop D466; Los Alamos National Laboratory, Los Alamos, NM 87545.

(Received: _____;
revised: _____;
accepted: _____.)

Paper number 94JA_____.

FIGURE CAPTIONS

Figure 1. Lockheed Fabry-Perot camera optical set-up for the CRRES low-altitude Caribbean campaign. Camera installation was along the aircraft fuselage, facing into a large elliptical gyro-stabilized pointing mirror stationed at one of the 30-inch diameter optical grade windows.

Figure 2. Camera fields of view. Orion's belt shows relative alignment and scale. Both images are in white light (filters removed). The Fabry-Perot wheel is in the no-etalon position. Both fields are mirror-reversed, and one camera is inverted relative to the other.

Figure 3. Caribbean release area. Location of barium releases and corresponding aircraft coordinates at the time of each release are shown. Views of the releases are looking toward sunrise from the night side of the terminator. A few minutes after each release the direction of flight was slowly changed to follow ions southward along the magnetic field. Aircraft were temporarily based on the island of Aruba near the coast of Venezuela.

Figure 4. G-12 barium release filtered image sequence. Wide-field and narrow-field images at 8, 19, and 28 seconds after release show the ion cloud evolution. Fringes from the 2-mm Fabry-Perot etalon in the narrow-field camera reveal the double-peaked nature of the ion radial velocity distribution.

Figure 5. Selected Fabry-Perot images from the G-9 release. The time after release is indicated for each image. The decrease of fringe width is clearly evident.

Figure 6. Fabry-Perot images and profiles from the G-9 release illustrate the differing free spectral ranges for the 8-mm, 2-mm, and 0.5-mm etalons. Calibration lamp images and profiles provide the zero-velocity fringe radii (a spurious neon emission line in the lamp is disregarded). Profiles calculated for an infinitely narrow line are shown for comparison.

Figure 7. Fabry-Perot profiles from 2-mm etalon images: Stacked series from the first minute or two of releases G-9, G-11A, and G-12. Profiles are truncated after the innermost (highest resolution) fringe. Times are indicated. The bottom profile in each series is of the calibration lamp, used to locate the zero-velocity position. As in the previous figure, the abscissa is linear in image-space, but labeled in Doppler velocity.

Figure 8. Release geometries: Azimuthal plane projections at the release points, with north upward, of the satellite velocity vector, the geomagnetic field direction, and vectors toward the sun and toward the observer, for the G-9, G-11A, and G-12 releases. Ion trajectories southward along the field lines are illustrated schematically.

Figure 9. The solar spectrum in the vicinity of the 455.4-nm BaII resonance (Fraunhofer) line. Intensity is given both in $W/m^2/nm$ and as a fraction of the solar continuum, versus wavelength (angstroms) and the corresponding Doppler velocity. [Adapted from Stenbaek-Nielsen, 1989.]

Figure 10. Monte Carlo (PTRACE) simulations of the Fabry-Perot Doppler profiles for G-9 and G-11A as would be observed from the aircraft at four different times after release. The narrowing of the modeled profiles with time represents energy loss from ion-neutral collisions only. Modeled profiles compare well with observations shown in Figure 7.

Figure 11. Average ion velocity vs time after release, for three events, as modeled by the PTRACE Monte Carlo simulation code. Momentum loss calculations are due to ion-neutral collisions only, where the ambient neutral atom population varies with altitude.

Figure 12. Observed ion velocity decrease with time during the first six minutes following three releases. The early energy loss rate is steepest for G-11A, released at the lowest altitude, and shallowest for G-12, released at the highest altitude, an ion-neutral collisional effect. The width of the G-12 profile begins at a lower value than that of the other releases because a smaller component of the satellite orbital velocity is perpendicular to the geomagnetic field.

Figure 13. Wide field and Fabry-Perot image data obtained during the sudden ion energy loss observed in the G-9 release. The wide field images verify that no appreciable change in the camera look direction was responsible for the rapid decrease in fringe width. No qualitative change in the structure of the wide field barium ion scene is evident. (The third image is brighter because the frame integration time was doubled at this point.)

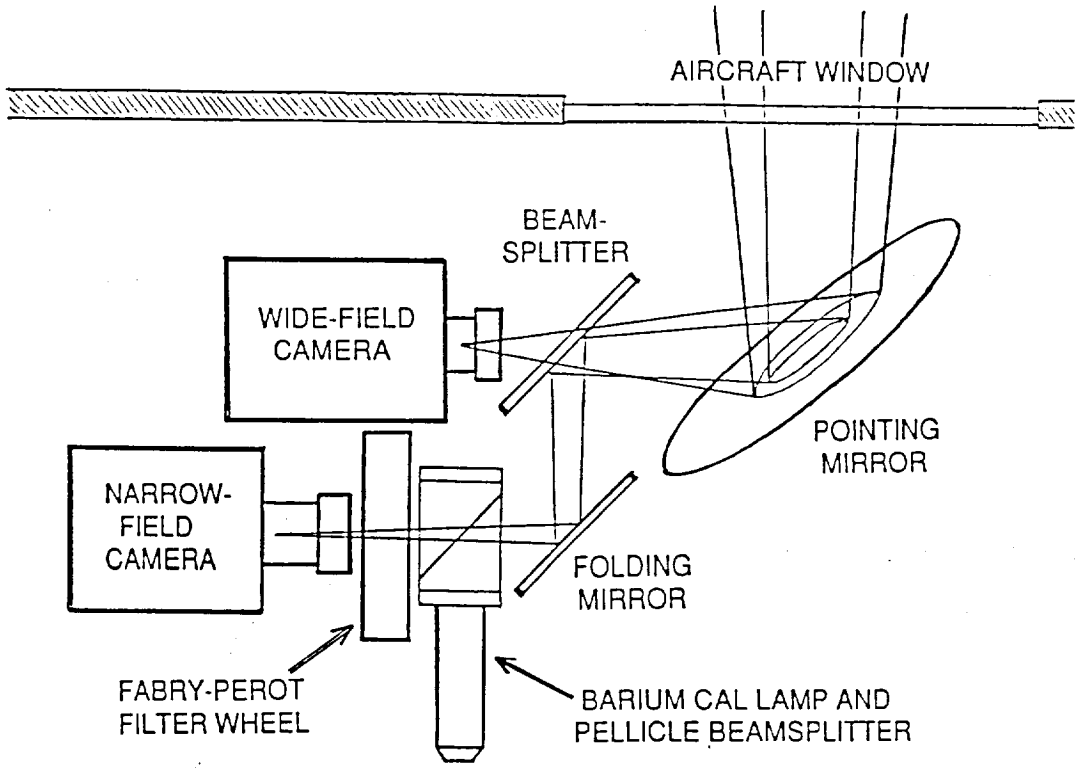

FIGURE 1. Lockheed Fabry-Perot camera optical set-up for the CRRES low-altitude Caribbean campaign. Camera installation was along the aircraft fuselage, facing into a large elliptical gyro-stabilized pointing mirror stationed at one of the 30-inch diameter optical grade windows.

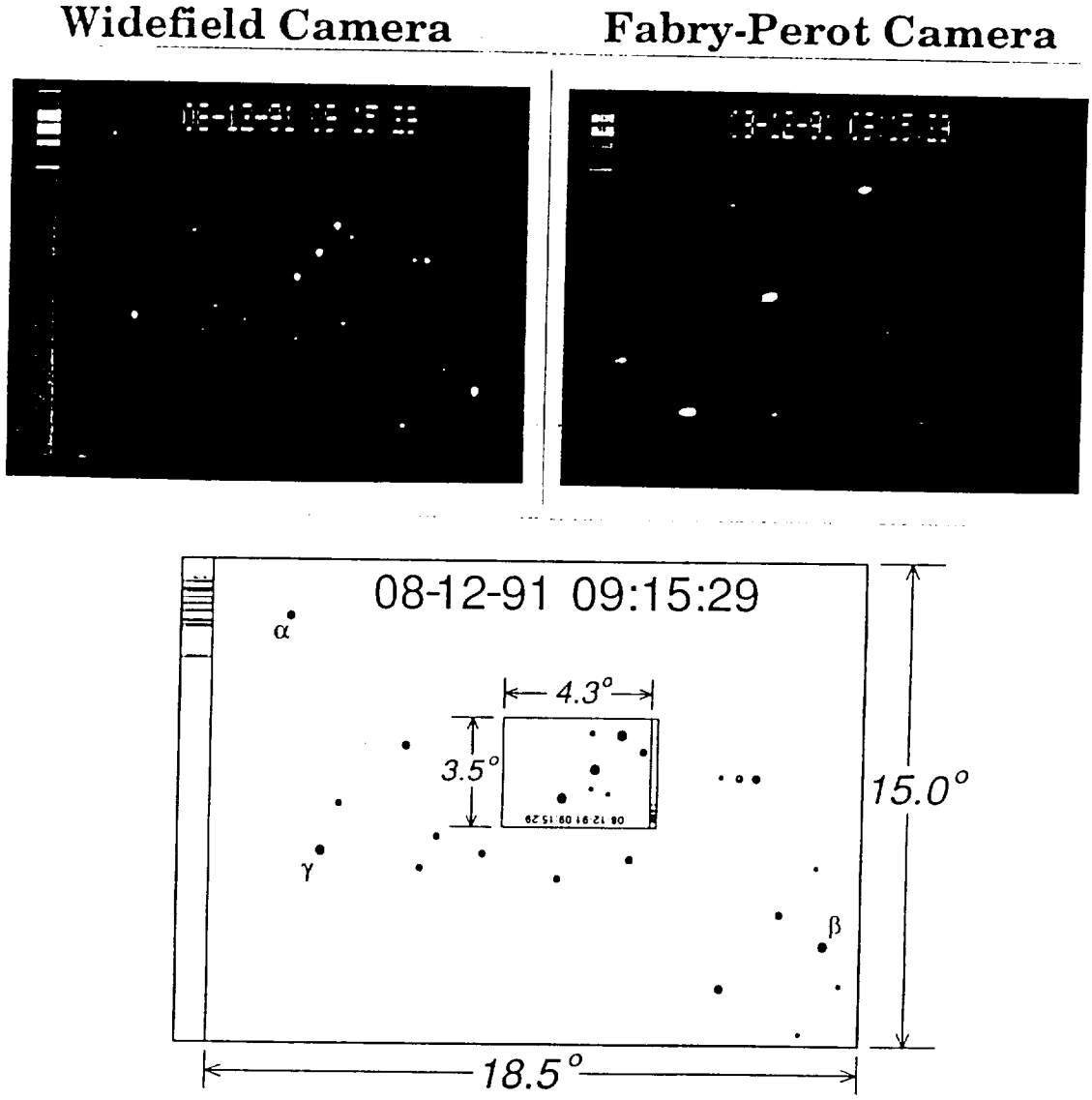

FIGURE 2. Camera fields of view. Orion's belt shows relative alignment and scale. Both images are in white light (filters removed). The Fabry-Perot wheel is in the no-etalon position. Both fields are mirror-reversed, and one camera is inverted relative to the other.

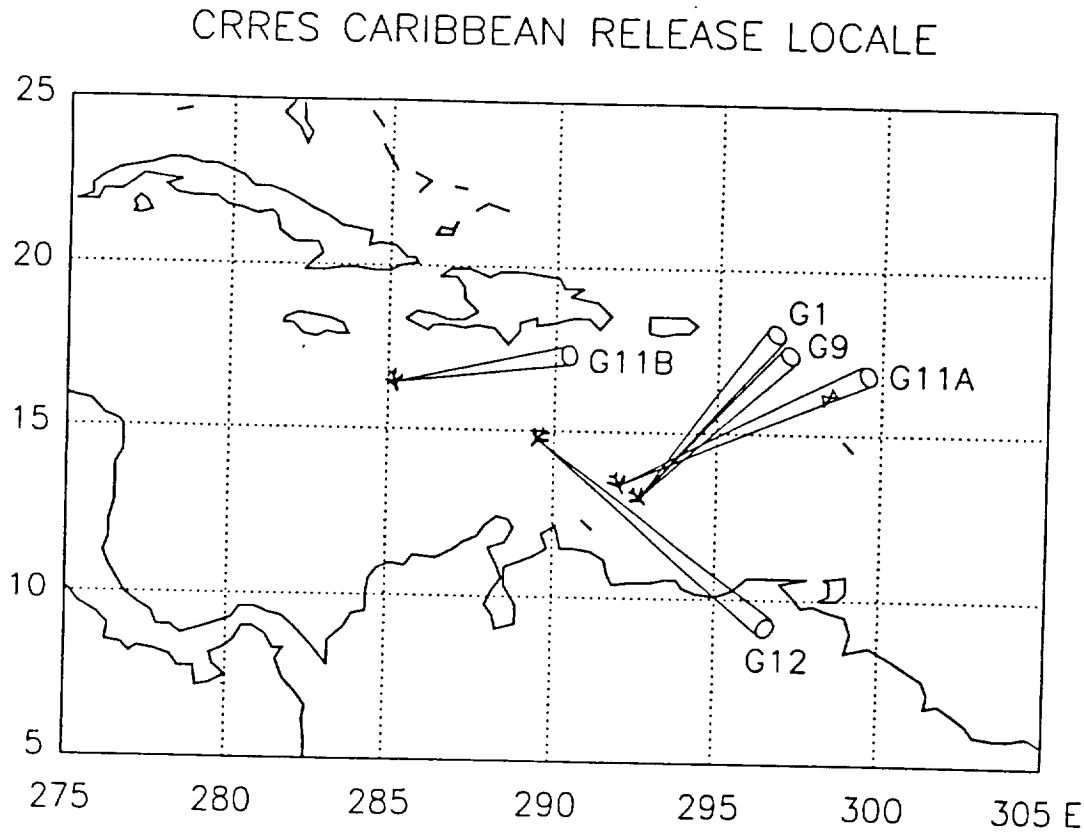

FIGURE 3. Caribbean release area. Location of barium releases and corresponding aircraft coordinates at the time of each release are shown. Views of the releases are looking toward sunrise from the night side of the terminator. A few minutes after each release the direction of flight was slowly changed to follow ions southward along the magnetic field. Aircraft were temporarily based on the island of Aruba near the coast of Venezuela.

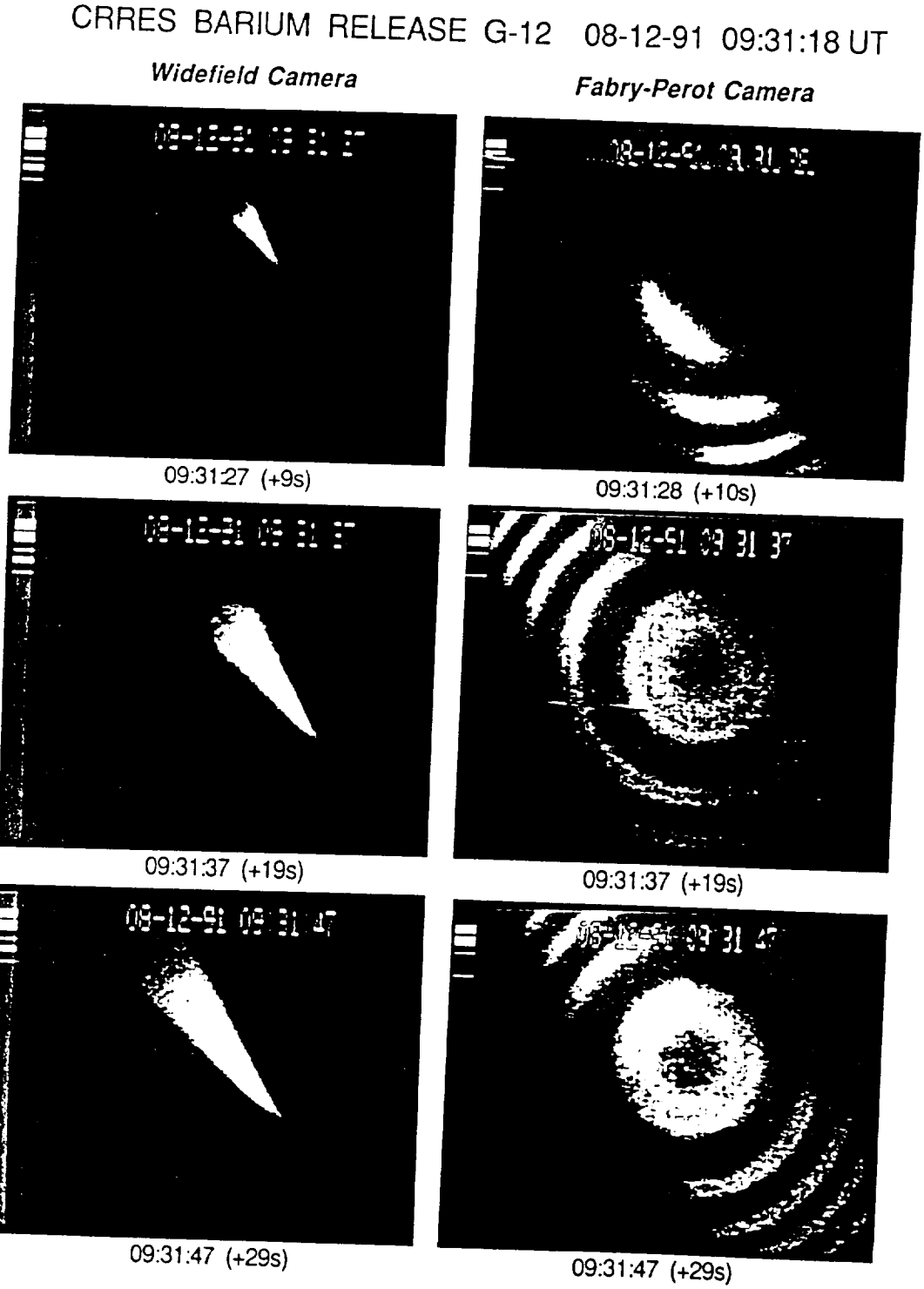

FIGURE 4. G-12 barium release filtered image sequence. Wide-field and narrow-field images at ~9, 19, and 29 seconds after release show the ion cloud evolution. Fringes from the 2-mm Fabry-Perot etalon in the narrow-field camera reveal the double-peaked nature of the ion radial velocity distribution.

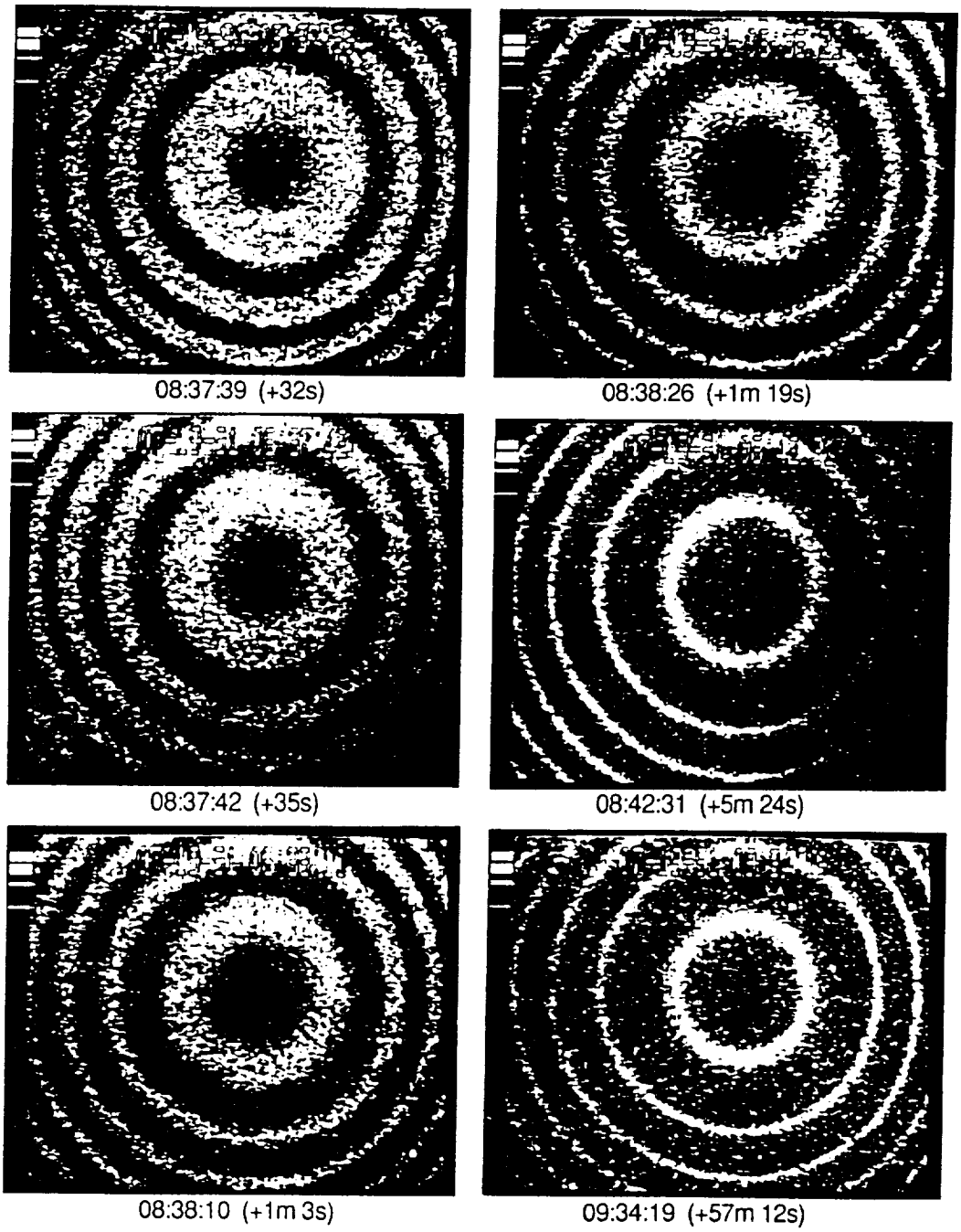

FIGURE 5. Selected Fabry-Perot images from the G-9 release. The time after release is indicated for each image. The decrease of fringe width is clearly evident.

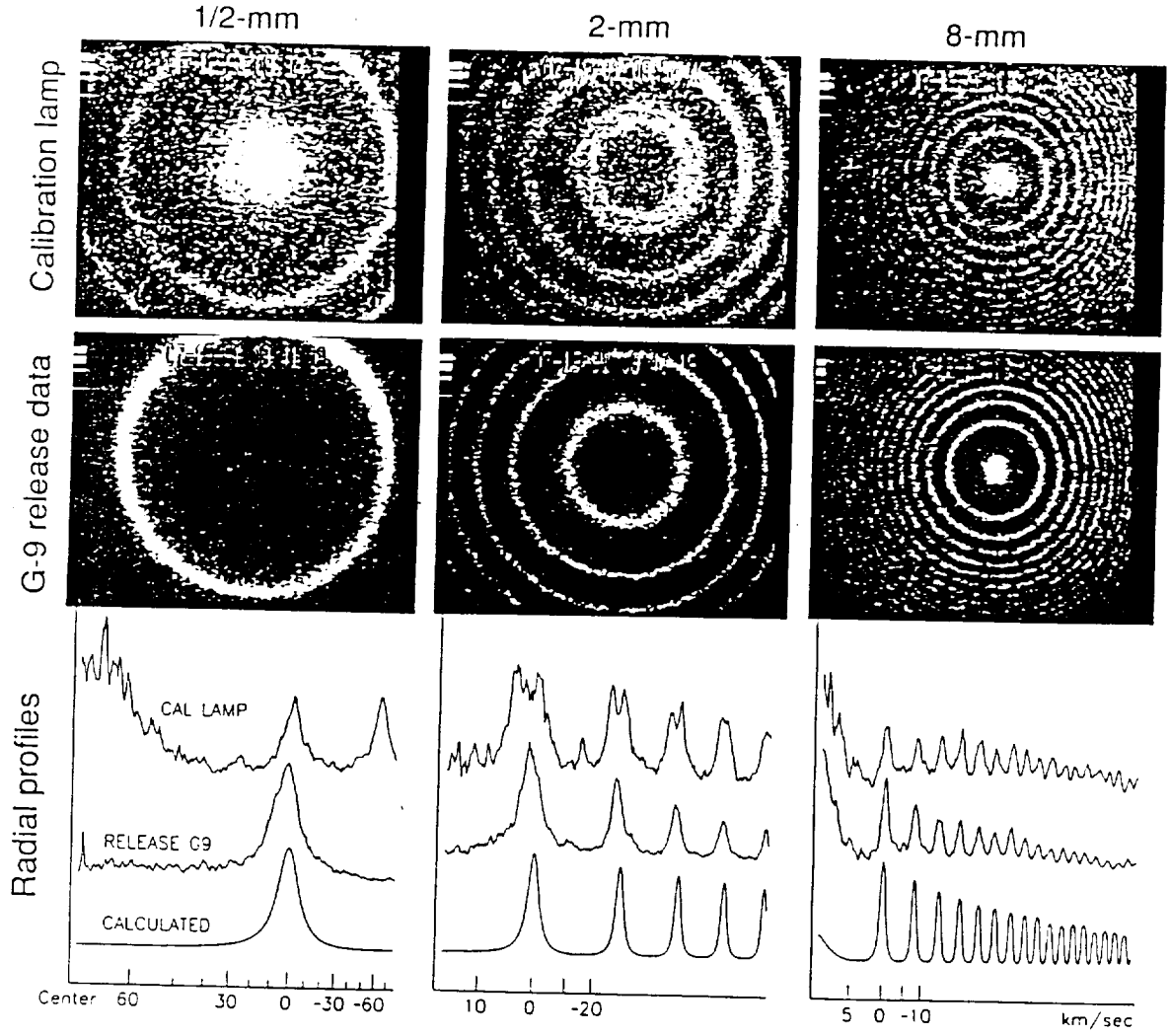

FIGURE 6. Fabry-Perot images and profiles from the G-9 release illustrate the differing free spectral ranges for the 8-mm, 2-mm, and 0.5-mm etalons. Calibration lamp images and profiles provide the zero-velocity fringe radii (a spurious neon emission line in the lamp is disregarded). Profiles calculated for an infinitely narrow line are shown for comparison.

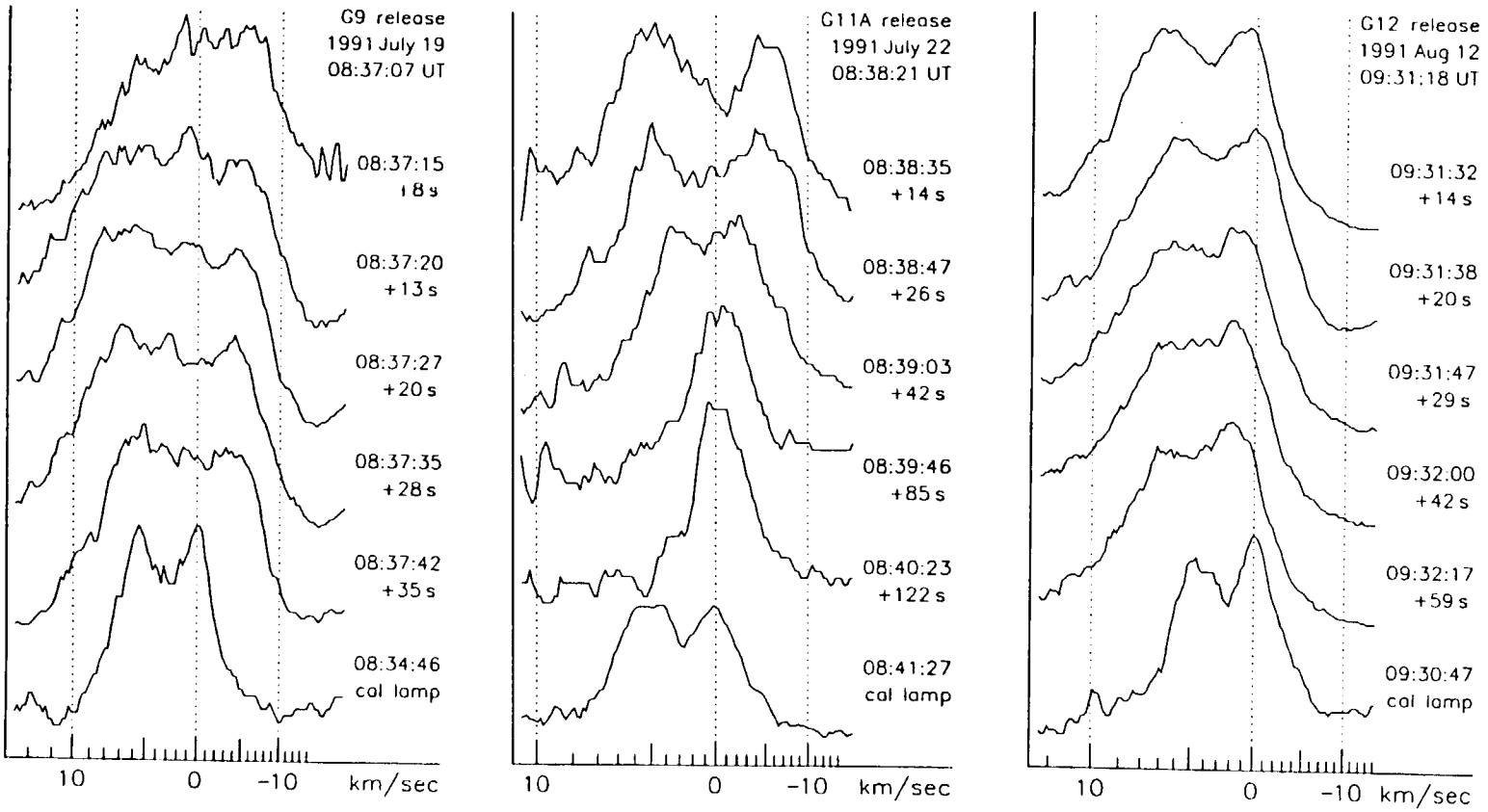

FIGURE 7. Fabry-Perot profiles from 2-mm etalon images: Stacked series from the first minute or two of releases G-9, G-11a, and G-12. Profiles are truncated after the innermost (highest resolution) fringe. Times are indicated. The bottom profile in each series is of the calibration lamp, used to locate the zero-velocity position. As in the previous figure, the abscissa is linear in image-space, but labeled in Doppler velocity.

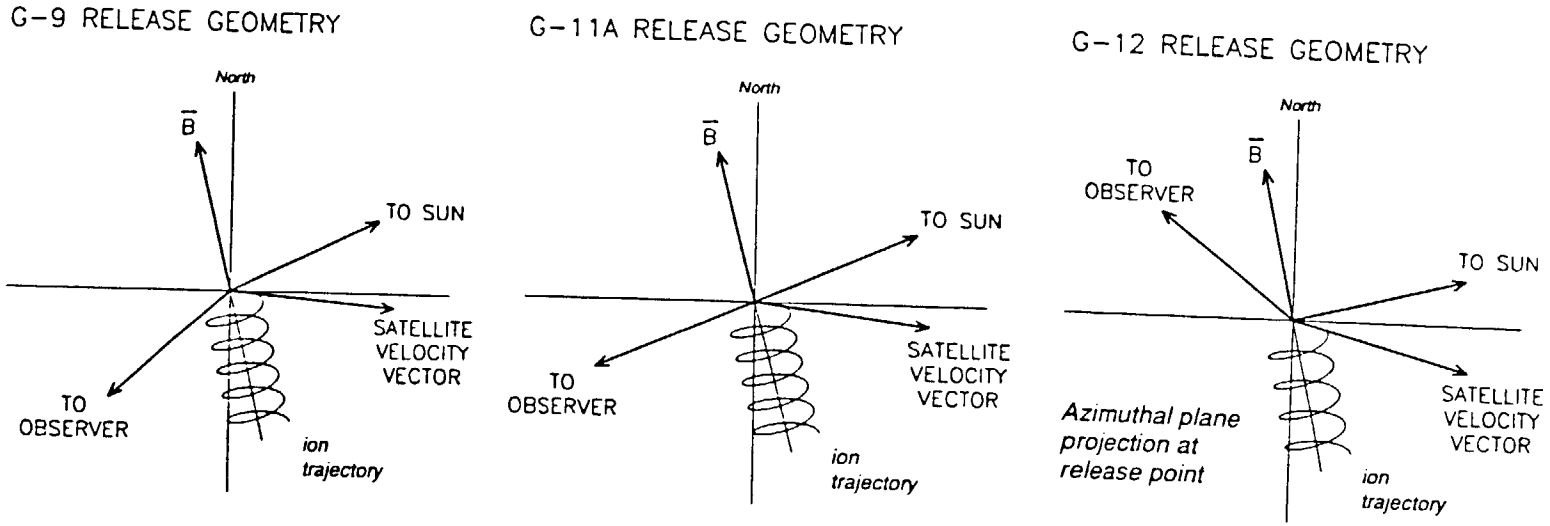

FIGURE 8. Release geometries: Azimuthal plane projections at the release points, with north upward, of the satellite velocity vector, the geomagnetic field direction, and vectors toward the sun and toward the observer, for the G-9, G-11a, and G-12 releases. Ion trajectories southward along the field lines are illustrated schematically.

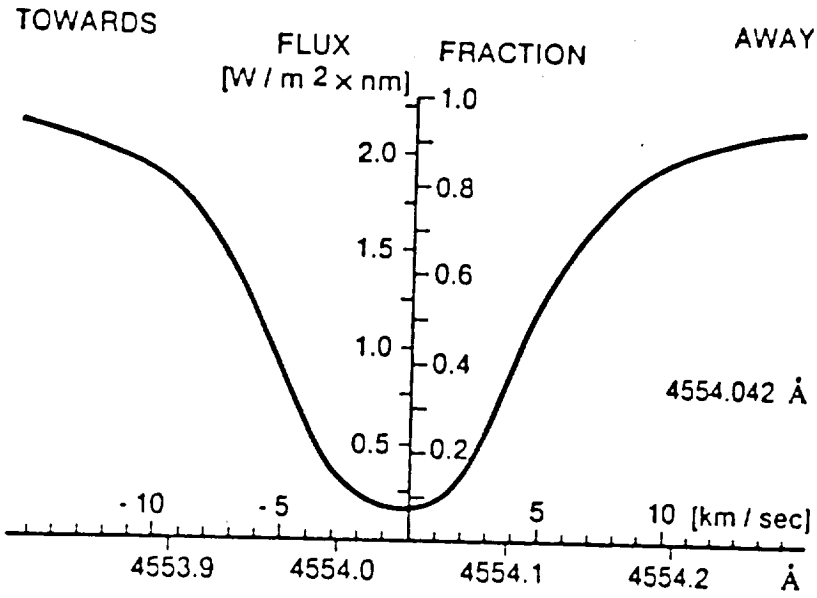

FIGURE 9. The solar spectrum in the vicinity of the 455.4-nm BaII resonance (Fraunhofer) line. Intensity is given both in W/m2/nm and as a fraction of the solar continuum, versus wavelength (angstroms) and the corresponding Doppler velocity. [Adapted from Stenbaek-Nielsen, 1989.]

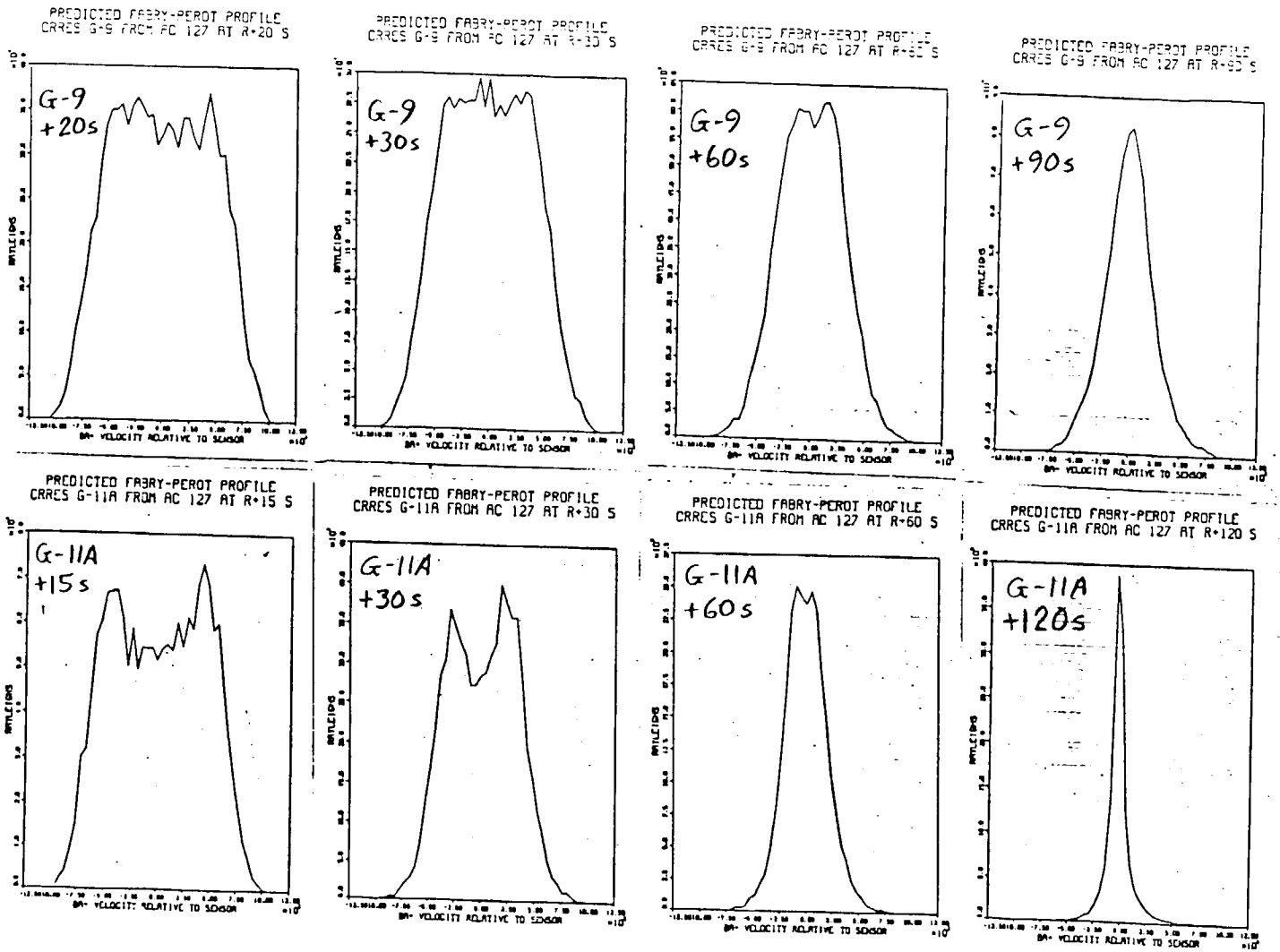

Figure 10. Monte Carlo (PTRACE) simulations of the Fabry-Perot Doppler profiles for G-9 and G-11A as would be observed from the aircraft at four different times after release. The narrowing of the modeled profiles with time represents energy loss from ion-neutral collisions only. Modeled profiles compare well with observations shown in Figure 7.

PTRACE Monte-Carlo Simulation of effect of ion-neutral collisions

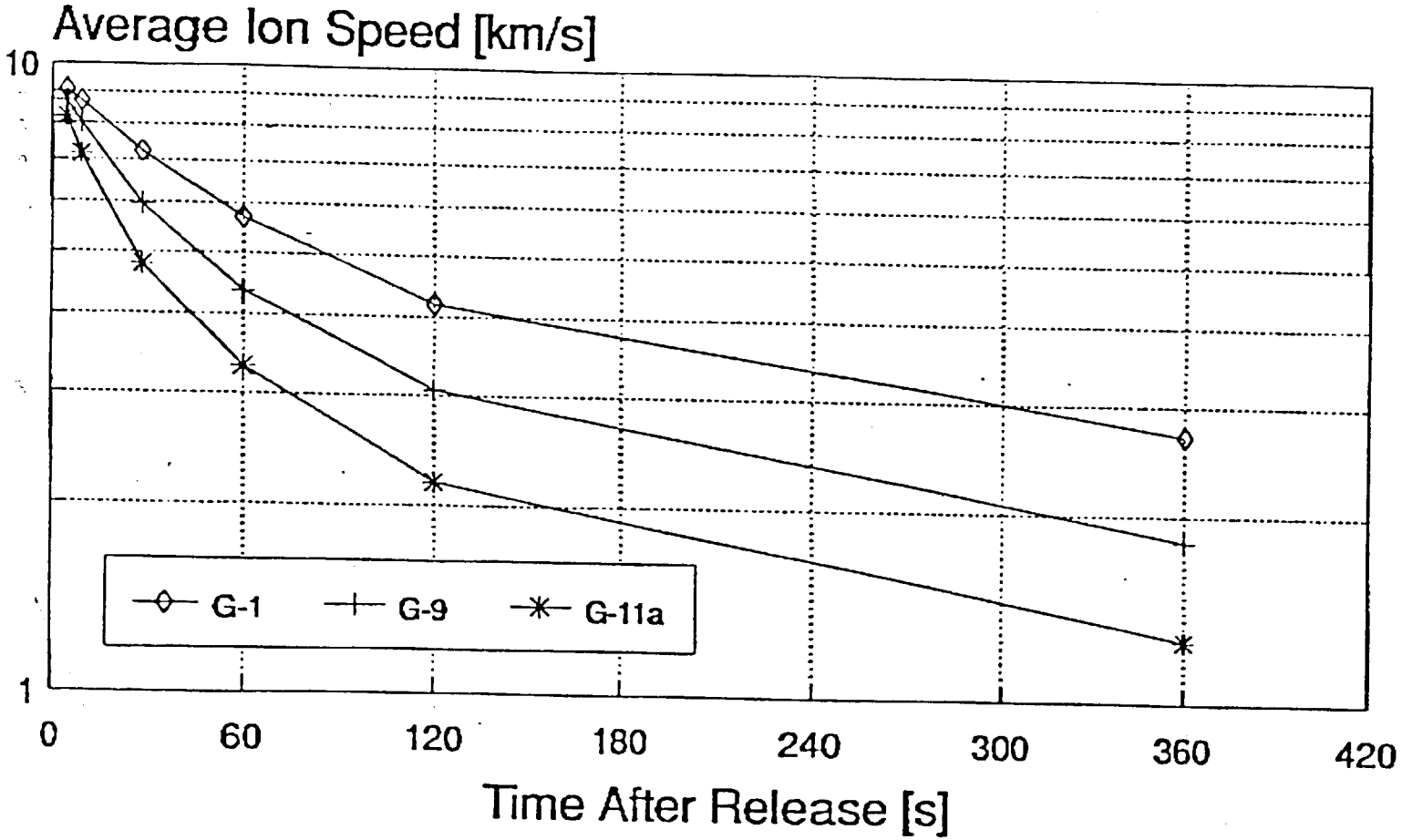

Figure 11. Average ion velocity vs time after release, for three events, as modeled by the PTRACE Monte Carlo simulation code. Momentum loss calculations are due to ion-neutral collisions only, where the ambient neutral atom population varies with altitude.

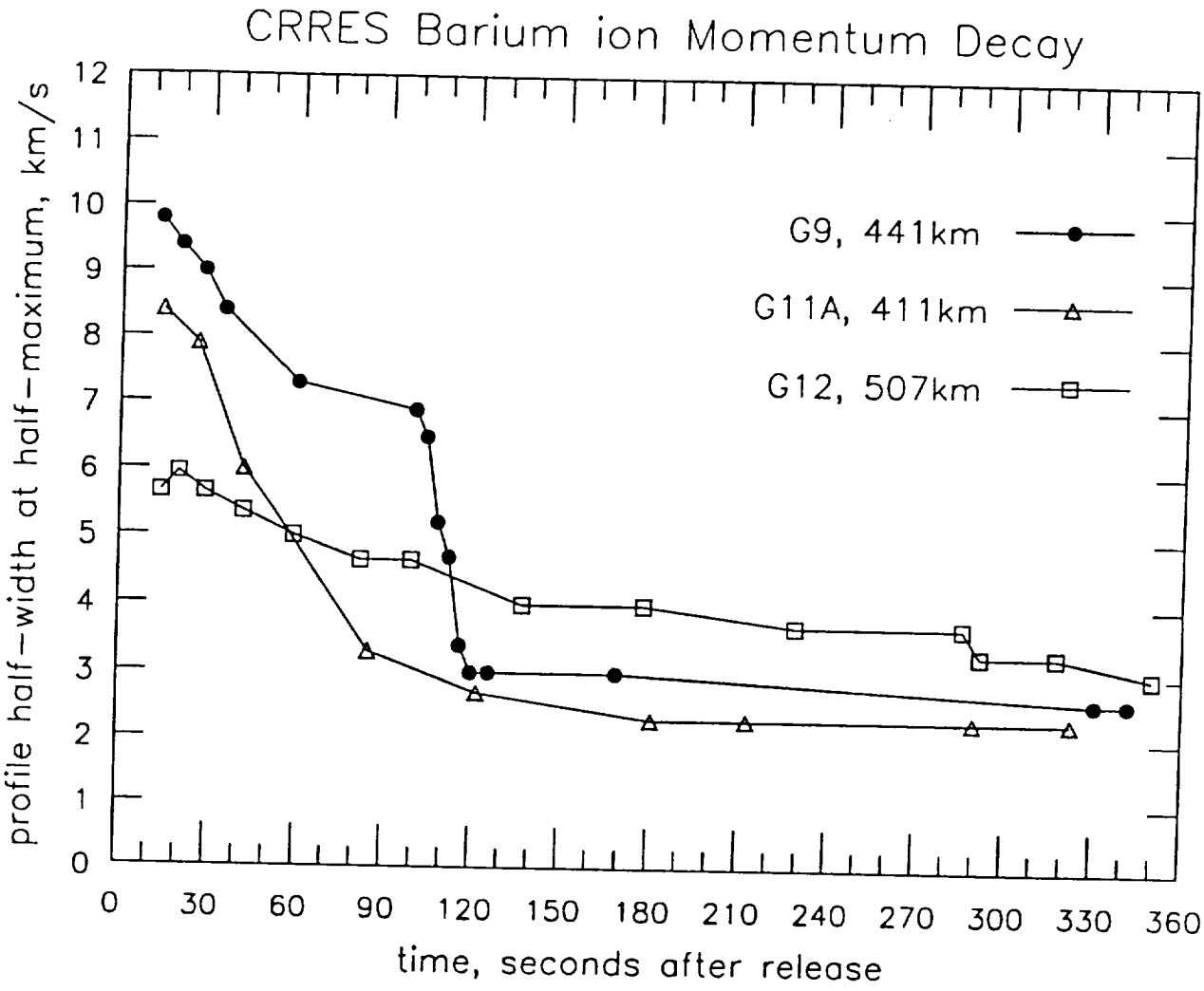

Figure 12. Observed ion velocity decrease with time during the first six minutes following three releases. The early energy loss rate is steepest for G-11A, released at the lowest altitude, and shallowest for G-12, released at the highest altitude, an ion-neutral collisional effect. The width of the G-12 profile begins at a lower value than that of the other releases because a smaller component of the satellite orbital velocity is perpendicular to the geomagnetic field.

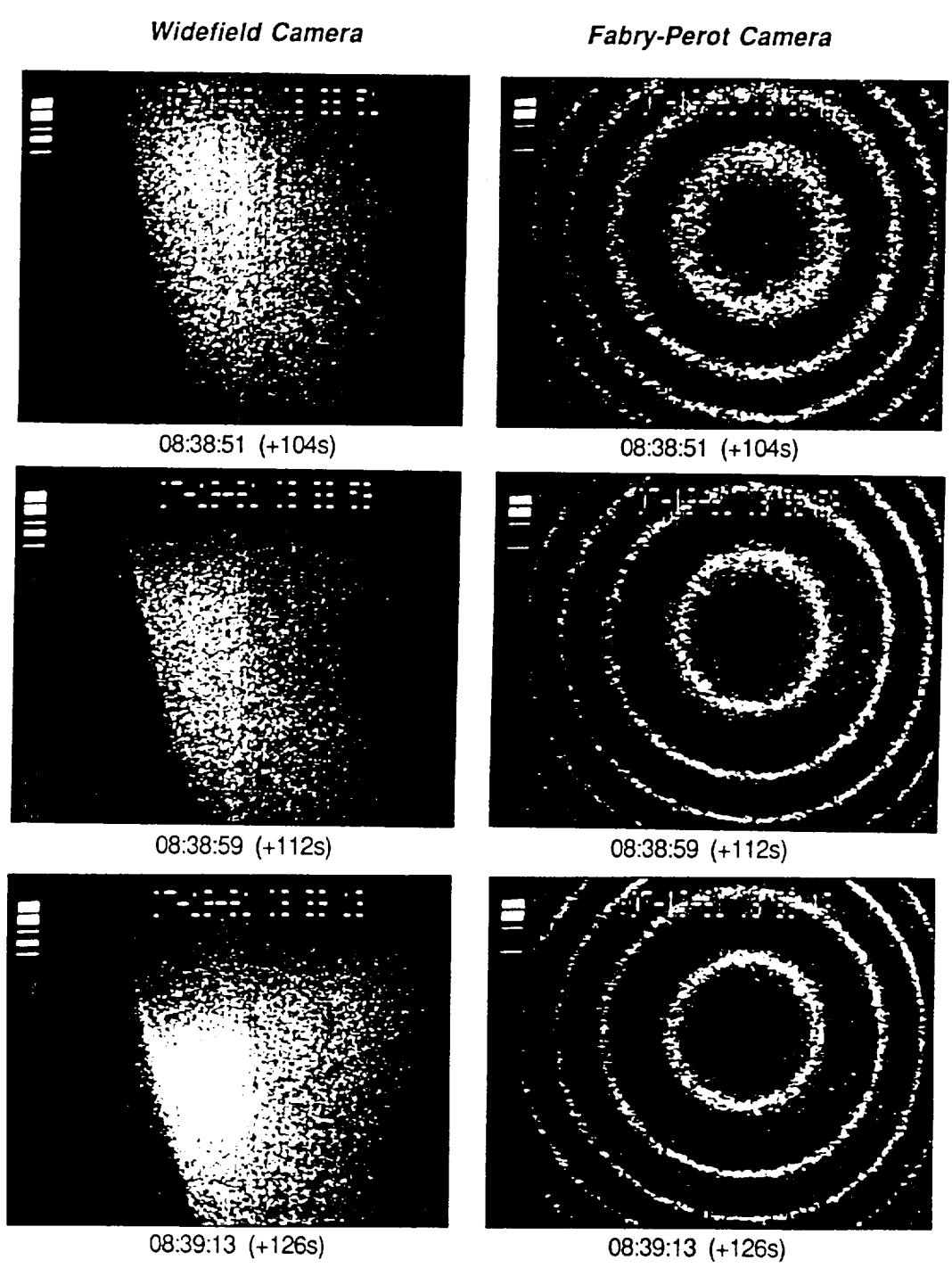

Figure 13. Wide field and Fabry-Perot image data obtained during the sudden ion energy loss observed in the G-9 release. The wide field images verify that no appreciable change in the camera look direction was responsible for the rapid decrease in fringe width. No qualitative change in the structure of the wide field barium ion scene is evident. (The third image is brighter because the frame integration time was doubled at this point.)

APPENDIX C

Report

CRRES Program G-6 Release

by

S.B. Mende

CRRES Program G-6 Release

by S. B. Mende

Contract number: NAS-8-36630

12 February 1991, 04:15:00 UT

EXPERIMENT OBJECTIVES:	Stimulation of Ion-Cyclotron Waves and Artificial Ion Precipitation
Principal Investigator:	S. B. Mende
Collaborative Investigators:	P. Bernhardt, G. Haerendel, T. Fritz, W. Peterson E. Wescott, D. Papadopolous, R. Smith, M. Pongratz, D. Simons, A. Valenzuela, R. Anderson
Location:	Approximately 6 Re outside plasmapause on field line accessible to Millstone Hill Radar.
Time:	Pre-Midnight Local Time Sector (2200-2400 LT)
Other Conditions:	Darkness over North America, Local Plasma Density $N < 1/cm^3$
Chemicals:	20 kg. Lithium (2 Large Canisters)

It is expected that the pre-midnight sector will be dominated by energetic protons which precipitate to form the pre-midnight proton aurora. The injection of an artificial cloud of cold Lithium plasma will lead to the generation of ion-cyclotron waves and these waves, in turn, will scatter protons into the loss cone leading to enhanced proton aurora. The enhanced precipitation will be detected by optical instruments at the foot of the field line and the CRRES/GTO wave and particle instrumentation will aid in determining the optimum conditions for release.

POINT OF CONTACT:

Steve B. Mende
LPARL
3251 Hanover St.
O/91-20, B/255
Palo Alto, CA 94304

SPAN - LOCKHD::MENDE
PHONE (415) 424-3282
FAX (415) 424-3333

EXPERIMENT ELEMENTS:

Coordinates of Release: 4.9N 76.1W 32249 km
Canister Type: Large
Chemicals:
6A TI 5770 gms, B 2604 gms, LI 457 gms, EU 299 gms
6B TI 5767 gms, B 2603 gms, LI 457 gms, EU 299 gms
Delay: None

RELEASE STRATEGY

The original goals of this release were to enhance ion cyclotron waves and thereby induce proton precipitation in the pre-midnight auroral oval. However, the earlier G5 release on the 18th of January failed to make a detectable electron precipitation event using whistler mode wave enhancements through cold plasma seeding. Thus it was argued that a successful repeat of the G5 release experiment would have satisfied the cold plasma induced precipitation goals of the CRRES program and the G-6 release was attempted to be released in conditions which would satisfy both the G5 and G6 requirements.

The experiment released produced a large ion cloud. Since Lithium ions are invisible, there was relatively little emphasis in monitoring the cloud development optically. The important optical observations were made by the two instrumented aircrafts which made observations of the aurora at the foot of the field line. If the experiment worked, the hot electrons which were measured in situ by the spacecraft should have been disturbed by the cold plasma and the waves produced inside of the cloud should have precipitated causing the artificial auroras. The airplanes were used to assure that the observations were not obscured by clouds. Operationally, the satellite control center gave the release command.

RELEASE CONDITIONS

For the successful release and detection of cold plasma injection produced precipitation, we required some very stringent release conditions.

The release conditions were as follows:

1. Lack of ambient cold plasma. Ambient plasma density as measured by the satellite should be less than 1 ~ 2. This condition was monitored by the University of Iowa experiment (R. Anderson).

2. Abundance of hot plasma mainly energetic electrons. This was monitored by the Lockheed or the AFGL experiment. The following basic considerations apply:

Synchronous altitude particles which are required to create plasma sheet precipitation can be obtained from Eather et al.[1976]. According to this, the plasma sheet precipitation is probably of the order of 1 ergs/cm^2/sec precipitation energy flux. This is equivalent to about 200 Rayleighs of 4278 and perhaps kR of 557 and probably about 3 kR of white light.

This energy intensity is equivalent to $1/\pi$ times this value or in particle flux per steradian, it is .318 ergs/cm^2/sec/sterad.

Thus, the .318 ergs/cm^2/sec/sterad is equivalent to 2×10^{11} eV (1.6×10^{-12} ergs/eV). Table 1 summarizes the required flux levels for various particles of different energy.

Table 1. kR Rayleigh Local Auroral Minimum Criteria

Omnidirectional energy flux of 2.0×10^8 keV/cm^2/sterad/sec

Particles of energy	Total Particle flux	Flux per keV
1keV	2.03×10^8	
2keV	1.04×10^8	5.20×10^7/keV
5keV	4.17×10^7	8.53×10^6/keV
10keV	2.03×10^7	2.03×10^6/keV
20keV	1.00×10^7	5.00×10^5/keV

These fluxes are absolute minimum for release criterion. During big substorms, the particle intensities go up by factors of 10 and 20.

The release had to be initiated 30 minutes prior. The G6 release was called around 3:45 UT to take place at 4:15. The release was called on the basis of geophysical parameters which would assure that the above conditions were met.

Although for a Lithium release the weather at the ground sites was not critical, the STC operation center monitored the weather. The weather is summarized in Table 2.

3. No discrete aurora. (Absence of confusing auroral precipitation at the foot of field line)

Table 2. Weather Conditions Prior to the G6 Release

Time	St Croix	Arecibo	Bonaire	El Leon	Cerro
2:11	Cld 50%	o.cast	Few clouds	Bad	
2:38	Clearing		OK		
3:00	Clearing		60%clear		
3:05	90%clear		60%clear	Bad	Good
3:26				Clearing	
4:38	90%clear		not good		

Time	Goddard	Wht Sands	Los Alamos	Lincoln Lab
2:11	90%clear	60%clear	clear	
2:38				
3:00	good	O. cast	Thin clouds	clearing
3:05	80%clear		good	
3:36				
4:38		Bad	OK	

At the STC operation center, the satellite auroral electron and cold plasma density were also monitored. The cloud release was based on these parameters. These parameters were documented as a function of time in Table 3.

Table 3. Geophysical Parameters for the G6 Release

	Time	K indx	Aurora 5577	GLf flux	GL anstr	Iowa density
2/11	18:56			1.1×10^9		
	19:16					2.0
	01:56	$3 \rightarrow 2$				
	02:26					
	02:30			2.4×10^9 streamers decreasing	1.9×10^9	
	02:31			2.5×10^9		2.0
	02:35	3		2.1×10^9 streamers gone	1.4×10^9	2.0 strong AKR
	02:55	4		1.8×10^9	1.2×10^9	2.0 AKR
	03:00	4	Diffuse aurora 4kR	2.7×10^9	1.9×10^9	2.0
	03:09			2.7×10^9	1.8×10^9	
	03:15	4		1.8×10^9	1.4×10^9	2.0
	03:30		6kR post break op			
	03:40	4		1.1×10^9	9.3×10^9	1.5 AKR
	04:37		1.8-3.5kR pulsating			
	05:03					
	03:59			8.4×10^8	7.1×10^8	
	04:05			7.5×10^8	6.2×108	
	04:10			8.2×10^8	6.7×108	
	04:15			7.2×10^5	5.6×10^5	
	04:18			5.9×10^8	4.8×10^8	
	04:23			7.4×10^8	4.4×10^8	
	04:28			5.4×10^8	4.0×10^8	
	04:32			5.2×10^5	3.9×10^5	

It can be seen that the electron threshold was above the 2×10^8 keV/cm^2/sterad/sec. An additional consideration for the release was the position of the satellite. In Table 4, we summarize the satellite parameters near apogee.

Table 4. Ephemeris Extrapolation for CRRES

Day	UT	Rev	GLAT	WLON	ALT	BTOT	BINT	GMLAT	GMLON	GMLT	L	SDANG
02/12/91	04:00:00	491	5.65	74.77	31535.	145.	157.	16.39	356.08	22:44	6.592	10.15
02/12/91	04:15:00	491	4.93	76.25	32242.	135.	147.	15.65	354.56	22:54	6.662	08.67
02/12/91	04:30:00	491	4.24	77.81	32797.	127.	140.	14.92	352.96	23:03	6.708	07.37
02/12/91	04:45:00	491	3.55	79.43	33203.	122.	135.	14.20	351.32	23:13	6.730	06.25
02/12/91	05:00:00	491	2.87	81.09	33462.	117.	131.	13.46	349.64	23:22	6.728	05.35
02/12/91	05:15:00	491	2.19	82.76	33576.	115.	129.	12.73	347.94	23:31	6.704	04.70
02/12/91	05:30:00	491	1.51	84.45	33545	113.	129.	11.98	346.25	23:41	6.658	04.32
02/12/91	05:45:00	491	0.83	86.12	33370.	113.	130.	11.22	344.57	23:50	6.589	04.25
02/12/91	06:00:00	491	0.13	87.77	33049.	115.	132.	10.44	342.93	23:59	6.500	04.50
02/12/91	06:15:00	491	- .58	89.38	32581.	118.	136.	09.64	341.35	00:09	6.388	05.05
02/12/91	06:30:00	491	-1.31	90.92	31962.	122.	142.	08.82	339.83	00:19	6.255	05.89
02/12/91	06:45:00	491	-2.06	92.39	31189.	128.	150.	07.97	338.41	00:29	6.100	07.00
02/12/91	07:00:00	491	-2.84	93.74	30256.	137.	161.	07.09	337.10	00:40	5.923	08.34
02/12/91	07:15:00	491	-3.67	94.95	29158.	150.	175.	06.18	335.95	00:51	5.722	09.92
02/12/91	07:30:00	491	-4.54	95.98	27887.	166.	194.	05.23	334.99	01:03	5.498	11.71

For the positioning of the air plane several field models were evaluated for the time of the release. The 4:15 position of the foot of the field line is shown in Table 5. Note at the time of release, the K_p was 4, therefore, it is the last line of Table 3 which is applicable. This model is based on the TU model.

On Figure 1, we show the Millstone Hill radar convection plots. The Millstone Hill group has also inserted their prediction of the foot of the field line for 04:15 UT. The convection plot was generated from data taken at 04:05.

SUMMARY

The G6 release did not accomplish its stated scientific goals and the results are inconclusive. Operationally every condition was satisfied. The ambient cold plasma density was down to 1.5 electrons per cm^3, the energetic electrons were above the 2×10^8 keV/cm2/sterad/sec threshold. However it was very difficult to predict the situation in advance and the auroral situation over the airplanes were very confused at the time the effect should have manifested itself. A small enhancement in the aurora, which was expected to occur following the plasma injection could not be detected in the presence of the natural auroral displays which occurred. Just before calling the release at 04:37 the airplane reported auroral pulsations of 1.8 - 3.5 kR in strength. It was hoped that this level of aurora would not be detrimental to the observations and that it would weaken with time. This weakening did not occur. Thus the G6 release experiment could not be used to show that cold plasma releases can be responsible for increased precipitation.

Table 5. Satellite (Lat, Lng, Ht)

1991 2/12 4:15: 0
Field Line Base (100 Km Height) is:

KP =	0	N.LAT =	52.09	E.LONG =	-77.92
KP =	0+	N.LAT =	52.80	E.LONG =	-78.01
KP =	1-	N.LAT =	52.66	E.LONG =	-78.03
KP =	1	N.LAT =	52.52	E.LONG =	-78.08
KP =	1+	N.LAT =	52.45	E.LONG =	-77.99
KP =	2-	N.LAT =	52.36	E.LONG =	-78.07
KP =	2	N.LAT =	52.13	E.LONG =	-78.09
KP =	2+	N.LAT =	52.31	E.LONG =	-78.07
KP =	3-	N.LAT =	52.05	E.LONG =	-78.07
KP =	(3,3+)	N.LAT =	51.76	E.LONG =	-78.07
KP =	>3+	N.LAT =	51.21	E.LONG =	-78.27

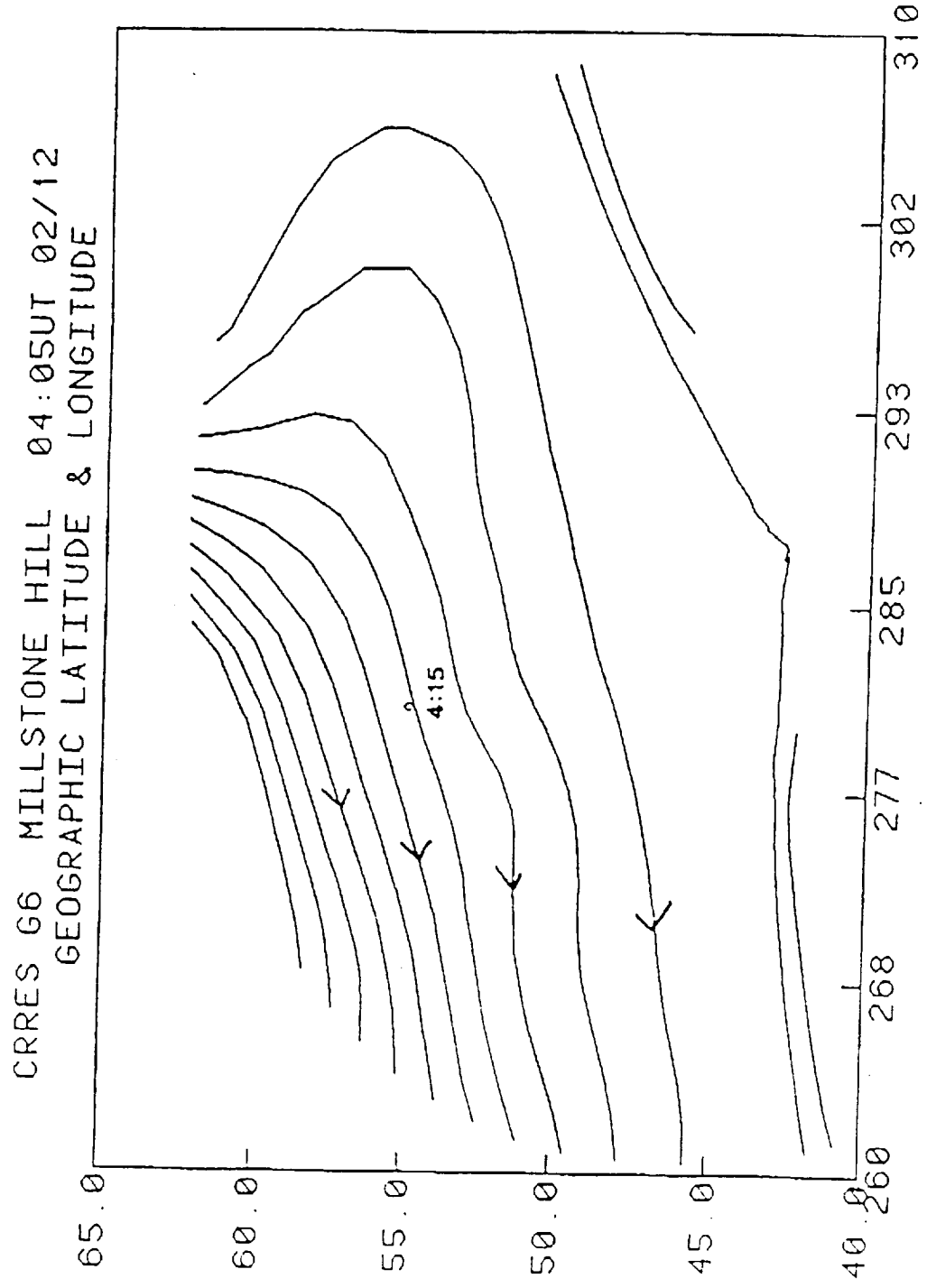
CRRES G6 MILLSTONE HILL 04:05UT 02/12
GEOGRAPHIC LATITUDE & LONGITUDE
65.0
60.0
55.0
50.0
45.0
40.0
260
268
277
285
293
302
310
4:15

APPENDIX D

Report on CRRES Program G-4

Release by S.B. Mende

EXPERIMENT G-4

By S. B. Mende

16 January 1991, 06:25:00 UT

EXPERIMENT OBJECTIVES: Diamagnetic Cavity, Plasma Coupling

Principal Investigator:	S. B. Mende
Collaborative Investigators:	M. B. Pongratz, D. Papadopolous, R. Smith, R. Anderson, Young, H. Singer, E. Szuszczewicz, E. Wescott, H. C. Stenbaek-Nielsen, G. Haerendel, A. Valenzuela, P. A. Bernhardt, J. D. Huba.
Location:	0.7 degrees S, 53.8 degrees W
Time:	06:25:00 UT.
EXPERIMENT ELEMENTS:	Coordinates of Release: 0.7S 53.8W 23977 km Canister Type: Small Chemicals: TI 1271 gms, B 574 gms, BA 1471 gms, SR 19 gms Delay: None
Model Calculations:	Ted Fritz LANL MS-D438 Los Alamos, NM 87545 SPAN - ESSDP1::FRITZ PHONE (505) 667-9234 FAX (505) 665-3332
POINT OF CONTACT:	Robert Hoffman GSFC CODE 696 Greenbelt, MD 20771 SPAN - DE696::U6RAH PHONE (301) 286-7386 FAX (301) 286-9240

STATION COVERING THE RELEASE:
Caribbean - St. Croix, USVI Arecibo, PR
North America - Boston, MA Long Key, FL Los Alamos, NM White Sands, NM
South America - Cerro Tololo, Chile El Leoncito, Argentina

Note: The results of the G-4 release and its relationship to G-2 and G-3 are summarized in the following report.

CRRES G-4 Release Triangulation and its Relationship to the G-2 and G-3 Releases

S. A. Fuselier, S. B. Mende 7-22-93

From 13 to 16 January, 1991, a series of 3 small barium canisters were released by the CRRES spacecraft at different altitudes. The objectives of this series of releases were to study diamagnetic cavity formation, unstable velocity distribution and coupling of the cavity to the ambient plasma. Table 1 shows the dates, times, geographic coordinates and altitudes of the three releases.

Name	Date	Time	Latitude	Longitude	Altitude
G-2	13 Jan 1991	0217:03 UT	16.9°	-103.1°	6,180 km
G-3	15 Jan 1991	0411:00 UT	17.9°	-97.5°	15,063 km
G-4	16 Jan 1991	0625:00 UT	-0.7°	-53.8°	23,977 km

This report describes the results of the G-4 triangulation. However, the relationship between this release and the other two in Table 1 is important for understanding the coupling of the cavity to the ambient plasma. Therefore, this report also contains a comparison of the G-4 releases with the other releases in the series.

Several ground stations participated in the G-4 release. However, not all stations provide favorable baselines for triangulation of the cloud. The plasma cloud that forms in a barium release of this type striates along the magnetic field, which is approximately perpendicular to the equator in geographic coordinates. Newly formed barium ions are relatively free to move along the magnetic field but motion perpendicular to the magnetic field direction is controlled by the coupling of the plasma cloud to the ambient plasma. Understanding this coupling is a major objective of this series of Barium releases, so it is desirable to obtain the motion of the cloud perpendicular to the magnetic field (through triangulation from two different ground stations). This favors ground stations with large east-west ground baselines, and not baselines with primarily north-south baselines.

Triangulation of the G-4 release was initially done using Arecibo (PR) and Long Key (FL) data. However, these stations were only ~14° apart in longitude. Triangulation errors due to the small longitude spread and distance of the release (~4 R_E altitude) were relatively large (~0.03 R_E).

To improve the triangulation, we chose to use a larger baseline consisting of Breezy Point (Los Alamos, NM) and Arecibo (PR) ground stations. These stations have the advantage that they are separated by almost 40° in longitude and, because the Arecibo data is in video tape form, essentially all images from Breezy Point can be paired with an Arecibo image.

The drawback of this baseline is that after the first minute, the Breezy Point data does not have a time code. However, extremely accurate timing (~ seconds) was not necessary since observable changes in the cloud position occurred over time intervals closer to 30 seconds. The station leader for Breezy Point (Morrie Pongrantz) reviewed the Breezy point data and, using simultaneous video images taken at the same location, has been able to reconstruct the time sequence of the Breezy Point images with reasonable accuracy.

We have triangulated the first 7 minutes of data from the two ground stations. After this, multiple striations and fading of the cloud caused it to be nearly lost from the Breezy

Point images despite the fact that the cloud was tracked for over 45 minutes at Arecibo. Although this appears to be a short amount of time, it was sufficient to obtain a very good history of the cloud motion and deduce details of the coupling of the cloud to the ambient plasma.

As with the G-2 release, the triangulation was done using the "CRRESTR2" program in the CRRES directory on the Lockheed VICOM computer. The following is a list of the image pairs with some brief comments. The image data files can be found in the CRRES directory in the following format:

BP021758 - BP = Breezy Point, 021758 = the center time of the image in hhmmss

Also listed are the data files containing the triangulated points. These can also be found in the CRRES directory.

Images		Triangulated	comments
Breezy Point	Arecibo	data filename	
BP062501	AR062502	crrestr0625a1.pt	Just after release
BP062532	AR062529	crrestr0625a2.pt,	
BP062558	AR062557	crrestr0625a3.pt	
BP062631	AR062629	crrestr0626c1.pt	
BP062657	AR062656	crrestr0626c2.pt	
BP062727	AR062727	crrestr0627c.pt	
BP062806	AR062806	crrestr0628c1.pt	
BP062858	AR062858	crrestr0628c2.pt	
BP062937	AR062940	crrestr0629c1.pt	
BP063029	AR063028	crrestr0630c1.pt	
BP063134a	AR063433a	crrestr0631c1.pt	
BP063252	AR063252	crrestr0632c1.pt	

A typical triangulated data file contains the triangulated points at a few different positions along the ionized cloud. Since the Arecibo camera was filtered for the barium ion line it does not show the neutral cloud(?). At least in the first minute, the Breezy Point data do not show a separation of the cloud and trail.

Triangulation Procedure

Triangulation was performed using the triangulation computer codes developed for the AMPTE barium releases [Mende et al., 1989]. Arecibo images were digitized from video tape at the Lockheed Palo Alto Research Laboratory image data analysis facility. Breezy Point images were digitized from 35 mm film by Mary Miller at GSFC. These digitized images were copied onto the Lockheed VICOM computer. Using a star catalog on the VICOM computer with the position of stars down to 9th magnitude, the star field in the image was matched and positions of the stars were overlayed onto the video image to verify that the conversion from video image pixel location to right ascension and declination was accurate. Once this was accomplished, two stars (relatively far from one another) were selected as reference stars for the triangulation. The triangulation program used these two stars to assign right ascension and declination values to arbitrary pixel locations on the image by linear interpolation. After reference stars for an image pair were selected, triangulation was performed using software designed to determine the geographic coordinates of a location on the cloud. An example of a triangulated point on one of the G-4 release image pairs that illustrates the procedure is shown in Figure 1. The upper panel of that figure shows the Arecibo image at 0631:33 UT (6 min, 33 s after release) while the

lower panel shows the Breezy Point image at the same time (note that the images are rotated relative to one another.

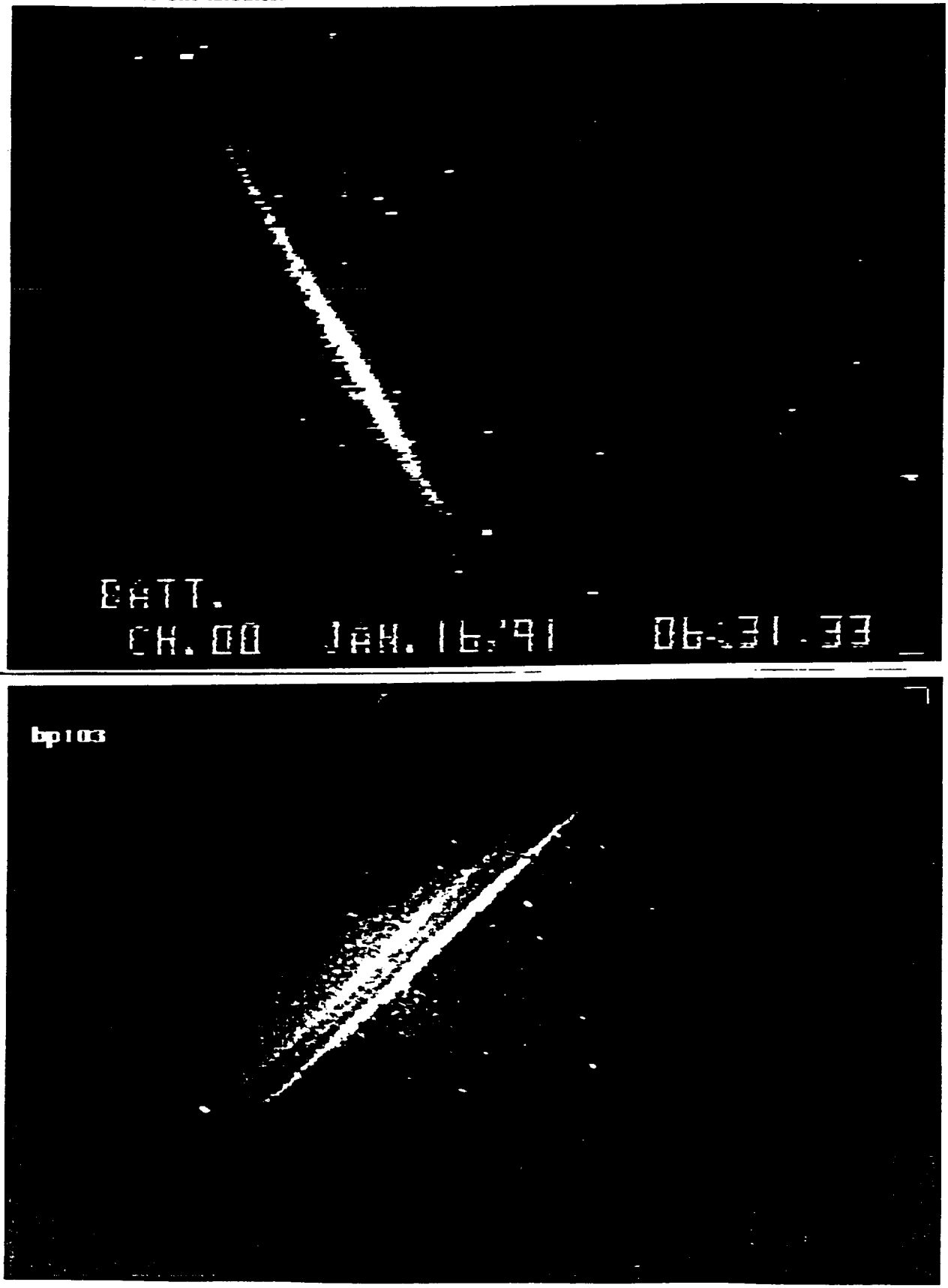

Figure 1

To triangulate the point on the image, the operator selects a point on the first image (shown by the cross in the upper panel of Figure 1), then, using an assumed cloud distance, the computer swaps images on the video display and draws a line centered on the assumed cloud distance (initially, this is chosen to be the spacecraft distance) and with length equal to 0.2 R_E on the second image. An example of the line is shown in the lower panel in Figure 1. This line is centered on an assumed distance of 4.61 R_E. The operator now chooses the location on the second image along the line that appears to correspond best with the point chosen in the first image. In the example in the lower panel of Figure 1, this point would be where the line drawn by the computer and the white cloud intersect. Once selected, the geographic coordinates of the triangulated point are stored in a data file. The process is repeated until several points along the cloud are triangulated.

The fact that the line drawn by the computer and the cloud are nearly perpendicular is simply the result of the fact that the baseline is nearly east-west while the cloud striates along the nearly north-south magnetic field. For north-south baselines, the angle between the line and the cloud would be much smaller and would result in significant uncertainty in the triangulated position.

Because of the large distance between the observer and release point, the uncertainty in the measurements was relatively large for the G-4 triangulation. The error was reduced somewhat by using a large baseline (one of the largest available) than the other releases (discussed below). The error in the triangulated measurement appears to be about 0.008 R_E based on the scatter in the points used to define the center of the cloud and on the computed distance between adjacent pixels on the image.

To illustrate the improvement in the triangulation procedure when the cloud distance is much smaller, Figure 2 shows a pair of images taken approximately 1 minute after the G-2 release. The upper panel of Figure 2 shows the digitized image from Rosemary Hills (FL) while the lower panel shows the digitized image from Breezy Point. The baseline is somewhat smaller but still comparable to the baseline used in the G-4 triangulation and the identical camera system was used at Breezy Point for both the G-2 and G-4 releases. The cross in the upper panel in Figure 2 shows a selected position on the Rosemary Hills image while the lower panel shows the 0.2 R_E long line centered on the assumed distance (in this case, 1.97 R_E). Comparing the lower panels of Figures 1 and 2, it is clear that the uncertainty in the cloud position due to the finite size of a pixel on the image is much smaller for the G-2 release near the Earth compared to the G-4 release almost 2.5 times further away.

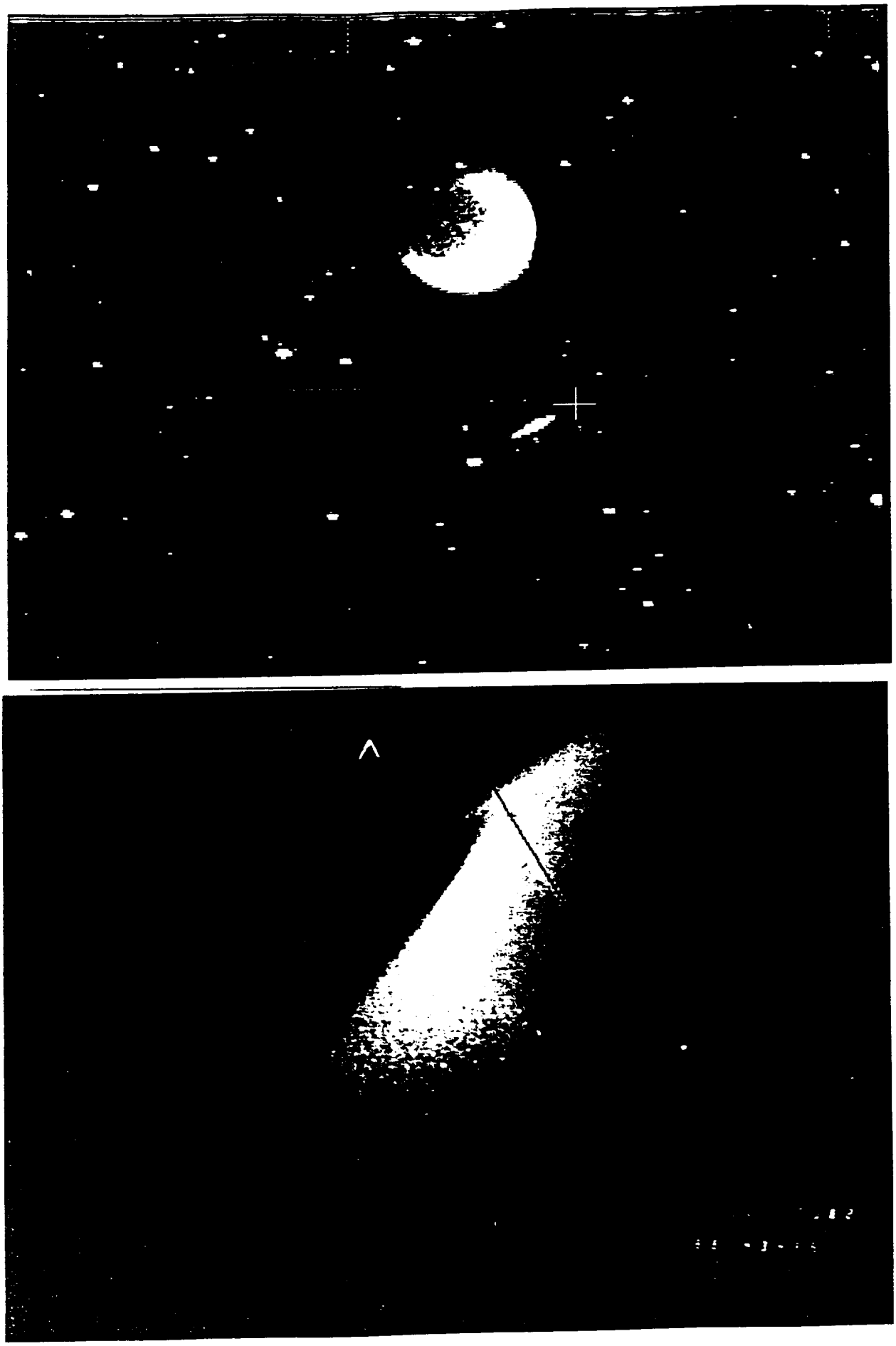

Figure 2

Analysis of Triangulation Results

Early chemical releases at high altitudes showed that the cloud striates along the local magnetic field [e.g., Mende et al., 1973]. We use this fact as a consistency check on the triangulated data and also to simplify the determination of the motion of the cloud with respect to the background plasma.

As a consistency check, the triangulated positions along the cloud should line up along the local magnetic field. To test this, we use the model magnetic field contained in the CRRES spacecraft ephemeris. Differences between the triangulated magnetic field direction and the model direction indicate that either the triangulation is in error or the model magnetic field is not correct. In fact, the differences between the two directions for all three releases were quite small. Table 2 shows the angle between the triangulated magnetic field direction (B_{tri}) and the model magnetic field direction (B_{mod}) obtained by taking the dot product of the two vectors. The only large angle is the first triangulated direction in the G-4 release and is the result of the fact that the cloud dimensions were quite small and prone to large error in the triangulated direction. Otherwise, the triangulated and model magnetic field direction agree to within 5 to 10°.

Table 2.

G-2 Release hmmss	13-Jan-1991 B_{tri}•B_{mod}	G-3 Release hmmss	15-Jan-1991 B_{tri}•B_{mod}	G-4 Release hmmss	16-Jan-1991 B_{tri}•B_{mod}
21700	(release)	41100	(release)	62500	(release)
21759	4.7	41200	1.9	62557	30.4
21935	1.6	41231	0.6	62629	14.5
22011	1.3	41300	1.1	62656	5.6
22048	1.0	41331	5.3	62727	5.7
22125	2.2	41400	3.7	62806	6.4
22233	3.3	41500	0.9	62858	10.7
22339	1.8	41600	3.0	62940	8.7
22407	2.3	41900	4.8	63028	6.8
22453	2.6	42000	4.4	63133	10.1
22703	8.8	42100	7.0	63252	7.0
		42202	9.4		
		42303	10.4		
		42400	9.0		
		42505	12.1		
		42600	9.9		

We also use the fact that the cloud striates along the magnetic field to simplify the determination of the motion of the cloud. To do this, we note that, collectively, the ions in the cloud have two motions, perpendicular and parallel to the ambient magnetic field. The parallel motion presents somewhat of a problem. The fields of view of the cameras that photographed the clouds were typically small (~ few degrees). When the angle the cloud subtends becomes greater than the field of view of a given camera, only a portion of the cloud could be tracked. Therefore, different stations usually were tracking different parts of the cloud. This problem is illustrated in Figure 1, where it is evident that the cloud in the Breezy Point image (lower panel) is not completely contained in the field of view. By triangulating different parts of the cloud from image pair to image pair as the cameras are moved to keep some portion of the cloud in the center of the field of view, apparent motions along the magnetic field are introduced. Because of this, we cannot accurately

analyze the motion along the magnetic field except in the very early stages of the cloud formation and we want to remove this motion from the analysis.

To remove the parallel motion, we define a coordinate system where the magnetic field is along the z-axis and the spacecraft velocity perpendicular to the magnetic field at the time of release is along the y-axis. For accuracy, we use the triangulated magnetic field direction to determine the rotation from the triangulated geographic coordinates to the B-$V_\perp$ coordinate system although it is evident in Table 2 that using the model field would produce similar results. Finally, we translate the points so that the spacecraft position at the time of the release is located at the origin. Figure 3 illustrates this coordinate system.

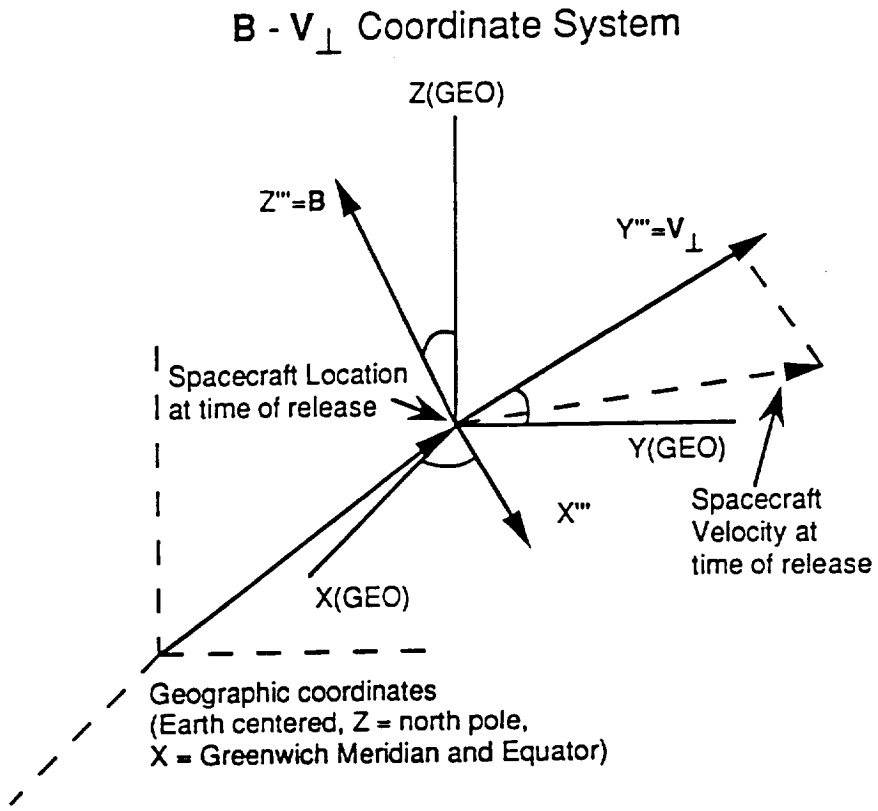

Figure 3

By rotating into the B-$V_\perp$ coordinate system, we de-couple the motion along the magnetic field and the motion perpendicular to the magnetic field. Also, since we relate the coordinate system to fixed locations and directions, we can compare the triangulated position from image pair to image pair without biasing the comparison. Since we cannot accurately describe the motion along the magnetic field, we will consider only the projection of the triangulated points into the x'''-y''' plane.

Figure 4,5, and 6 show the projected position of the triangulated points for the three releases into the x'''-y''' plane. For the G-2 release, we also had the opportunity to triangulate the neutral cloud for the first few minutes of the release. As expected, the

neutral cloud for the G-2 release (Figure 4) simply moved in the x'''-y''' approximately in the direction of the spacecraft velocity vector at the time of the release. Some residual motion in the x''' direction has not been explained at this time.

It is particularly interesting to compare and contrast the G-2, G-3 and G-4 results in Figures 4, 5 and 6. First, if all uncertainties in the triangulated points were equal, then the projection of the triangulated points for a given image pair should produce a small cluster in the x'''-y''' plane centered on the average location of the intersection point of the magnetic field with that plane. However, all uncertainties are not equal. In the triangulation procedure, the uncertainties in the determination of the location perpendicular to the line of sight are inherently much smaller than that in the radial direction. Thus instead of a cluster of points, the projected points form short line segments approximately in the radial direction. These line segments are evident in both Figures 5 and 6.

The plasma cloud motion perpendicular to the magnetic field direction was different for all three releases. For the G-2 release, the plasma cloud simply moved a short distance from the release point and spent the remaining 10 minutes very close to it. For the G-3 release, the plasma cloud moved away from the release point at about a 45° angle for the first minute and a half, stopped, then moved in the $-V_{y'''}$ direction for approximately a minute and a half and finally drifted approximately in the $V_{x'''}$ direction for the remaining 10 minutes. For the G-4 release, the plasma cloud moved away from the release point almost uniformly for the first 6 minutes after the release at which time it stopped. Triangulation beyond this time was not possible due to the loss of data at the Breezy Point site. We are currently in the process of analyzing this motion and are preparing a paper on the results for publication in the Journal of Geophysical Research.

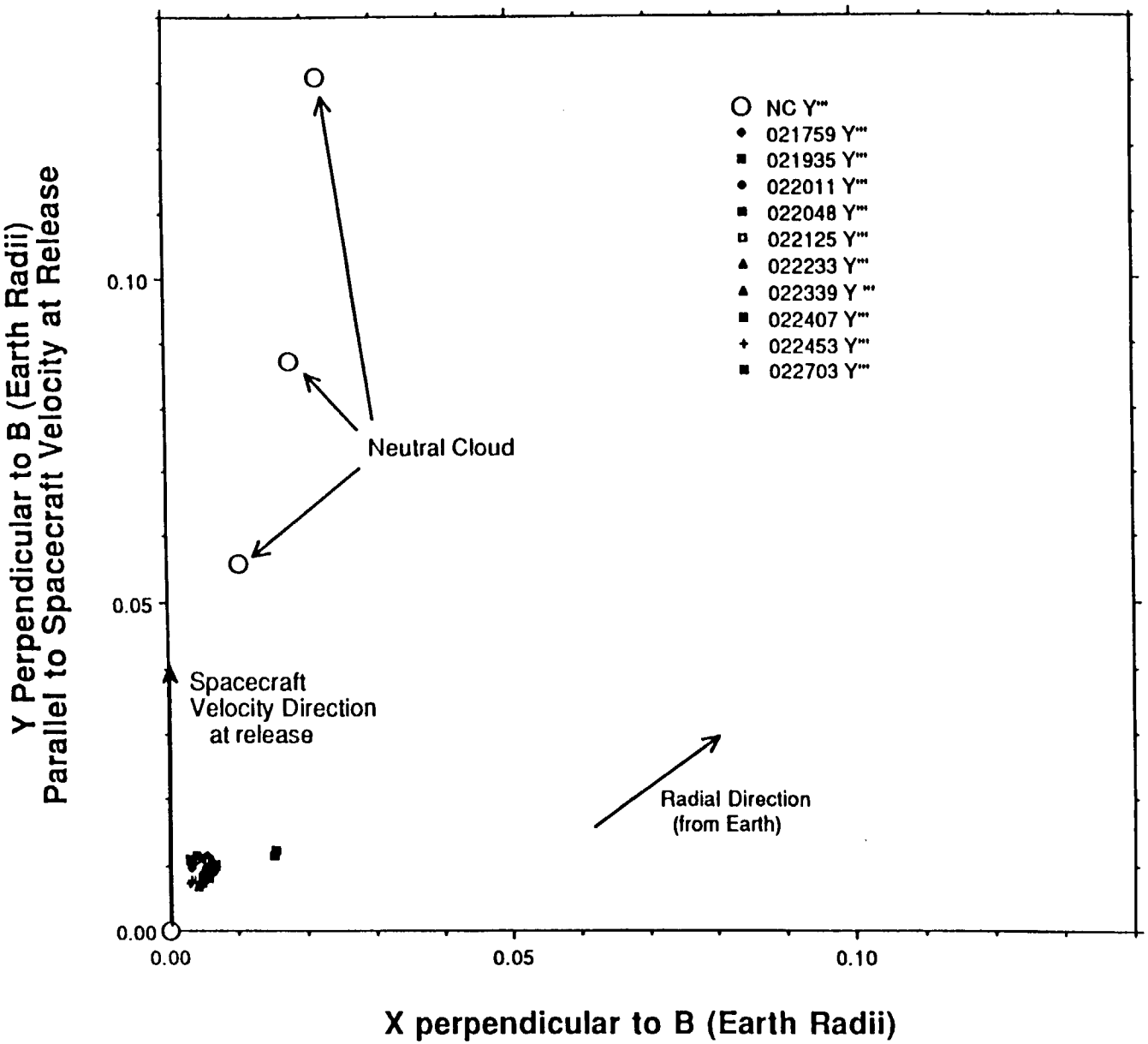
Data from "G2 trlang perp to B coord"
NC Y'''
021759 Y'''
021935 Y'''
022011 Y'''
022048 Y'''
022125 Y'''
022233 Y'''
022339 Y '''
022407 Y'''
022453 Y'''
022703 Y'''
Neutral Cloud
Spacecraft
Velocity Direction
at release
Radial Direction
(from Earth)
0.00
0.05
0.10
0.00
0.05
0.10
Y Perpendicular to B (Earth Radii)
Parallel to Spacecraft Velocity at Release
X perpendicular to B (Earth Radii)

Figure 4

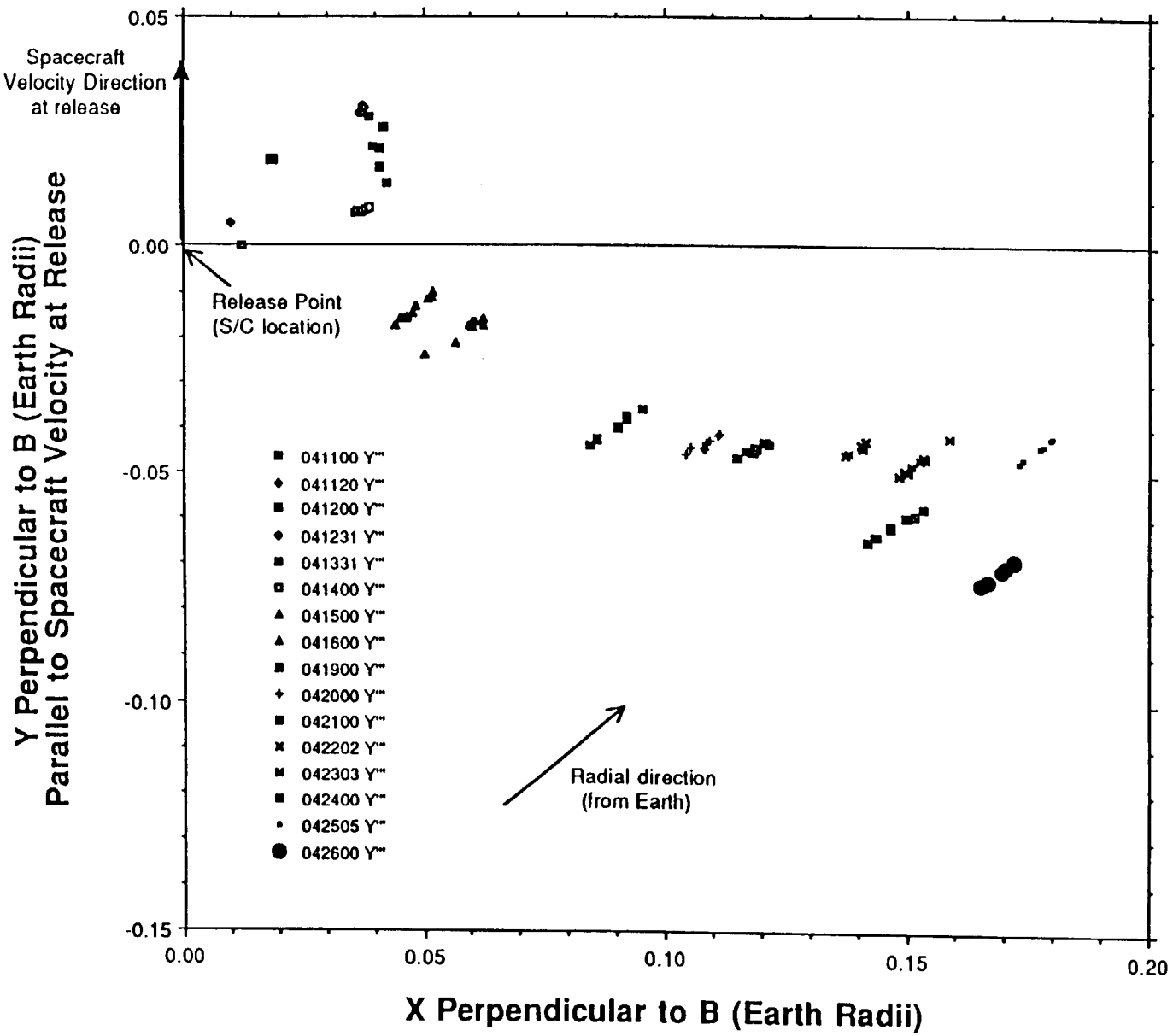
Data from "G-3 trlang rotated to B"
Spacecraft
Velocity Direction
at release
Release Point
(S/C location)
Radial direction
(from Earth)
041100 Y'''
041120 Y'''
041200 Y'''
041231 Y'''
041331 Y'''
041400 Y'''
041500 Y'''
041600 Y'''
041900 Y'''
042000 Y'''
042100 Y'''
042202 Y'''
042303 Y'''
042400 Y'''
042505 Y'''
042600 Y'''
0.05
0.00
-0.05
-0.10
-0.15
0.00
0.05
0.10
0.15
0.20
Y Perpendicular to B (Earth Radii)
Parallel to Spacecraft Velocity at Release
X Perpendicular to B (Earth Radii)

Figure 5

Data from "G-4 BP-AR trlang rot coord"

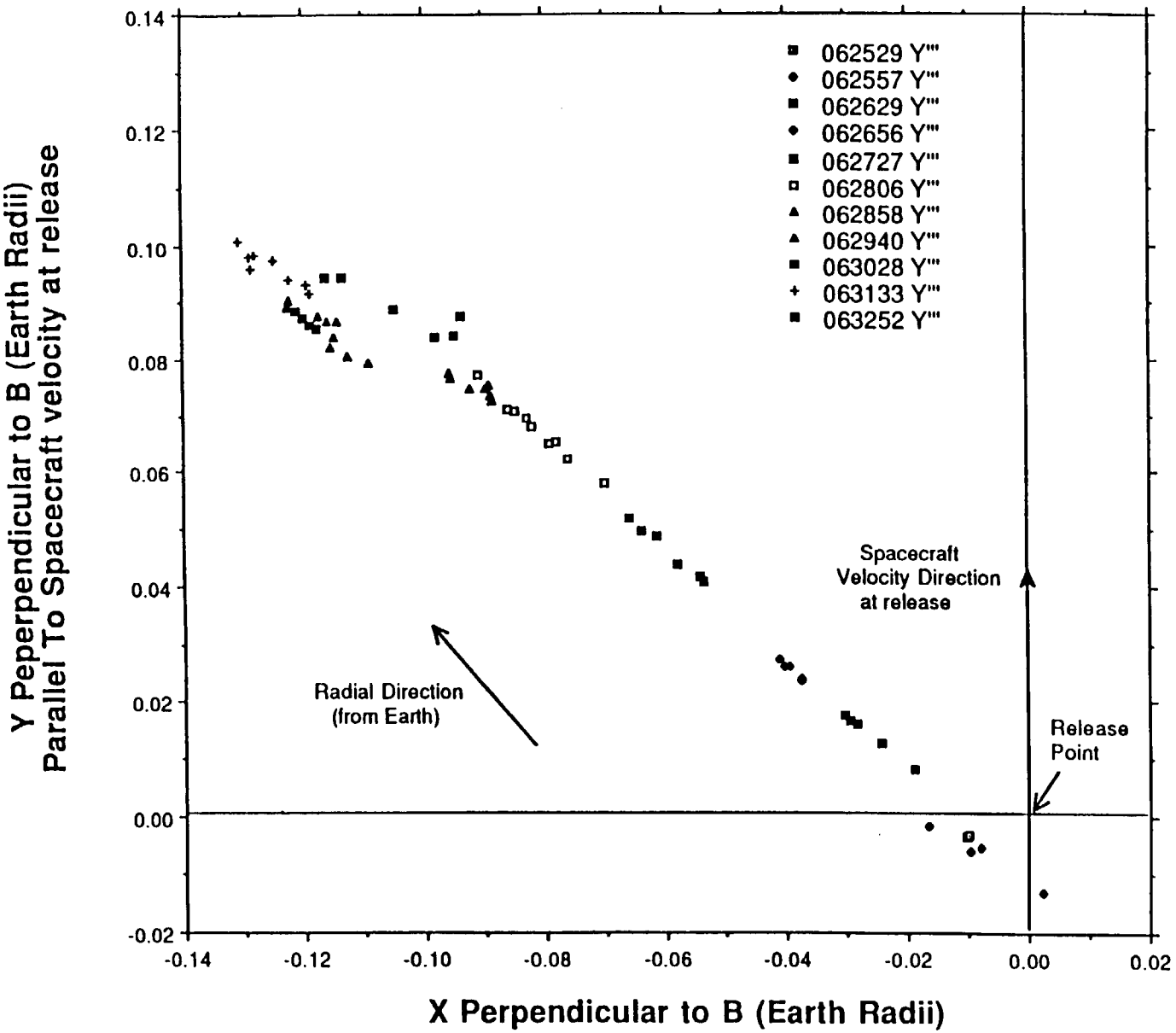

Figure 6

REPORT DOCUMENTATION PAGE

Form Approved
OMB No. 0704-0188

1. AGENCY USE ONLY (Leave blank)	2. REPORT DATE	3. REPORT TYPE AND DATES COVERED
	1/21/94	Final Report 4/12/85 - 12/23/93

4. TITLE AND SUBTITLE
Artificial Plasma EXperiments.
Chemical release observations associated with the CRRES program.

5. FUNDING NUMBERS
Contract
NAS8-36630

6. AUTHOR(S)
S.B. Mende

7. PERFORMING ORGANIZATION NAME(S) AND ADDRESS(ES)
Lockheed Missiles & Space Company
Research and Development Division
0/91-20, B/255, Fac 2
3251 Hanover Street
Palo Alto, CA 94304-1187

8. PERFORMING ORGANIZATION REPORT NUMBER

9. SPONSORING / MONITORING AGENCY NAME(S) AND ADDRESS(ES)
NASA
George C. Marshall Spaceflight Center
Marshall Spaceflight Center, Alabama 35812

10. SPONSORING / MONITORING AGENCY REPORT NUMBER

11. SUPPLEMENTARY NOTES

12a. DISTRIBUTION / AVAILABILITY STATEMENT
Unlimited/Unclassified

12b. DISTRIBUTION CODE

13. ABSTRACT (Maximum 200 words)

This report submitted is the Final report and covers work performed under the contract for the period as shown in Block 3.

14. SUBJECT TERMS
space plasma physics, ionosphere, magnetosphere, plasma clouds, barium clouds

15. NUMBER OF PAGES
87

16. PRICE CODE

17. SECURITY CLASSIFICATION OF REPORT	18. SECURITY CLASSIFICATION OF THIS PAGE	19. SECURITY CLASSIFICATION OF ABSTRACT	20. LIMITATION OF ABSTRACT
Unclassified	**Unclassified**	**Unclassified**	**Unlimited**